2015-03-01

Re-Calibration of the Periods of Selected Cepheids from the Hubble Space Telescope Key Project Using Time Correction

Muxue Liu
Brigham Young University - Provo

Re-Calibration of the Periods of Selected Cepheids

from the Hubble Space Telescope Key Project

Using Time Correction

Muxue Liu

A thesis submitted to the faculty of
Brigham Young University
in partial fulfillment of the requirements for the degree of

Master of Science

Eric Hintz, Chair
Mike Joner
Denise Stephens

Department of Physics and Astronomy

Brigham Young University

March 2015

ABSTRACT

Re-Calibration of the Periods of Selected Cepheids
from the Hubble Space Telescope Key Project
Using Time Correction

Muxue Liu
Department of Physics and Astronomy, BYU
Master of Science

The Hubble Space Telescope (HST) was originally proposed and funded in the 1970's with a launch planned for the early 1980's. However, the launch finally occurred on April 24, 1990, largely due to the Challenger accident. Once launched in 1990, one of HST's earliest projects was the Key Project. One of the main purposes of the Key Project was to calibrate the distances to nearby galaxies and determine a definitive value of the Hubble constant H_0. All secondary distance determination methods were based on the period-luminosity relation of Cepheid variable stars. This thesis examines the Cepheid data from the Key Project by first redetermining the periods of Cepheids in selected galaxies and then applying a time correction to the data. This time correction is to compensate for the effects of the recessional motion of each galaxies, as caused by the finite speed of light. The recovery stage of the project was mostly successful, but revealed concerns with the original data set. This result led to less compelling results for the time-correction stage due to the larger than anticipated errors. A further examination was performed on part of the sample by using a more accurate form of the time input as found in the HST image headers. Overall we conclude that the short observation baseline of the Cepheids, with medium to long periods, is a major deficiency of the Cepheid data from the Key Project with regard to testing for the effects of recessional motion. Future studies on the effects of the time correction need to be done using data with longer time coverage that spans at least 4 pulsational cycles, perferably more than 30 cycles.

Keywords: [Cepheids, $P-L$ relation, time correction, Hubble Space Telescope Key Project, Peranso, variable star period search]

ACKNOWLEDGMENTS

There are a lot of people who I want to acknowledge. I must first thank my parents and grandparents who are back in China for all the financial and spiritual support they have given me throughout the years I have been studying in the United States. I must also thank Xiaogang Gao, my beloved one, for sharing with me courage and hope in the most difficult time of my life.

I must thank my advisor Dr. Eric Hintz for giving me the opportunity to do research, Dr. Denise Stephens and Dr. Mike Joner for being my committee members, and Dr. Eric Hirschmann for his help as the Department Graduate Coordinator. I must thank Miss Rachel Hunter for sharing data with me, which have made valuable contributions to the conclusion part of this thesis. I must acknowledge Derek Felli, Adam Johanson, and Brandon Wiggins for being fabulous colleages and all the good times we have spent as office mates since I joined the graduate student office in 2012.

Finally, I must acknowledge the Department of Physics and Astronmy of Brigham Young University for their support and being my "home" in the United States since I first landed here in 2007.

Contents

Chapter 1

Introduction and Background

1.1 The Cepheid $P-L$ Relation

Cepheid variables, especially the classical type (or type I), play a significant role in our understanding of the scale of the Universe. They obey a period-luminosity ($P-L$) relation, which makes them favorable standard candles to measure the distances to extragalactic objects which are within the local region near the Milky Way. As demonstrated in the Hubble Space Telescope (HST) Key Project on the Extragalactic Distance Scale (Freedman et al. 2001), Cepheids can be measured with sufficient accuracy out to a distance of about 20 Mpc. They provide an early rung in the distance ladder and provide the calibration for techniques used to reach out to much greater distances.

The change in brightness seen in Cepheids had been observed long before the underlying physical reasons were understood. It was once thought that the light variations were caused by tidal effects in the atmosphere of binary stars. However, Shapley (1914) argued that the binary theory was fatally flawed, because the size of the star would exceed the size of the orbit for some variables. Plummer (1913) and Martin & Plummer (1914) discussed the possibility that the light variations seen could be the result of radial pulations. The true landmark paper on the pulsational nature of Cepheids came a few years later from Eddington (1919) where an actual mechanism was discussed. Later it was understood that classical Cepheids are supergiant stars of luminosity class I_b. They are about fifty times the size of the Sun and thousands of times more luminous. These stars have long since left the main sequence stage and are moving through the upper portion of the instability strip in the H-R diagram. Their pulsation periods change in a regular pattern as well as mean radii and temperature (Berdnikov & Turner 2001). Stars evolving towards the lower-temperature side of the H-R diagram at nearly constant luminosity are gradually increasing in size, and they exhibit increasing pulsating periods. On the other hand, stars evolving towards the higher-temperature side of the H-R diagram at nearly constant luminosity are gradually decreasing in size and exhibit shorter periods. Both scenarios have been confirmed by the observed rates of period change in Cepheid pulsation periods (Berdnikov & Ignitova 2000; Turner 1998; Turner et al. 2001; 1999). Observations have shown results that closely match what is expected from stellar evolutionary models.

Henrietta Swan Leavitt (1868-1921), played a major role in the history of Cepheids and made critical contributions to the first formulation of the period-luminosity relation. Over many years of work she discovered 2400 classical Cepheids with periods between 1 and 50 days, most of them located in the Small Magellanic Cloud (SMC). From this work Leavitt & Pickering (1912) presented the $P-L$ relation for 25 Cepheids in the SMC, as shown in Table 1.1. Although neither understood the full implications of their results at the time of publication, we now know that by plotting the average magnitude of each star versus the log of the period (in days) as seen in Figure 1.1, one finds a clear linear relation. The fit determined from this original data is given by the relation:

$$m_{ave} = -2.0332 log_{10} P_d + 16.163, \tag{1.1}$$

where m_{ave} is the average apparent magnitude, P_d is the Cepheid's pulsating period in days. The quantity -2.0332 is the slope of the $P-L$ fit, and 16.163 is the zero point. It should be noted that the magnitudes listed in Table 1.1 are apparent magnitudes on a photographic magnitude scale that doesn't match modern values with proper standardized filters. Therefore the intercepts quoted should not be used for comparison with later determinations shown in this thesis.

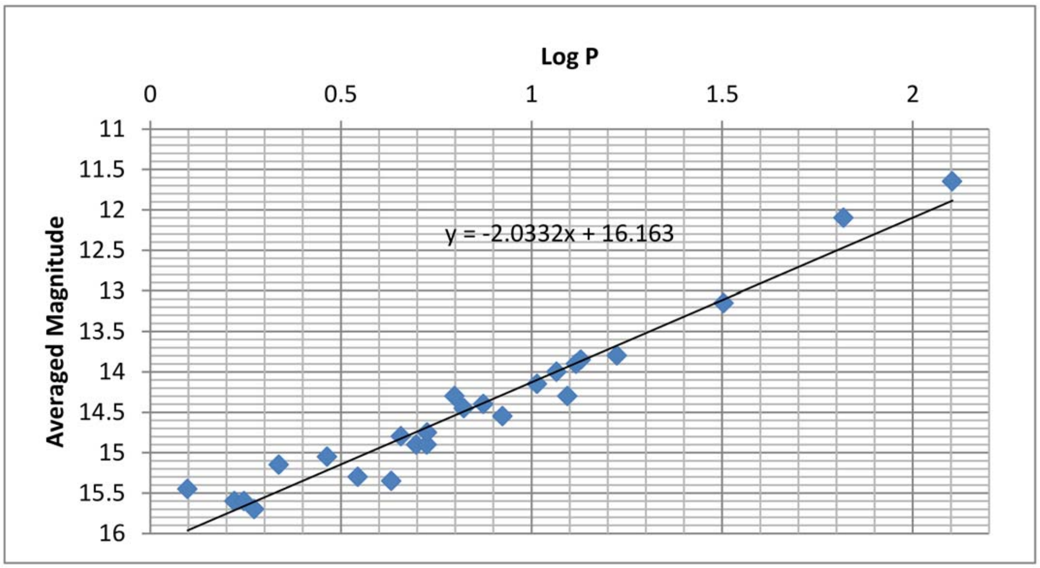

Figure 1.1 The $P-L$ relation of the 25 Cepheids in the SMC.

Since the first discovery of the $P-L$ relations many projects have been undertaken to provide greater understanding of this relation in a range of bandpasses. For example, in 2002, Sebo and Rawson's team used the data of 34 Cepheids in the Large Magellanic Cloud (LMC) taken from the Siding Spring (Australia) and Las Campanas (Chile) Observatories and reported

$$M_V = -2.760(log_{10}P_d - 1) - 4.218 \tag{1.2}$$

and

$$M_I = -2.962(log_{10}P_d - 1) - 4.904 \tag{1.3}$$

for the V and I wavebands respectively (Sebo et al. 2002) using absolute magnitude in this case. In 2006, Macri's team derived $P-L$ relations for the Cepheids in the galaxy NGC 4258 using data

Table 1.1. Periods and Magnitudes of the 25 Cepheids in the SMC

Period [Days]	Log Period	Maximum Magnitude	Minimum Magnitude	Average Magnitude
1.25336	0.098076	14.8	16.1	15.45
1.6637	0.221075	14.8	16.4	15.6
1.762	0.246006	14.8	4	15.6
1.87502	0.273006	15.1	16.3	15.7
2.17352	0.337164	14.7	15.6	15.15
2.913	0.46434	14.4	14.7	15.05
3.501	0.544192	14.7	15.9	15.3
4.2897	0.632427	14.6	16.1	15.35
4.547	0.657725	14.3	15.3	14.8
4.9866	0.697805	14.3	15.5	14.9
5.311	0.725176	14.4	15.4	14.9
5.323	0.726156	14.3	15.2	14.75
6.2926	0.79883	13.8	14.8	14.3
6.65	0.822822	14.1	14.8	14.45
7.483	0.874076	14	14.8	14.4
8.397	0.924124	13.9	15.2	14.55
10.336	1.014353	13.6	14.7	14.15
11.645	1.066139	13.4	14.6	14
12.417	1.094017	13.8	14.8	14.3
13.08	1.116608	13.4	14.4	13.9
13.47	1.129368	13.4	14.3	13.85
16.75	1.224015	13	14.6	13.8
31.94	1.504335	12.2	14.1	13.15
65.8	1.818226	11.4	12.8	12.1
127	2.103804	11.2	12.1	11.65

from the HST Advanced Camera for Surveys/Wide Field Camera (ACS/WFC) (Ford et al. 2009). They reported

$$M_B = -2.439(log_{10}P_d - 1) + 14.929, \tag{1.4}$$

$$M_V = -2.779(log_{10}P_d - 1) + 14.287, \tag{1.5}$$

and

$$M_I = -2.979(log_{10}P_d - 1) + 13.615 \tag{1.6}$$

for the B, V, and I wavebands respectively (Macri et al. 2006), returning to apparent magnitudes. In 2008, Ngeow's team derived $P-L$ relations for the fundamental mode Cepheids in the LMC. They used the data from the third phase of observation of the Optical Gravitational Lensing Experiment (OGLE-III) (Soszynski et al. 2008). They reported $P-L$ relations for multiple wavebands as demonstrated in Table 1.2 (Ngeow et al. 2009). Just for consistancy we note that these are again apparent magnitudes in the respective bands.

Interstellar extinction is one of the major problems in the measurement of Cepheid $P-L$ relations, especially in the visible wavelengths. Various researchers have been able to substantially decrease the scatter in the $P-L$ relation by making observations in the infrared where extinction is less of a problem and thus lower the uncertainty. One such fit was made by Persson's team using magnitudes measured in the infrared H band (centered at $1.654\mu m$) over a 3-year baseline. The data was of 92 Cepheids in the LMC taken by three different telescopes. The period-luminosity relation before color correction was given by

$$H = -3.324log_{10}P_d + 16.079. \tag{1.7}$$

And the relation after color correction was given by

$$H = -3.428log_{10}P_d + 1.54 < J - K_s > +15.637, \tag{1.8}$$

Table 1.2. The LMC Period-Luminosity Relations in Various Bands Derived from OGLE-III Data

Band	Slope	Zero Point
V	-2.769 ± 0.023	17.115 ± 0.015
I	-2.961 ± 0.015	16.629 ± 0.010
J	-3.115 ± 0.014	16.293 ± 0.009
H	-3.206 ± 0.013	16.063 ± 0.008
K	-3.194 ± 0.015	15.996 ± 0.010
3.6μm	-3.253 ± 0.010	15.967 ± 0.006
4.5μm	-3.214 ± 0.010	15.930 ± 0.006
5.8μm	-3.182 ± 0.020	15.873 ± 0.015
8.0μm	-3.197 ± 0.036	15.879 ± 0.034
W	-3.313 ± 0.008	15.892 ± 0.005

where $J-K_s$ is the infrared color index (Persson et al. 2004). In 2012, Riess's team used the near-infrared data of Cepheids in M31 and derived the slope of the $P-L$ fit to be -3.43±0.17 (Riess et al. 2012). This is in good agreement with Persson's result (Persson et al. 2004).

Simultaneous comparison is needed for the study of the $P-L$ slopes from different samples (Ngeow et al. 2009). A proper study of Cepheid period variation also requires a sufficiently long baseline of observations with reasonably thorough temporal coverage in order to sort out clearly the various factors that affect period variations in the stars. Light travel time effects are generally difficult to establish within the standard constraints associated with observational scatter but can be detected in data sets of sufficiently good quality (Berdnikov & Turner 2001).

Some effects superimposed on the regular long-term luminosity variation can cause subtle changes to the measured periods. Such effects include light travel time differences resulting from orbital motion about a companion (Szabados 1977; 1980; 1981; 1989), random fluctuations in period (Berdnikov et al. 2000; Turner et al. 2001), etc. Another challenge to the standart $P-L$ relation is that it can be nonlinear even if the short- and long-period slopes are within roughly 1 to 2σ of each other, as analytical studies (Ngeow & Kanbur 2008) have shown. Statistical tests are needed to detect nonlinear $P-L$ relations (Ngeow & Kanbur 2006). This thesis project will assume linear $P-L$ relations for all of the galaxies in the sample and focus on the effect of recessional motion of those galaxies on their measured periods. Details about this effect will be discussed in Section 1.3.

In general, the Cepheid $P-L$ relation is the most important of the primary distance indicators of nearby galaxies. There are a number of advantages to using Cepheids as standard candles for these nearby objects. First, Cepheids are relatively common in those nearby spiral galaxies. In general this means that each galaxy will have a reasonable size sample that contains Cepheids over a range of periods. Another important characteristic of Cepheids is their distinctively shaped light curve with its fairly large amplitudes. Those two together make the discovery of Cepheids reasonably easy compared to other types of variable stars. Another important advantage to Cepheids is that they are periodic in nature and the pulsations are stable for long periods of time. This allows us to return to observe the same variable many times. This is not possible with other standard candles such as supernovae where the brighting means the destruction of the star. Finally, the Cepheid $P-L$ relation has relatively small scatter. It has been shown that that the dispersion amounts in the I band are only about ± 0.1 mag (Udalski et al. 1999). These ideas are all covered extensively in Freedman et al. (2001).

Another major advantage to working Cepheid variables is the many years of study that have gone into understanding their natures and the extensive amount of modeling which has been done. From this the reason for their variability is well understood: it is a consequence of motion of the upper regions of the stellar interior that result from valve-like driving mechanism as helium is cycled from a singly to doubly ionized state and therefore causing an opacity flip at different points in the cycle as detailed by Cox & Whitney (1958).

However, there are also some disadvantages to using Cepheids as standard candles. Perhaps the most difficult disadvantage to deal with are the corrections needed for extinction across many filters at many wavelengths. To minimize the extinction effects one must either use multi-color observations or move to data from longer wavelengths. There is also a great deal of concern with the effects of metallicity on $P-L$ relations. To ensure one is using the correct $P-L$ relation it would be best if the metal content could be determined spectroscopically. However, this is unlikely for the majority of Cepheids in external galaxies, especially as the distances increase. In fact the discovery of Cepheids becomes increasingly more difficult as we move to more distant galaxies due to their apparent magnitude decreasing and the effects of crowding in the fields. Many of these concerns are again summarized in Freedman et al. (2001).

1.2 The Hubble Space Telescope Key Project

The HST Key Project used Cepheid based distances to 31 nearby galaxies (see Table 1.3) to calibrate far reaching secondary methods of distance determination in these galaxies, which were then used to provide distance estimates to more remote galaxies. Then the objects over a wide range of distances were used to determine H_0, the Hubble constant. In Table 1.3 the 31 nearby galaxies from the Key Project are listed in order of recessional velocity.

When first proposed in the 1970's one of the primary missions of the Hubble Space Telescope was to measure an accurate value for H_0 (The Hubble Constant) and how that value impacts the Hubble Law:

$$v = H_0 d, \tag{1.9}$$

where v is the recessional velocity of a galaxy at a distance d. Therefore the value of H_0 is the expansion rate of the Universe at the current epoch. Once an accurate value of the Hubble Constant is determined, a number of other astrophysically significant determinations follow. The inverse, ${H_0}^{-1}$, provides a model dependent estimate for the age of the universe, t_0, and the size of the observable universe, $R_{obs} = ct_0$. The square of H_0 relates the total energy density of the universe to the underlying geometry (Kolb & Turner 1990; Peacock 1999a). Finally, H_0 defines the critical density of the universe as

$$\rho_{crit} = (3H_0^2)/(8\pi G). \tag{1.10}$$

.

Beyond determining the grand scale of the Universe the Hubble Law is also critical as a method to determine distance to astrophysically significant objects throughout the observable Universe. To determine the physical properties such as mass, luminosity, energy output, etc. of objects such as galaxies, galaxy clusters, and quarsars we need to know their distance. In many instances that distance can only be measured by using the Hubble Law. Therefore, the measurement of H_0 to an accuarcy of 10% was designated as one of three “Key Projects” of the HST. The team lead by Wendy L. Freedman was awarded “the Key Project on the Extragalactic Distance Scale” in 1986 (Freedman et al. 2001). They began their initial observations of the closest galaxies in their sample in 1991, which was shortly after the launch of HST. Starting with the now well established Cepheid $P-L$ relation, the goal was to calibrate a number of secondary distance indicators including the Tully-Fisher relation, Type I_a supernovae, surface brightness fluctuations, and Type II supernovae (Freedman et al. 2001). The combination of all these methods would then provide a high quality estimate for the value of H_0.

Table 1.3. List of Cepheid Galaxies Observed by the Key Project

Galaxy Name	Recessional Velocity [km/s]	Alternative Names
NGC 224	-301	M31, IRAS F00400+4059, Andromeda Galaxy
IC 1613	-234	IRAS F01024+0153, MCG+00-03-070
NGC 598	-182	M33, MCG+05-04-069, Triagulum Galaxy
NGC 3031	-42	M81, IRAS F09514+6918, Bode's Galaxy
NGC 2403	129	IRAS F07320+6543, MCG+11-10-007
NGC 300	144	IRAS 00525-3757, MCG-06-03-005
NGC 5457	267	M101, IRAS F14012+5434, Pinwheel Galaxy
IC 4182	324	IRAS F13035+3752, MCG+06-29-031
NGC 5253	403	IRAS F13370-3123, ESO 445-4, MCG-05-32-060
NGC 4258	462	M106, MCG+08-22-104, UGC 7353
NGC 4548	492	M91, MCG+03-32-075, UGC 7753
NGC 925	552	IRAS F02242+3321, MCG+05-06-045
NGC 2541	557	IRAS F08109+4912, MCG+08-15-054
NGC 3198	679	IRAS F10168+4547, MCG+08-19-020
NGC 3627	702	M66, IRAS F11176+1315, MCG+02-29-019
NGC 4414	717	IRAS F12239+3130, MCG+05-29-085
NGC 3621	727	IRAS F11158-3232, MCG-05-27-008
NGC 3319	752	IRAS 10361+4156, MCG+07-22-036
NGC 3351	777	M95, IRAS F10413+1157, MCG+02-28-001
NGC 7331	818	IRAS F22347+3409, MCG+06-49-045
NGC 3368	902	M96, IRAS F10441+1205, MCG+02-28-006
NGC 2090	923	ESO 363-23, IRAS F05452-3415
NGC 4639	978	IRAS F12403+1331, MCG+02-32-189

Table 1.3 (cont'd)

Galaxy Name	Recessional Velocity [km/s]	Alternative Names
NGC 4725	1207	IRAS 12480+2547, MCG+04-30-022
NGC 1425	1503	ESO 419-4, IRAS F03401-3003
NGC 4321	1570	M100, IRAS F12203+1605, MCG+03-32-015
NGC 1365	1665	ESO 358-17, IRAS F03316-3618
NGC 1326A	1718	ESO 357-28, MCG-06-08-013
NGC 4496A	1730	MCG+01-32-090, UGC 7668
NGC 4536	1808	IRAS F12319+0227, MCG+00-32-02
NGC 4535	1957	IRAS F12317+0828, MCG+01-32-104

1.3 The Time Correction

Because light travels at a finite speed the time it takes to travel from one object to another can be impacted by the relative motion of the two objects. This is clearly seen in the use of the Heliocentric Julian Date (HJD) or Modified Julian Date (MJD) in most studies of variable objects. This removes the motion of the Earth's orbit from the time measurement. Therefore, a time correction that contains the light traveling time is needed in principle for precise measurements of time-dependent quantities, such as the Cepheid pulsating periods, based on the motion of that object. Figure 1.2 demonstrates the effect in a simple, graphical way. In the published Key Project time-series the MJD was used to remove the Earth's motion, but a time correction was not applied for the motion of each galaxy. A simple 0.5 day conversion is used between HJD and MJD.

Time is measured in HJD in our study. HJD, or the Heliocentric Julian Dates is a high-precision time measurement that measures the time it would take light to travel from a celestial object to the center of the Sun rather than the Earth (Carroll & Ostlie 2007), since the Earth's orbit will cause

Figure 1.2 Light travels an additional distance due to the recessional motion of the distant galaxy.

inaccuracy in the measurement of time. A correction in HJD will slightly distort the shape of the magnitude vs. time curve. Theoretically, this distortion will affect the calculation of period and luminosity, which will eventually have some impact on the Hubble constant. Our aim is to do the time correction and verify whether this correction is necessary for accurate period calculations. In the study of variable stars, if this effect is uncorrected for, one would very likely obtain the period of revolution of the Earth rather than the star's true period.

The recessional velocities of the selected galaxies from the HST Key Project have been measured, and we used those values to correct the input time string for each Cepheid. The goal is to use these well established objects to see if the time correction will have any impact on the period determinations for each star as compared to the values published by the Key Project team. The traditional correction for the revolution of the Earth around the Sun was applied to the Key Project data, but a correction for the recessional velocities was not applied in the original project. We believe the Key Project data to be an ideal data set to test the need for additional time correction to all variable star data sets.

Some questions that will be addressed by this project include:

1. How large does the recessional velocity need to be in order to observe a period change?

2. Is the effect more significant on longer or shorter period Cepheids?

3. How accurate does the input time string need to be?

4. Overall, how critical is the time correction?

Chapter 2

Data

2.1 Overview

In our project, we have selected 17 galaxies from the sample list given earlier (Table 1.3) and calculated the periods of the Cepheids in each galaxy using both the original time-string and time-corrected data. There were two reasons for rejecting the remaining 14 galaxies from the Key Project. First we did not have access to the photometric data in an easily readable electronic format. Second, the published data appear to have a flaw or deficiency in the online data source that made it hard to recover the desired data. An example of such would be NGC 1425. As we will discuss later (Section 2.2), there are some errors in the publication, which makes the data inaccessible. Once we settled on the sample of 17 galaxies we followed the following stages for the project.

There are four stages in our study:

1. Period recovery using the original published data.

2. Period determinations using time-corrected data.

3. Use more accurate time from HST headers for selected galaxies

4. Evaluate the significance of time correction.

All the photometric data are directly taken from the Key Project publication series. These data include the time (in HJD) and apparent magnitudes for each observation of each Cepheid and its published period as calculated by the authors of the paper. The software we use for our period search is Peranso (version 2.51). This is a light curve and period analysis software package developed by Tonny Vanmunster at the Center for Backyard Astrophysics (CBA) Belgium Observatory (Peacock 1999b). In Peranso, there are 13 period-searching methods. Our first task was to select the most suitable methods to apply on our data. To do this, we randomly select about 30 Cepheids from different galaxies and use each method in Peranso to perform the period search. We then record the results and compare them to the published values. We find that the Date Compensated Discrete Fourier Transform (DCDFT), the CLEANest, and the Analysis of Variance (ANOVA) are the most reliable methods in recovering the published values. Therefore we choose to use these three for both the recovery and the time correction stages. Later we confirmed that the DCDFT and the CLEANest provided almost identical outputs based on the periods found for over 200 Cepheids.

Our data were taken by the HST using both the V and I filters. Table 2.1 presents the number of data points in the V and I filters for each of our 17 galaxies. It is obvious that the number of data points in the I filter is significantly smaller than that in the V filter. All galaxies have less than 10 data points in the I filter, which makes the period calculation difficult and inaccurate. Therefore, we decided to use only the V-filter data in this project.

2.2 Stage One: Recovery

The first stage of our project was to try and recover the published periods for each Cepheid using the original data. This provided a test of our period determination methods as compared to those

Table 2.1. Number of Data Points in the V and I Filters

Galaxy	Number of Points in V	Number of Points in I
NGC 925	12	4
NGC 1326A	12	8
NGC 1365	12	4
NGC 2090	13	5
NGC 2541	13	5
NGC 3031	22	6
NGC 3198	26	6
NGC 3319	26	8
NGC 3351	12	4
NGC 3621	12	4
NGC 4321	12	4
NGC 4414	13	4
NGC 4535	13	9
NGC 4548	13	8
NGC 4725	27	9
NGC 5457	25	5
NGC 7331	15	4

used on the Key Project. In the recovery stage, we are able to match most of our period determinations to the published values. At the same time, we also found some deviations that seemed to cluster around the longer period variables. Below we provide a brief introduction to each galaxy and present charts showing the comparison between the published periods and the periods determined with the DCDFT and ANOVA methods in Peranso.

Originally, NGC 1425 was going to be included in our sample. However, further examination indicates that there is a disagreement between the published results and the photometric data on the Project website. The authors published the periods of 29 Cepheids that were selected from 33 candidates. Cepheids C07, C10, C21, and C29 were excluded because their data could not be recovered by either ALLFRAME or DoPHOT. However, Table 6 in Mould et al. (2000) presents photometric data for 30 Cepheids instead of 29. The authors did mention that the numbering of Cepheids was not continuous due to the exclusion of the 4 Cepheids. It is possible that some error occurred in the table. This discrepancy in the number of Cepheids has caused ambiguity, and it is the reason why we decided to exclude this galaxy from our project.

As we present each individual galaxy in the section below we will follow a similar pattern. First we will give the basic background for the galaxy and why it might have been a primary target for the HST. We will then provide a table of all Cepheids reported for that galaxy by the Key Project, with their published period and our periods from the DCDFT and ANOVA methods. Finally we will show the $P-L$ plot for the published periods, the periods from the DCDFT method, and the periods from the ANOVA method. Each figure will contain the equation for the best fit to the data.

2.2.1 NGC 925

NGC 925 is classified as an SBcII-III galaxy by Sandage & Tammann (1981) and as an SBS3 galaxy by de Vaucouleurs et al. (1991). It is a member of the NGC 1023 galaxy group (Tully 1980). This galaxy has a favorable inclination angle of 57 degree, which makes it a popular target for application of the Tully-Fisher methods (Silbermann et al. 1996). The 80 Cepheids that were selected for observation in this galaxy are summarized in Table 2.2. The published period for Cepheid 1 is noted as long in the paper. The authors suggest that its period may be as long as 109 days (Silbermann et al. 1996). Along with the published periods the period determinations done for this project are included. In Figures 2.1, 2.2, and 2.3 the $P-L$ plot is shown for each column from Table 2.2, along with the best fit to the data.

Table 2.2. Recovery of Cepheid Periods in NGC 925

Cepheid	Published (days)	DCDFT (days)	ANOVA (days)	Cepheid	Published (days)	DCDFT (days)	ANOVA (days)
C1	Long	121.458	140.187	**C2**	80	106.572	93.139
C3	80	120.000	120.000	**C4**	80	83.333	103.591
C5	48.5	46.189	45.714	**C6**	43.2	47.337	48.900
C7	42.1	42.105	41.973	**C8**	37.3	37.500	37.313
C9	35.1	35.294	35.211	**C10**	32.7	31.513	32.189
C11	31.3	30.060	31.250	**C12**	31.1	31.315	30.992
C13	30.4	30.488	30.550	**C14**	30.2	31.185	31.983
C15	30.1	29.656	29.821	**C16**	29.8	29.574	29.014
C17	28.5	27.594	24.116	**C18**	27.5	26.608	26.667
C19	27.3	26.906	28.169	**C20**	26.7	28.302	26.786
C21	26.7	27.088	27.027	**C22**	26.5	27.088	26.667
C23	25.5	26.608	26.144	**C24**	25.3	25.586	25.210
C25	24	24.917	25.773	**C26**	23.7	23.292	23.810
C27	23.5	23.962	23.148	**C28**	23.3	22.321	22.255
C29	23.3	22.936	22.590	**C30**	22.5	22.523	21.930
C31	22.3	21.866	21.802	**C32**	21.9	21.067	10.760
C33	21.5	20.000	10.776	**C34**	21.1	21.368	21.247
C35	20.6	19.947	20.380	**C36**	20.2	22.321	20.718
C37	19.3	19.737	19.355	**C38**	18.9	18.868	18.293
C39	18.9	19.108	18.634	**C40**	18.7	18.293	5.245
C41	18.3	18.925	19.052	**C42**	18.2	18.072	18.182
C43	18	17.964	17.964	**C44**	18	18.519	18.072

Table 2.2 (cont'd)

Cepheid	Published (days)	DCDFT (days)	ANOVA (days)	Cepheid	Published (days)	DCDFT (days)	ANOVA (days)
C45	17.8	17.442	17.544	**C46**	17.3	17.241	17.241
C47	16.7	18.072	16.949	**C48**	16.7	16.043	16.484
C49	16.7	17.241	17.143	**C50**	16.4	16.251	16.251
C51	16	15.941	17.626	**C52**	15.7	15.790	14.940
C53	15.7	15.496	15.736	**C54**	15.7	15.213	14.423
C55	15.5	15.814	16.146	**C56**	14.9	14.302	15.331
C57	14.8	14.671	15.060	**C58**	14.7	14.423	14.671
C59	14.6	14.799	14.928	**C60**	14.4	14.009	14.546
C61	14.4	16.053	14.183	**C62**	14.3	14.423	14.302
C63	13.6	12.967	13.682	**C64**	13.5	13.790	6.977
C65	13.5	13.575	13.575	**C66**	13.5	13.366	13.575
C67	13.3	13.366	9.652	**C68**	13.1	13.064	13.163
C69	12.9	12.987	12.987	**C70**	12.7	12.837	12.837
C71	12.5	12.547	12.270	**C72**	12.5	12.407	12.033
C73	12.2	12.005	12.270	**C74**	11.8	11.877	11.877
C75	11.1	12.422	12.406	**C76**	11	11.084	10.976
C77	10.8	10.870	10.976	**C78**	9.9	9.825	9.912
C79	9.8	9.825	9.259	**C80**	6.4	6.413	6.378

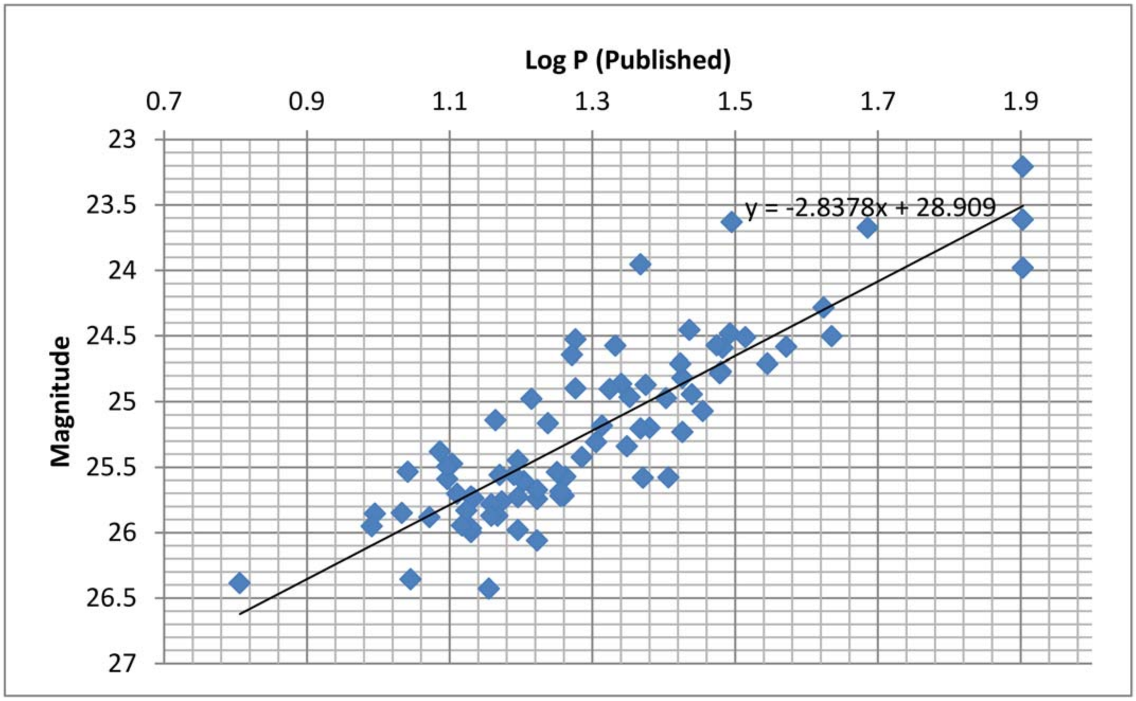

Figure 2.1 The Published $P-L$ Plot and Linear Fit for NGC 925.

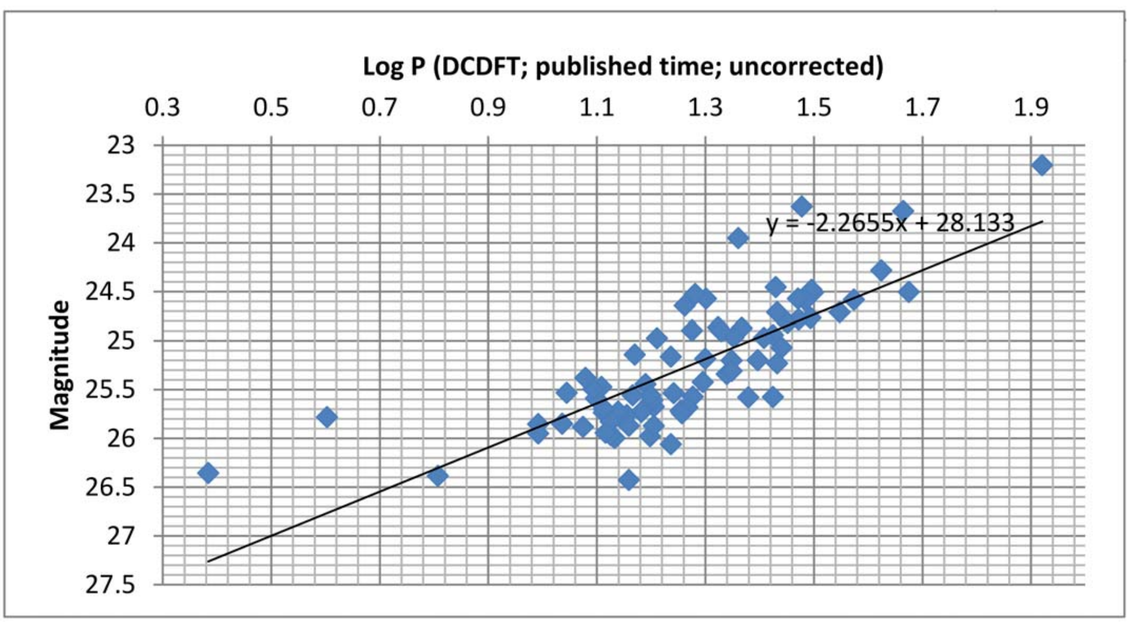

Figure 2.2 The $P-L$ Plot from DCDFT Period Recovery and the Linear Fit for NGC 925.

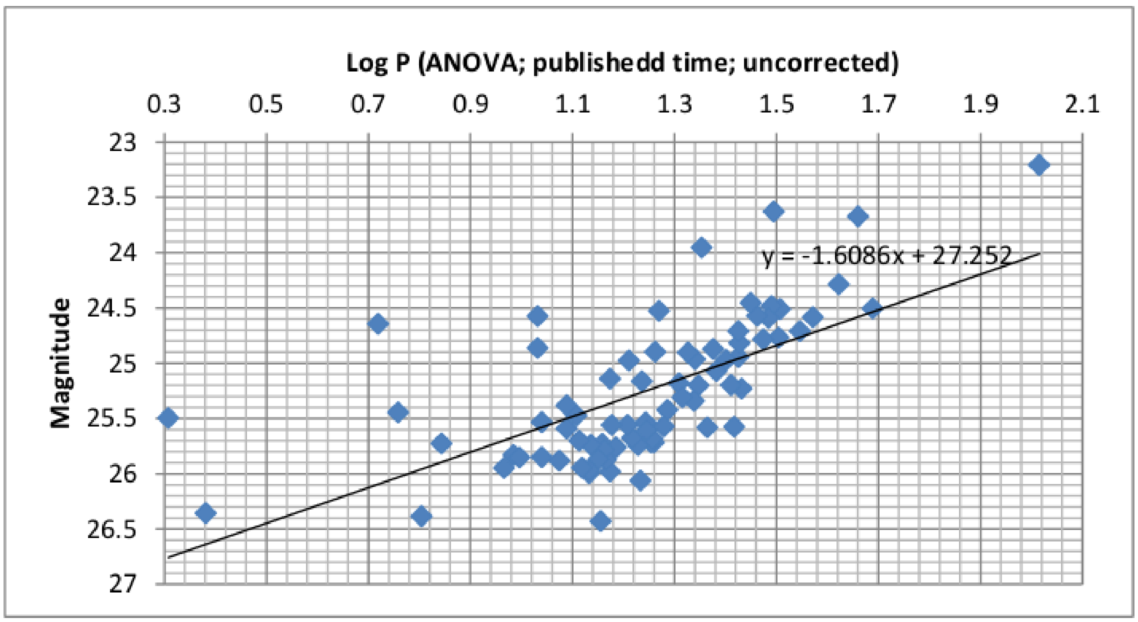

Figure 2.3 The $P-L$ Plot from ANOVA Period Recovery and the Linear Fit for NGC 925.

Table 2.3. Recovery of Cepheid Periods in NGC 1326A

Cepheid	Published (days)	DCDFT (days)	ANOVA (days)	Cepheid	Published (days)	DCDFT (days)	ANOVA (days)
C1	47.4	45.455	44.910	**C2**	39.5	42.614	40.215
C3	35.9	33.937	35.129	**C4**	33.7	33.557	33.708
C5	32	36.675	34.884	**C6**	30.8	30.706	31.780
C7	30.1	28.037	28.763	**C8**			
C9	25.2	26.709	26.824	**C10**			
C11	20.9	22.085	21.044	**C12**	19.7	19.623	19.623
C13	19.6	18.825	38.285	**C14**	20.3	19.512	39.448
C15	17.5	17.065	17.167	**C16**	14.7	14.151	13.393
C17	12.3	12.658	12.876	**C18**	10.3	11.539	23.256
C19	9.8	9.830	8.701				

2.2.2 NGC 1326A

The data for NGC 1326A is collected in Table 2.3. NGC 1326A is the third galaxy in the Fornax Cluster region that was studied in the Key Project series (The first two are NGC 1365 and NGC 1425). This galaxy is classified as type SBmpec by de Vaucouleurs et al. (1991). It lies about 2.5 arcmin away from another galaxy (NGC 1326B) and may be interacting with that system (Prosser et al. 1999). A total of 17 Cepheids were selected for observation in this galaxy. The sample size is smaller than most of the other galaxies in the Key Project due to the fact that NGC 1326A is one of the most distant galaxies and has relatively low luminosity. In Figure 2.4 the published $P-L$ relations is shown. The two recovered $P-L$ relations for DCDFT and ANOVA are shown in Figure 2.5 and Figure 2.6.

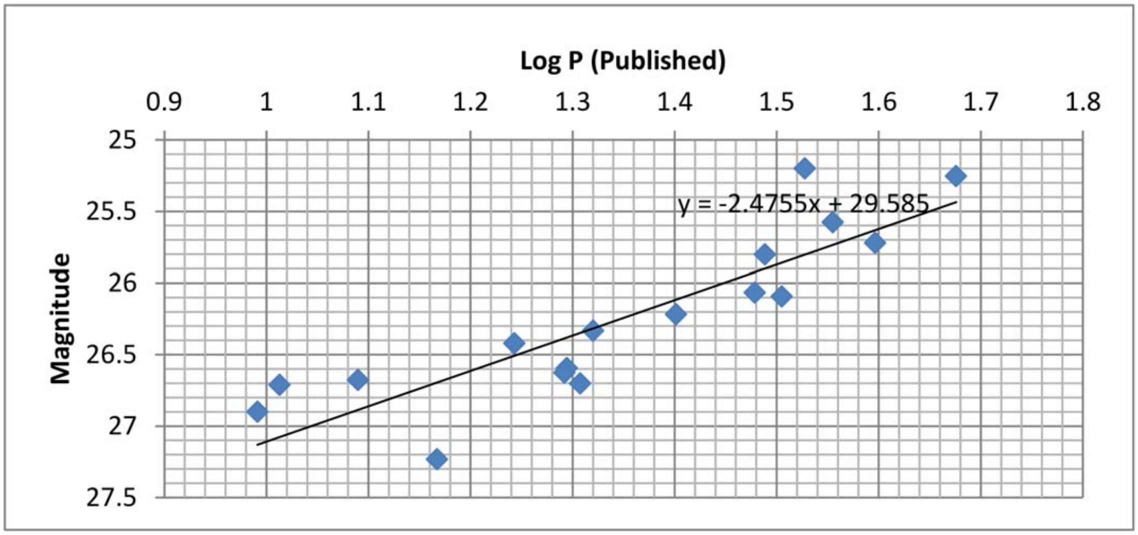

Figure 2.4 The Published $P-L$ Plot and Linear Fit for NGC 1326A.

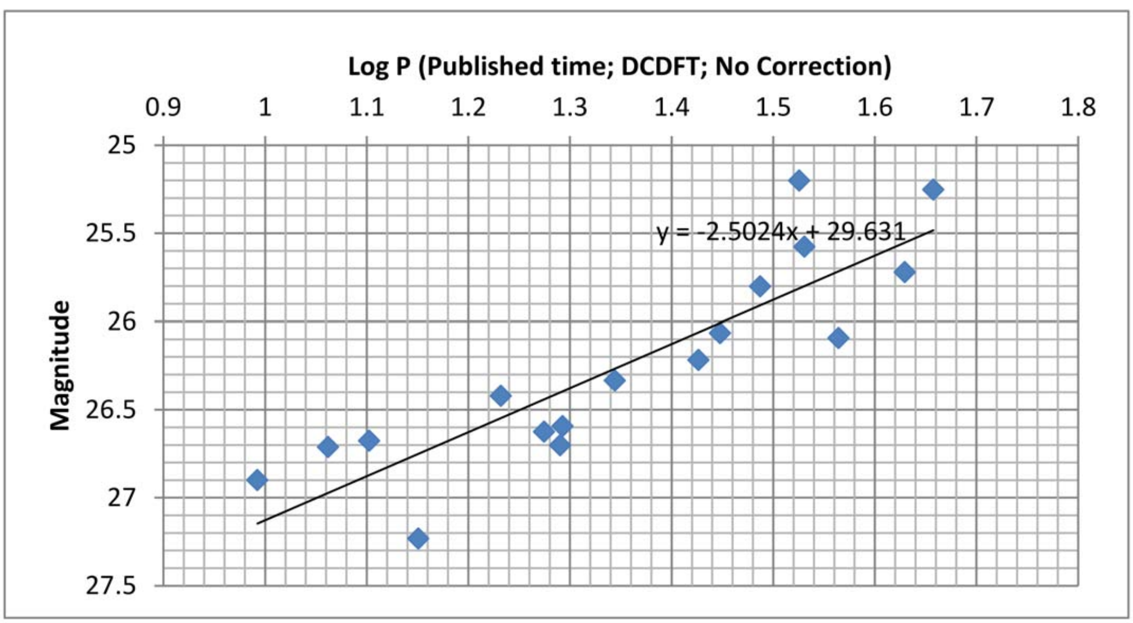

Figure 2.5 The $P-L$ Plot from DCDFT Period Recovery and the Linear Fit for NGC 1326A.

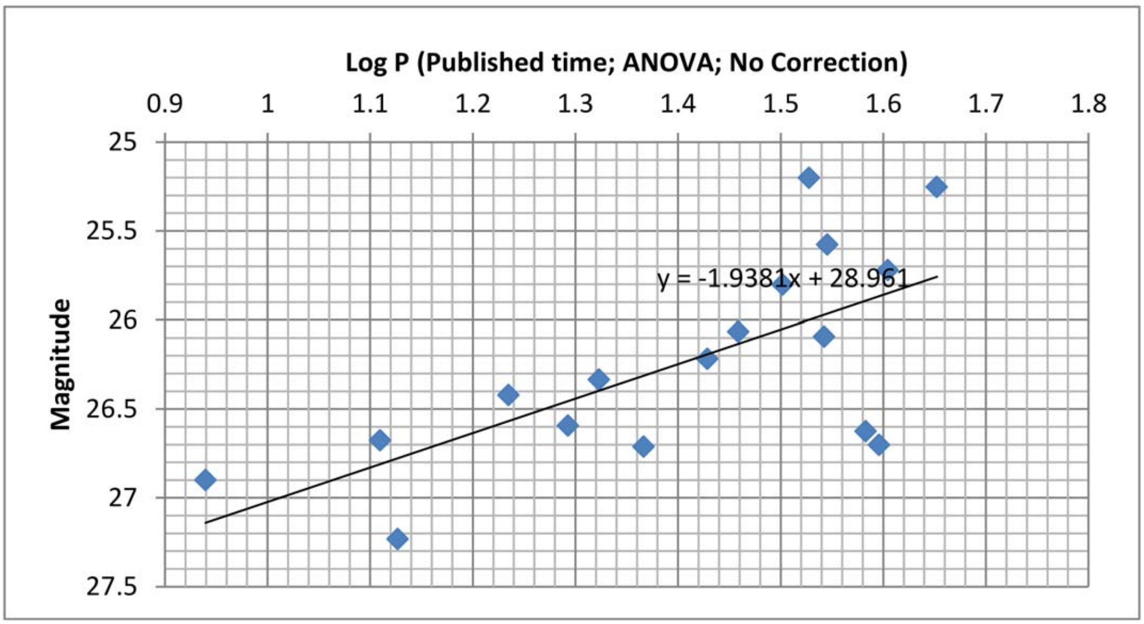

Figure 2.6 The $P-L$ Plot from ANOVA Period Recovery and the Linear Fit for NGC 1326A.

2.2.3 NGC 1365

NGC 1365 is a large, symmetric, barred spiral galaxy, sometimes called the *Great Barred Spiral*. The galaxy lies about 56 million light-years away in the direction of the Fornax constellation. It is classified as an SBb(s)I galaxy by Sandage & Tammann (1981) and as an SBs(b) galaxy by de Vaucouleurs et al. (de Vaucouleurs et al. 1991). It has been suggested that NGC 1365 contains a hidden Seyfert 1 nucleus (Veron et al. 1980). A total of 52 Cepheids were selected for observation in this galaxy as collected in Table 2.4. The various $P-L$ relations are showing in Figure 2.7, Figure 2.8, and Figure 2.9.

Table 2.4. Recovery of Cepheid Periods in NGC 1365

Cepheid	Published (days)	DCDFT (days)	ANOVA (days)	Cepheid	Published (days)	DCDFT (days)	ANOVA (days)
C1	60	187.266	67.039	**C2**	60	124.948	61.013
C3	55	355.282	54.478	**C4**	55	47.569	43.021
C5	53	47.170	42.776	**C6**	47	47.619	44.444
C7	44.2	40.230	41.543	**C8**	42.5	42.169	42.945
C9	41.5	39.106	39.326	**C10**	41.4	49.470	43.344
C11	41	41.791	43.210	**C12**	39.2	41.257	42.169
C13	38	37.824	38.126	**C14**	37.6	30.077	61.838
C15	35.2	33.333	33.926	**C16**	35.1	33.450	33.568
C17	35	36.383	36.803	**C18**	34.6	36.244	36.244
C19	34.5	35.971	36.383	**C20**	34.4	33.102	34.169
C21	34	34.665	34.047	**C22**	34	35.971	37.089
C23	34	31.362	30.756	**C24**	33.6	33.520	32.787
C25	33.1	30.000	31.915	**C26**	32.5	33.708	32.086
C27	31.3	30.000	26.316	**C28**	30.3	26.786	54.546
C29	29.8	28.169	28.302	**C30**	29.6	29.268	28.846
C31	29	27.778	27.907	**C32**	28.9	28.994	27.330
C33	28	30.479	9.694	**C34**	28	27.174	28.818
C35	27.5	27.330	28.305	**C36**	26.6	24.900	8.782
C37	26.5	26.717	41.684	**C38**	26.5	24.771	50.000
C39	26.1	25.031	24.143	**C40**	25	24.900	50.000
C41	23.5	20.773	19.577	**C42**	22.9	24.900	22.331
C43	21	21.331	19.030	**C44**	21	19.739	19.339

Table 2.4 (cont'd)

Cepheid	Published (days)	DCDFT (days)	ANOVA (days)	Cepheid	Published (days)	DCDFT (days)	ANOVA (days)
C45	20.3	19.183	19.339	**C46**	20.1	20.956	43.197
C47	20	19.339	20.417	**C48**	18.8	18.149	17.590
C49	18	17.483	35.088	**C50**	16.3	16.103	17.921
C51	16.2	17.491	6.458	**C52**	14.2	13.578	15.004

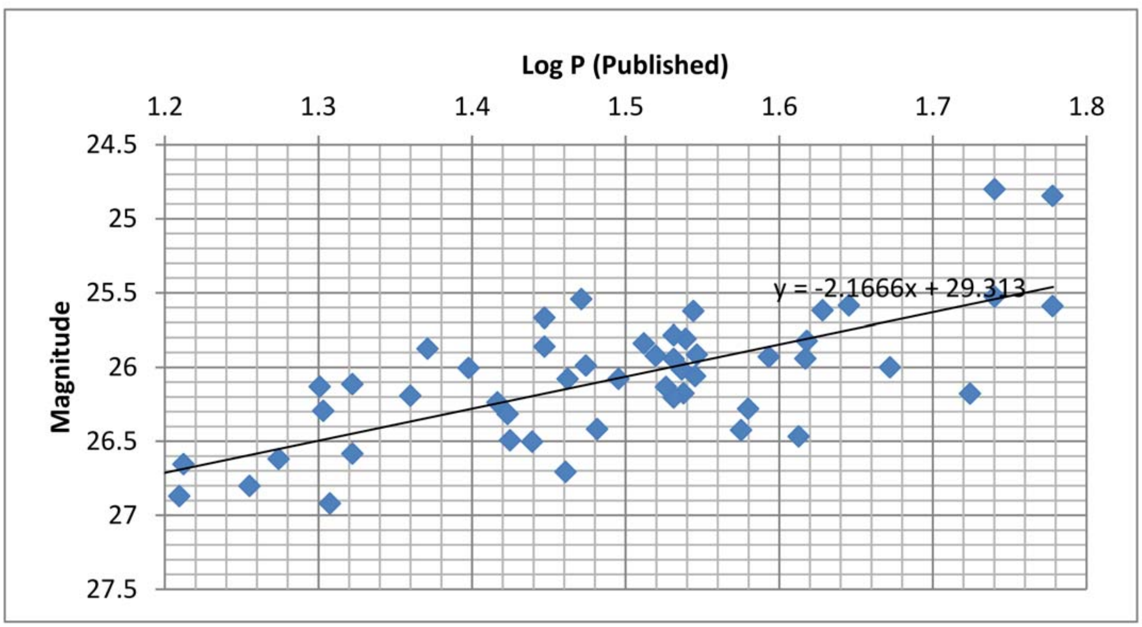

Figure 2.7 The Published $P-L$ Plot and Linear Fit for NGC 1365.

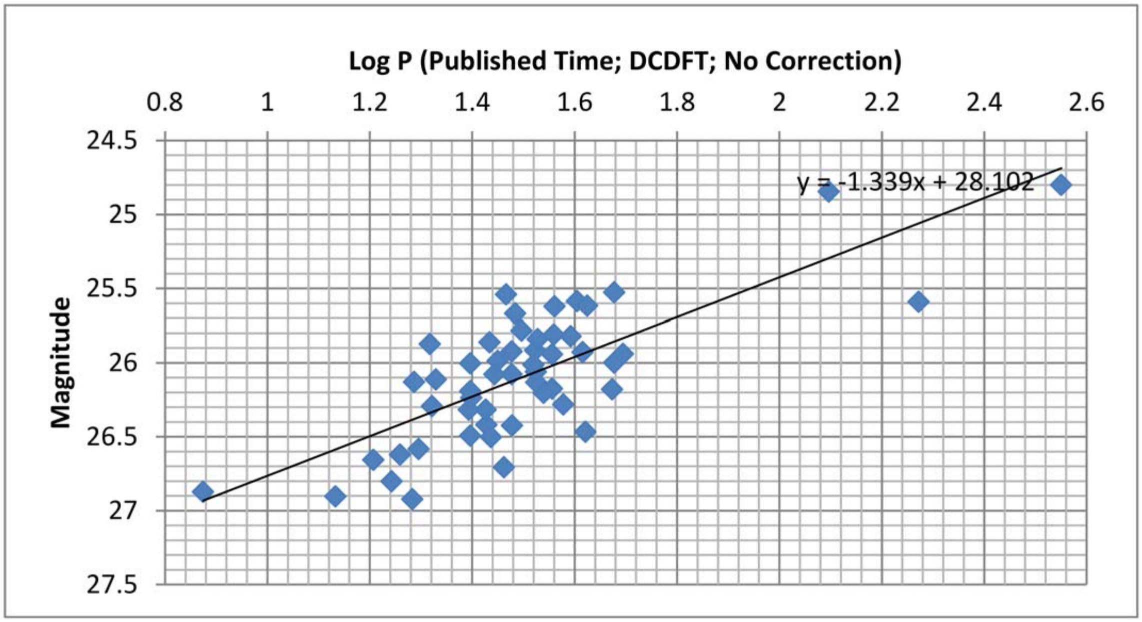

Figure 2.8 The $P-L$ Plot from DCDFT Period Recovery and the Linear Fit for NGC 1365.

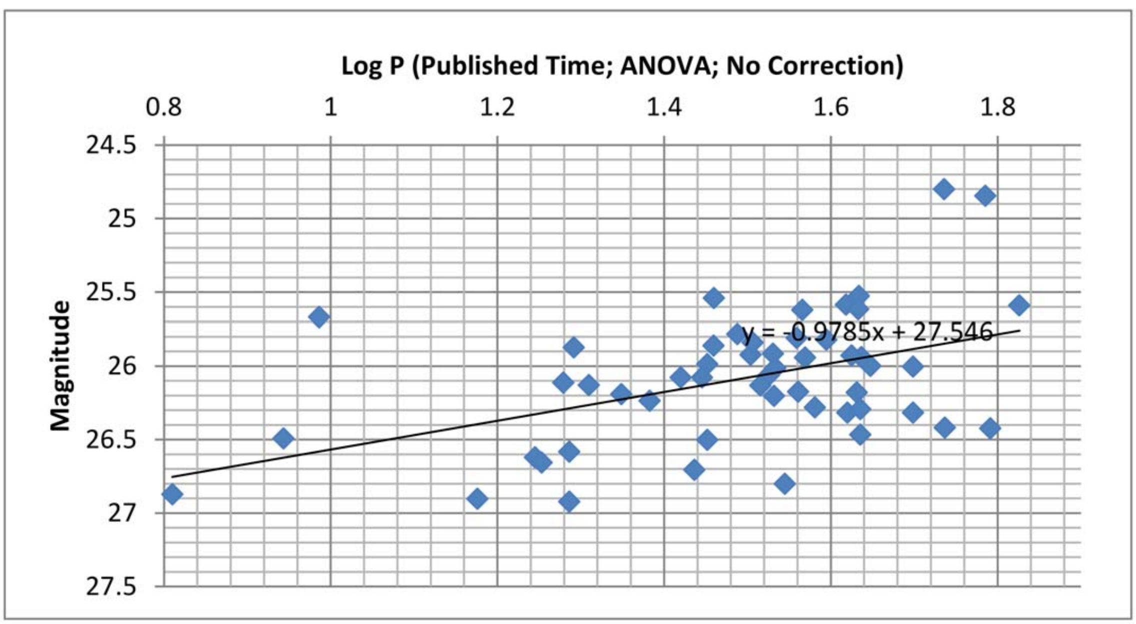

Figure 2.9 The $P-L$ Plot from ANOVA Period Recovery and the Linear Fit for NGC 1365.

2.2.4 NGC 2090

The galaxy NGC 2090 is an Sc II galaxy as defined by Sandage & Bedke (1985). The selection of NGC 2090 was based on the low surface brightness of those parts of the galactic disk that are threaded by spiral arms and on the fact that the spiral arms appeared sparse enough to be resolved into stars with crowding no greater than that observed in M33 and M101 from the ground (Phelps et al. 1998). The 34 Cepheids used for this galaxy can be found in Table 2.5. The $P-L$ relations are given in Figure 2.10, Figure 2.11, and Figure 2.12.

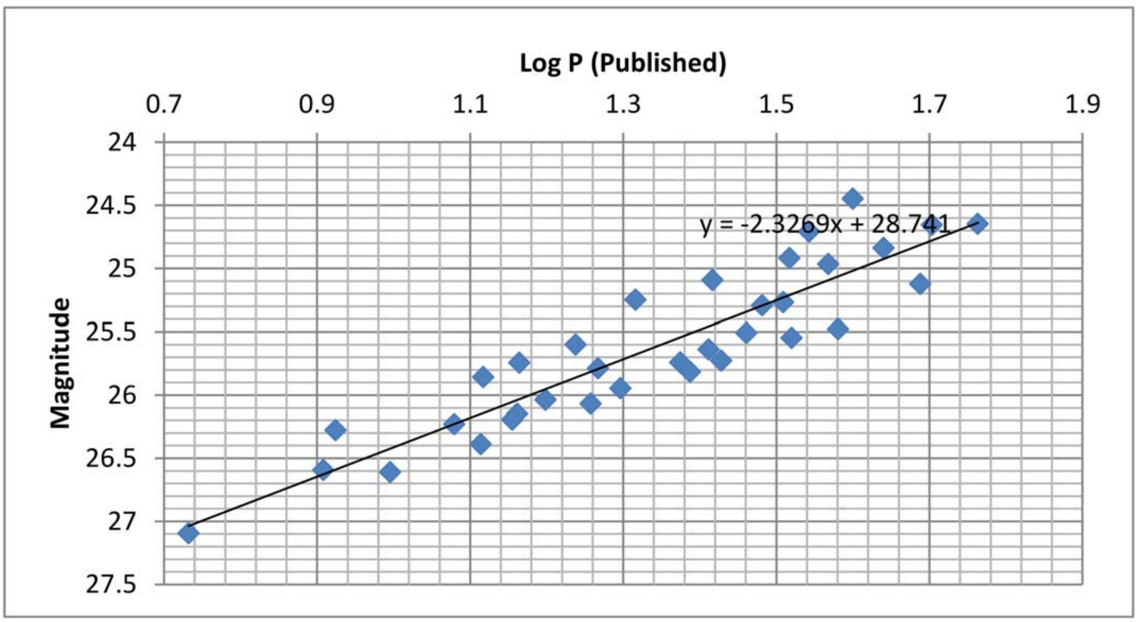

Figure 2.10 The Published $P-L$ Plot and Linear Fit for NGC 2090.

Table 2.5. Recovery of Cepheid Periods in NGC 2090

Cepheid	Published (days)	DCDFT (days)	ANOVA (days)	Cepheid	Published (days)	DCDFT (days)	ANOVA (days)
C1	58	85.6164	59.2417	**C2**	50.5	54.113	51.867
C3	48.8	62.7615	48.913	**C4**	43.7	42.878	42.735
C5	39.8	47.8469	46.2963	**C6**	38.1	35.180	34.965
C7	37	36.5297	36.7647	**C8**	34.9	34.130	34.130
C9	33.1	30.326	28.2287	**C10**	32.9	33.727	30.817
C11	32.3	31.6706	29.8507	**C12**	30.3	28.653	31.323
C13	28.9	27.3224	28.1558	**C14**	26.8	27.322	26.846
C15	26.1	27.9851	26.3852	**C16**	25.8	24.824	25.940
C17	24.4	22.9709	23.678	**C18**	23.7	8.470	8.929
C19	20.7	20.7972	20.5198	**C20**	19.8	19.763	19.623
C21	18.S	18.4502	18.4502	**C22**	18.1	18.825	18.825
C23	17.3	17.4095	16.7785	**C24**	15.8	17.194	15.913
C25	14.6	14.5773	14.6542	**C26**	14.5	15.051	14.810
C27	14.3	13.7137	13.1926	**C28**	13.1	12.887	12.652
C29	13	12.5376	11.7925	**C30**	12	11.793	22.124
C31	9.9	9.8555	4.7893	**C32**	8.4	8.661	8.456
C33	8.1	8.1345	8.1345	**C34**	5.4	5.338	10.638

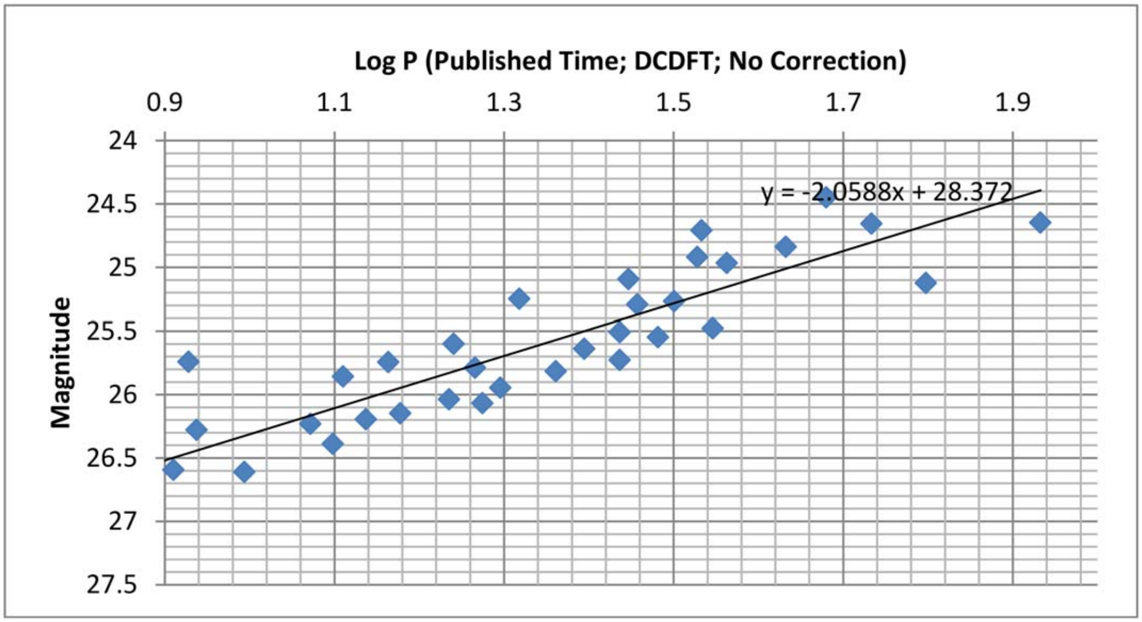

Figure 2.11 The $P-L$ Plot from DCDFT Period Recovery and the Linear Fit for NGC 2090.

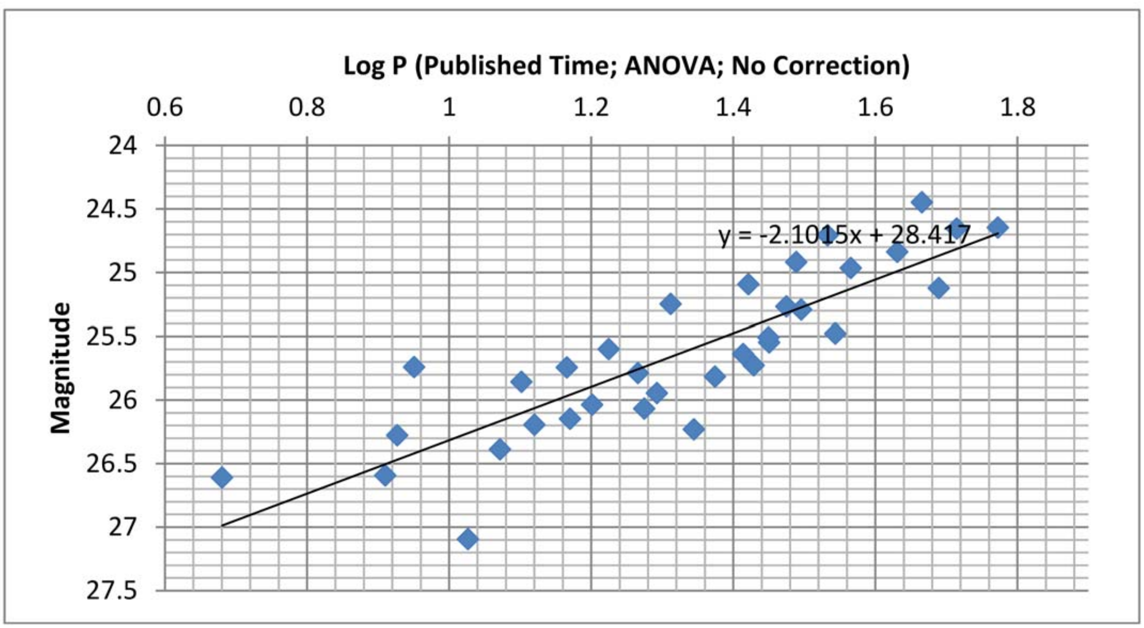

Figure 2.12 The $P-L$ Plot from ANOVA Period Recovery and the Linear Fit for NGC 2090.

2.2.5 NGC 2541

NGC 2541 is located about 40 million light-years away in a group with NGC 2500, NGC 2537, and NGC 2552. It is a SBc D galaxy (Pustilnik & Tepliakova 2011) and belongs to the NGC 2841 group (de Vaucouleurs 1978), which is located near the border of Ursa Major and Lynx. It was selected as part of the Key Project because of its potential as a Tully-Fisher calibrator. It was also considered to be a relatively easy target for the detection and measurement of Cepheid variables using HST (Ferrarese et al. 1998). A total of 34 Cepheids were used for this galaxy and are gathered in Table 2.6. The reconstructed $P-L$ relations are given in Figure 2.13, Figure 2.14, and Figure 2.15.

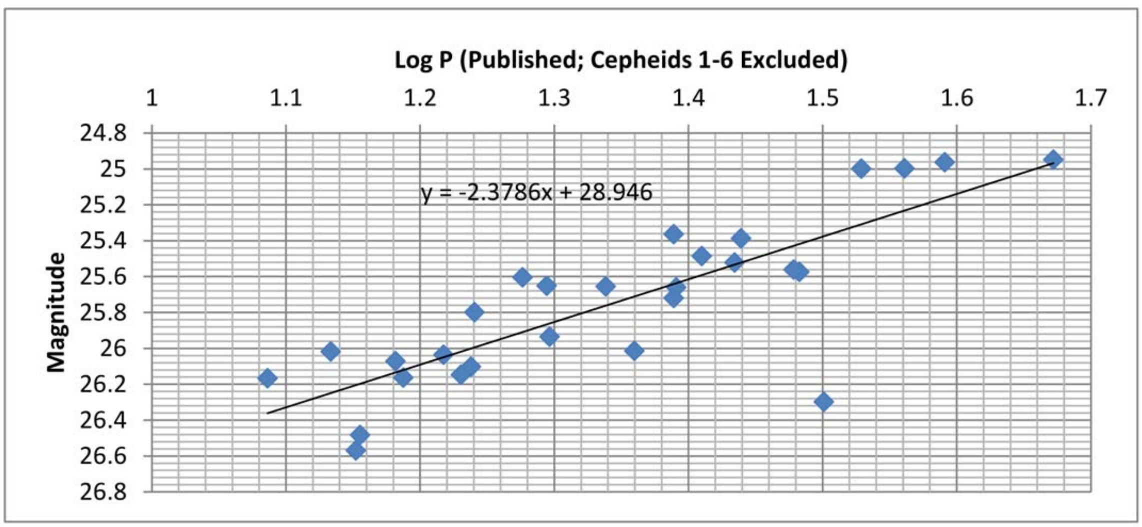

Figure 2.13 The Published $P-L$ Plot and Linear Fit for NGC 2541.

Table 2.6. Recovery of Cepheid Periods in NGC 2541

Cepheid	Published (days)	DCDFT (days)	ANOVA (days)	Cepheid	Published (days)	DCDFT (days)	ANOVA (days)
C1	>65	57.219	55.147	**C2**	>55	55.4S3	59.773
C3	>52	45.809	46.168	**C4**	>51	39.S47	51.116
C5	>50	60.181	51.414	**C6**	>43; <60	51.S46	75.901
C7	47	50.188	47.337	**C8**	39	38.462	35.088
C9	36.4	35.714	32.609	**C10**	33.8	33.520	33.708
C11	31.7	31.579	55.556	**C12**	30.4	32.967	29.851
C13	30.1	31.579	30.151	**C14**	27.5	25.317	27.149
C15	27.2	32.787	30.612	**C16**	25.7	23.904	20.761
C17	24.6	24.S90	24.291	**C18**	24.5	24.691	24.691
C19	24.S	22.901	24.S90	**C20**	22.9	21.429	21.978
C21	21.8	22.305	20.979	**C22**	19.8	18.868	19.782
C23	19.7	19.121	19.646	**C24**	18.9	20.060	18.744
C25	17.4	17.376	18.382	**C26**	17.3	17.376	10.225
C27	17	16.667	17.065	**C28**	16.5	16.0128	16.013
C29	15.4	14.695	14.695	**C30**	15.2	15.924	10.684
C31	14.3	13.708	28.169	**C32**	14.2	14.184	26.110
C33	13.6	12.453	13.450	**C34**	12.2	12.399	26.846

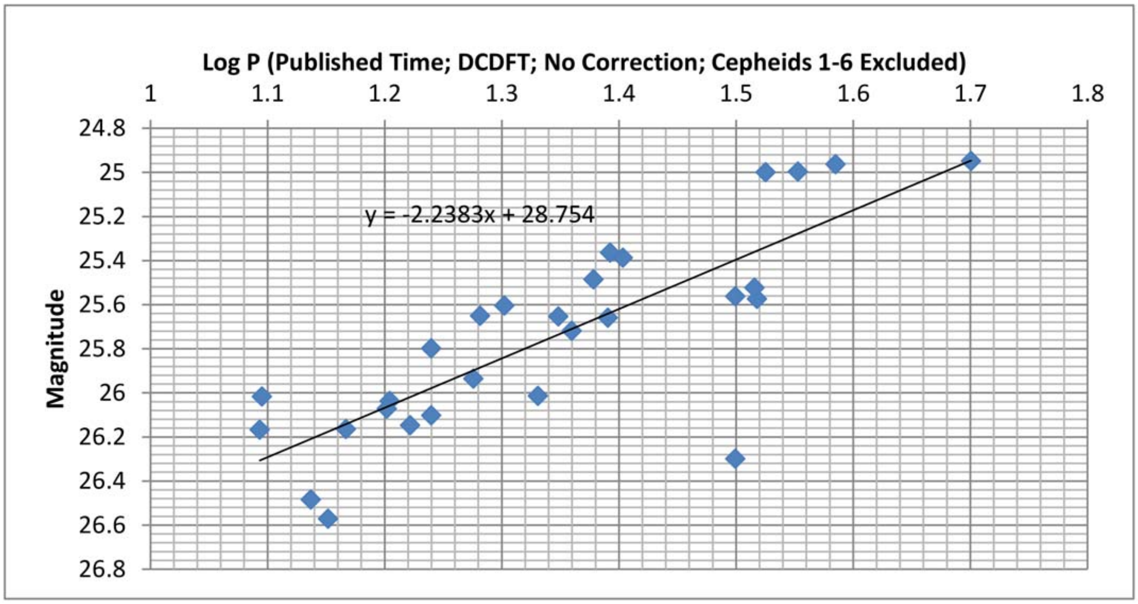

Figure 2.14 The $P-L$ Plot from DCDFT Period Recovery and the Linear Fit for NGC 2541.

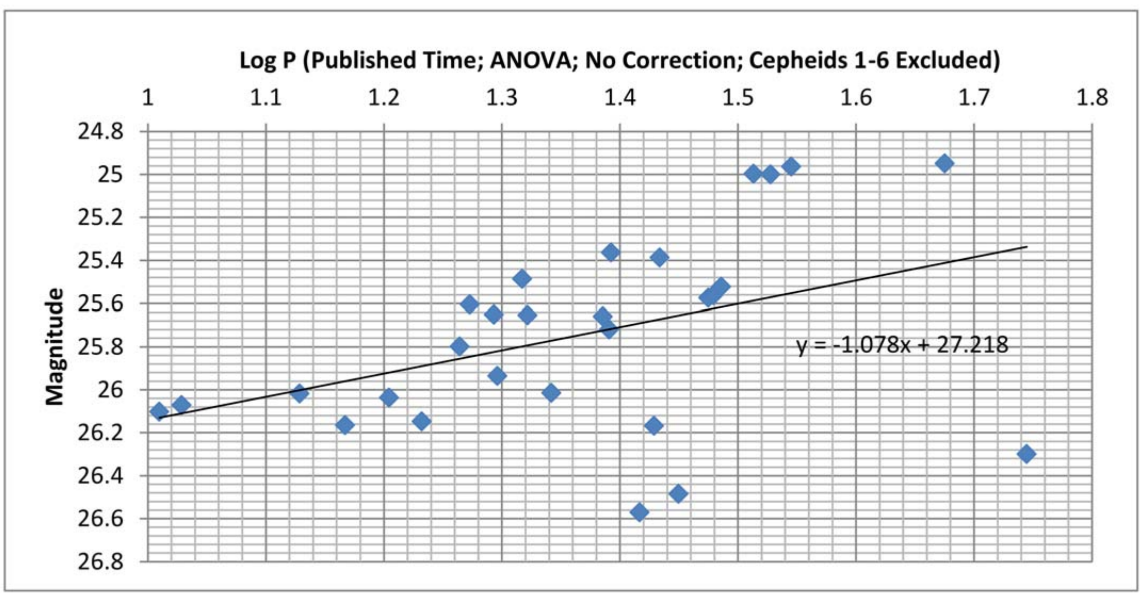

Figure 2.15 The $P-L$ Plot from ANOVA Period Recovery and the Linear Fit for NGC 2541.

2.2.6 NGC 3031

NGC 3031 is much better known by its Messier number M31 and it is sometimes known as Bode's Galaxy. The galaxy is classified as Sb(r)I-II (Sandage & Tammann 1981) and is similar in many respects to the Local Group galaxy M31. The high inclination of its disk and well-defined 21 cm velocity width make this galaxy an important Tully-Fisher calibrator. Its relatively large bulge makes it useful as a calibrator of surface brightness fluctuations and the planetary nebula luminosity function (Freedman et al. 1994b). A total of 31 Cepheids were recovered from this galaxy and have been listed in Table 2.7. The relations generated are shown in Figure 2.16, Figure 2.17, and Figure 2.18.

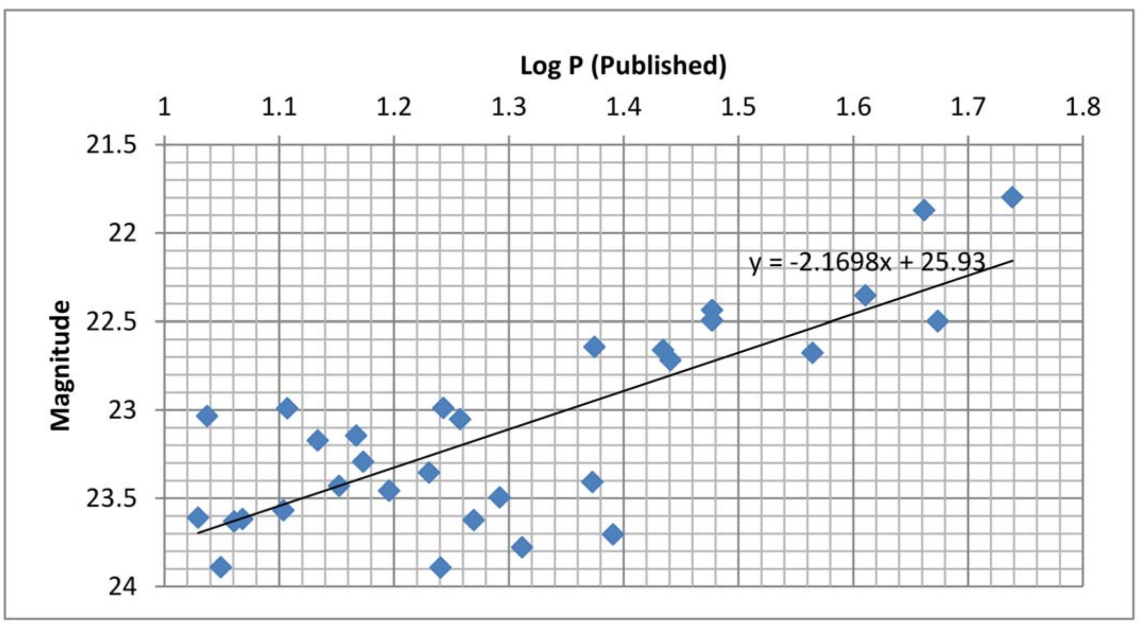

Figure 2.16 The Published $P-L$ Plot and Linear Fit for NGC 3031.

Table 2.7. Recovery of Cepheid Periods in NGC 3031

Cepheid	Published (days)	DCDFT (days)	ANOVA (days)	Cepheid	Published (days)	DCDFT (days)	ANOVA (days)
C1	20.5	20.4918	20.6441	**C2**	19.6	20.9556	39.3701
C3	17.5	16.6778	16.6778	**C4**	15.7	15.0512	31.3676
C5	10.7	10.3591	10.3591	**C6**	40.8	40.6977	40.9836
C7	27.2	27.0856	27.0856	**C8**	24.6	23.2342	6.0577
C9	14.7	15.2999	14.7319	**C10**	12.8	12.8271	12.8271
C11	47.2	63.2911	47.1698	**C12**	23.7	22.3015	22.3015
C13	18.6	16.8805	16.8805	**C14**	12.7	12.7097	25.355
C15	11.2	11.2208	11.2208	**C16**	10.9	4.0995	4.1402
C17	45.9	10.3734	10.6577	**C18**	36.7	40.1376	65.2985
C19	23.6	21.1149	19.9045	**C20**	17	17.4095	31.3676
C21	14.2	14.2045	14.8104	**C22**	13.6	5.9284	11.4521
C23	11.7	11.6442	12.0482	**C24**	11.S	11.8934	11.4995
C25	17.4	17.301	15.8228	**C26**	54.8	42.1348	54.878
C27	30	27.9018	27.9018	**C28**	27.6	30.012	29.6912
C29	30	30.012	27.9018	**C30**	18.1	17.1939	17.1939
C31	14.9	15.5569	14.8898				

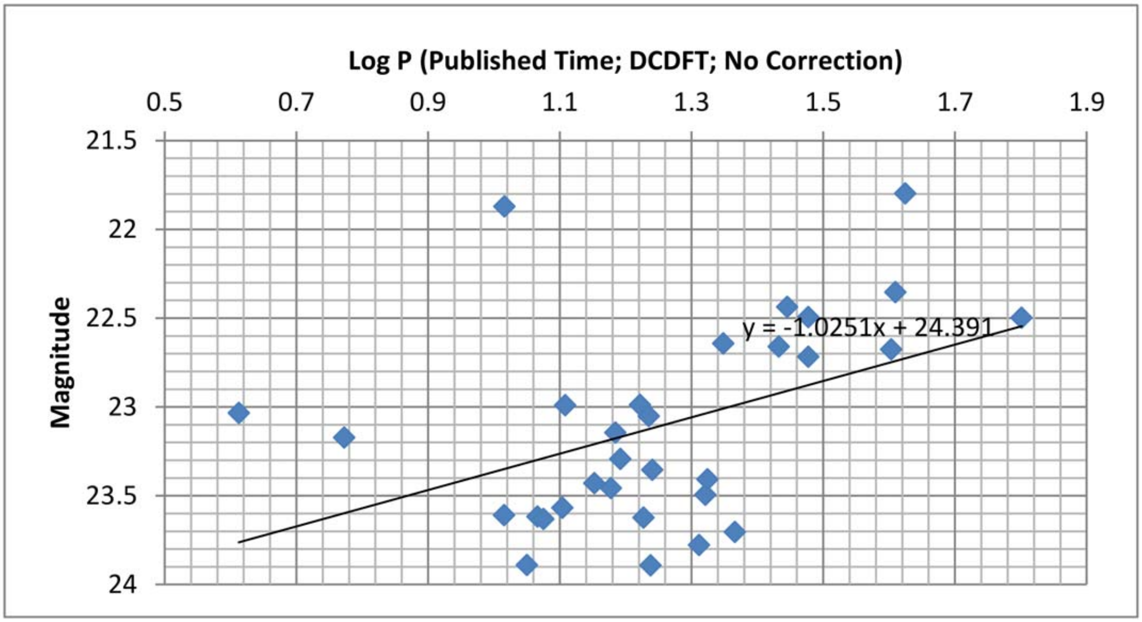

Figure 2.17 The $P-L$ Plot from DCDFT Period Recovery and the Linear Fit for NGC 3031.

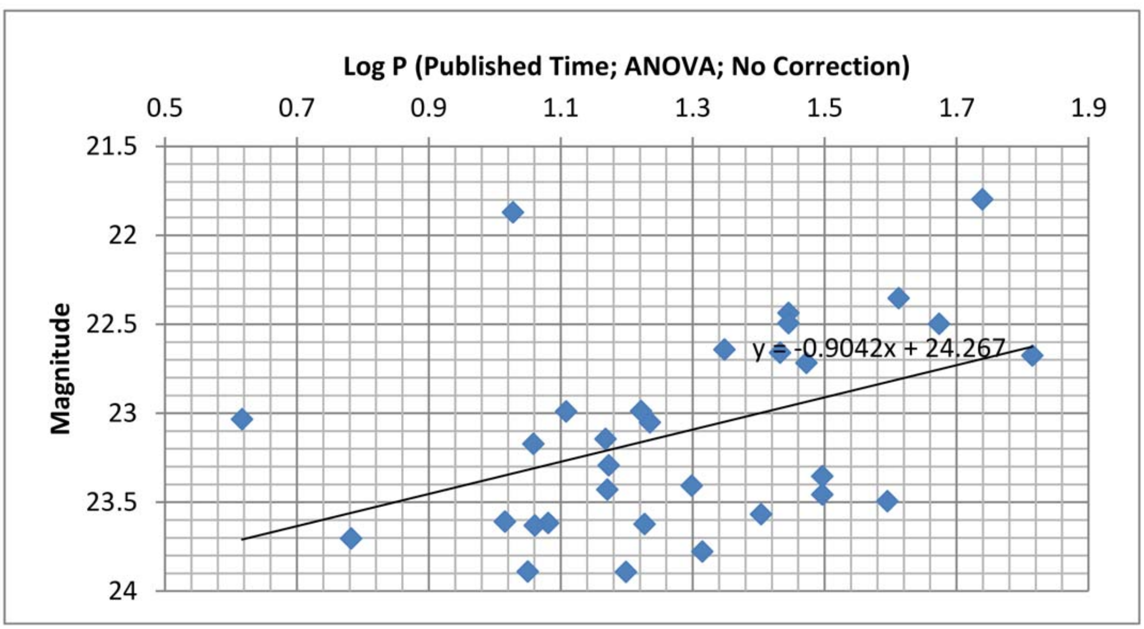

Figure 2.18 The $P-L$ Plot from ANOVA Period Recovery and the Linear Fit for NGC 3031.

2.2.7 NGC 3198

Although bright (B_T = 10.94 mag), and relatively nearby, NGC 3198 is not as well known as many other galaxies in this study. It is classified as a Sc(s)I-II galaxy (Sandage & Tammann 1981). However, de Vaucouleurs considered it a barred spiral, SB(rs)c (de Vaucouleurs et al. 1991). This galaxy was selected for inclusion in the Key Project primarily as a calibrator of the Tully-Fisher relation (Kelson et al. 1999). The galaxy contains 29 Cepheids as part of the Key Project which are shown in Table 2.8. The relations generated are shown in Figure 2.19, Figure 2.20, and Figure 2.21.

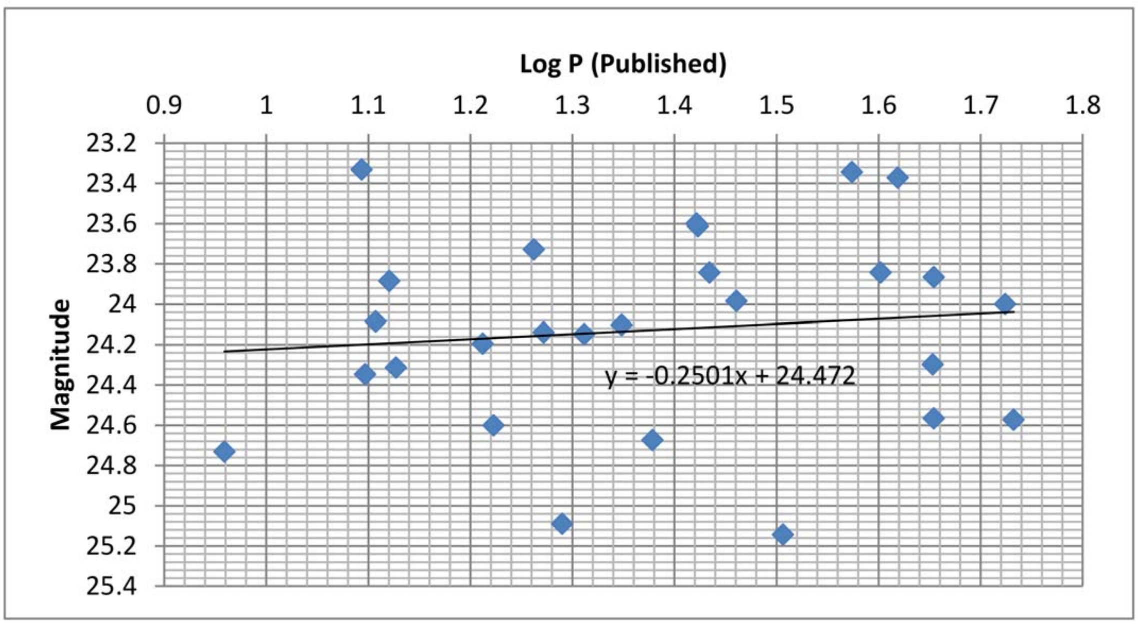

Figure 2.19 The Published $P-L$ Plot and Linear Fit for NGC 3198.

Table 2.8. Recovery of Cepheid Periods in NGC 3198

Cepheid	Published (days)	DCDFT (days)	ANOVA (days)	Cepheid	Published (days)	DCDFT (days)	ANOVA (days)
C1	40	58.7248	57.5658	**C2**	26.5	18.0897	36.2845
C3	26.4	14.7319	5.8411	**C4**	18.3	14.3266	14.3266
C5	37.5	46.875	47.2441	**C6**	18.7	10.2987	10.2987
C7	13.2	5.172	5.277	**C8**	41.6	41.3793	41.0959
C9	28.9	37.7644	38.2848	**C10**	45.1	37.73S8	37.500
C11	12.4	6.0478	11.5942	**C12**	27.2	33.6474	33.6474
C13	12.8	31.5956	31.5956	**C14**	>55	24.6063	38.7297
C15	13.4	19.7824	23.1481	**C16**	45	22.3048	22.2222
C17	16.3	16.38	7.3368	**C18**	20.5	12.8866	25.8264
C19	16.7	29.9401	9.2039	**C20**	12.5	5.4481	5.4481
C21	22.3	33.2447	33.244	**C22**	23.9	26.31S8	27.352
C23	53	25.8065	25.9067	**C24**	19.5	23.3372	8.107
C25	9.1	19.0355	9.2822	**C26**	45.1	17.7384	22.1607
C27	54	17.3913	5.6457	**C28**	>50	21.1745	42.2773
C29	32.1	11.9284	13.1291				

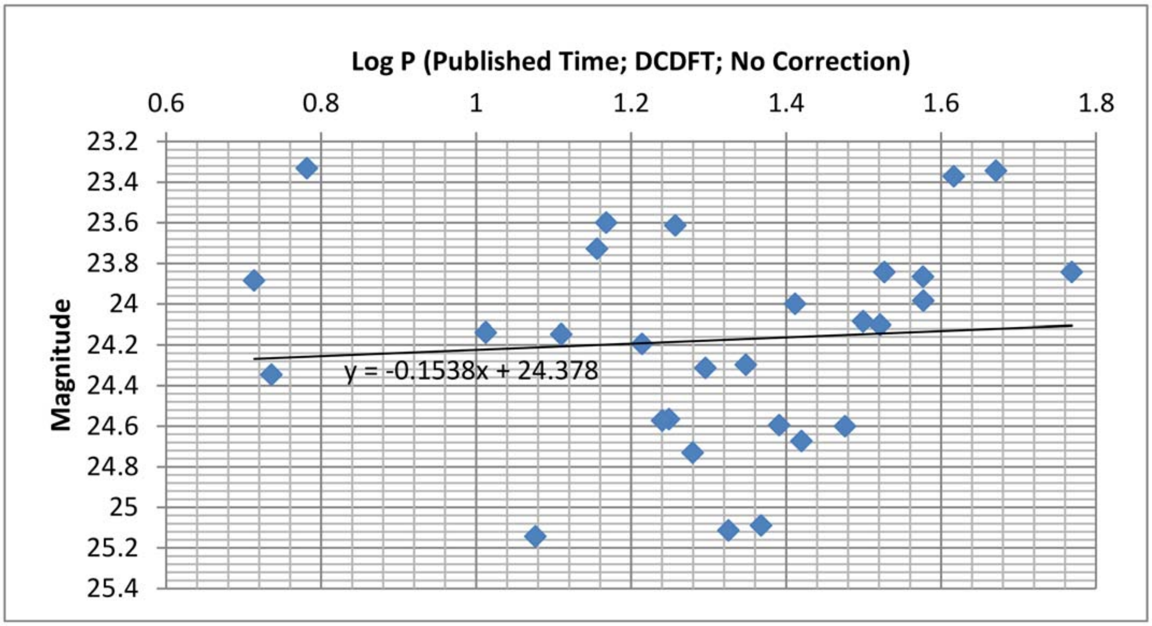

Figure 2.20 The $P-L$ Plot from DCDFT Period Recovery and the Linear Fit for NGC 3198.

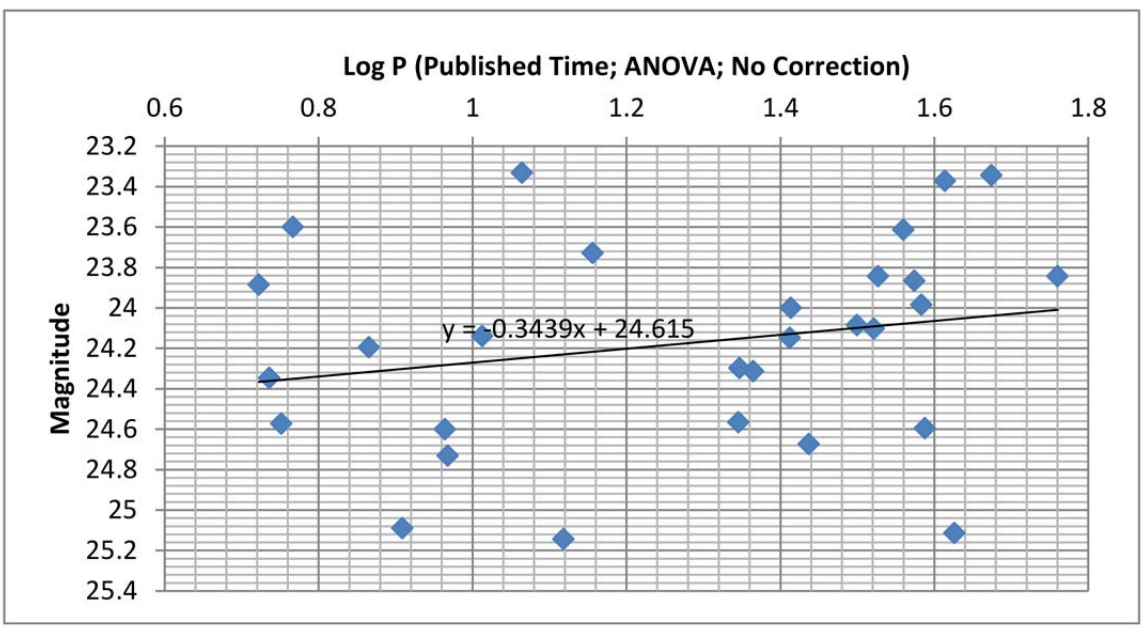

Figure 2.21 The $P-L$ Plot from ANOVA Period Recovery and the Linear Fit for NGC 3198.

2.2.8 NGC 3319

The barred spiral NGC 3319 was first examined by William Herschel in 1788. It is the last galaxy observed for the Key Project. It is an SB(rs)cd galaxy with a prominent bar (de Vaucouleurs et al. 1991). It shows no sign of interaction and is a fairly isolated galaxy. It was included in the Key Project primarily as a Tully-Fisher calibrator (Sakai et al. 1999). The 33 Cepheids selected by the Key Project and covered by this study are given in Table 2.9. The relations generated are shown in Figure 2.22, Figure 2.23, and Figure 2.24.

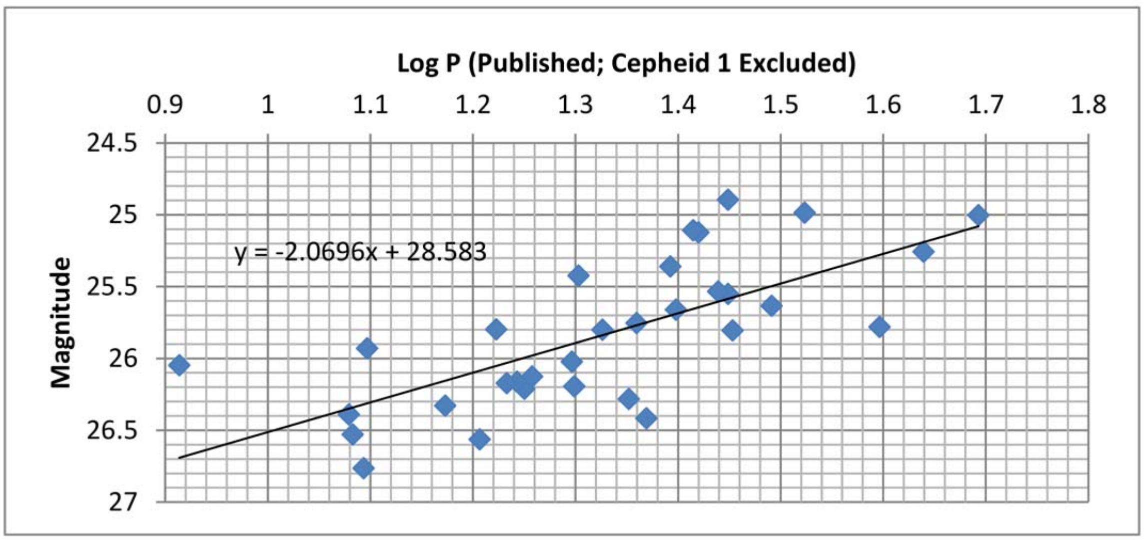

Figure 2.22 The Published $P-L$ Plot and Linear Fit for NGC 3319.

Table 2.9. Recovery of Cepheid Periods in NGC 3319

Cepheid	Published (days)	DCDFT (days)	ANOVA (days)	Cepheid	Published (days)	DCDFT (days)	ANOVA (days)
C1	>47	48.8281	50.2008	**C2**	49.3	68.8073	45.9418
C3	43.6	84.666	23.3827	**C4**	39.5	37.4883	38.2409
C5	33.4	41.8848	31.8471	**C6**	31	29.5421	30.9837
C7	28.4	25.974	25.5319	**C8**	28.1	30.6122	30.6122
C9	28.1	27.3973	27.2727	**C10**	27.5	25.5319	26.4317
C11	26.3	26.3158	28.436	**C12**	26	27.907	26.3158
C13	25	25.4237	21.6606	**C14**	24.7	23.1481	24.0385
C15	23.4	20.7469	18.5185	**C16**	22.9	20.9205	22.2222
C17	22.5	23.0415	24.8756	**C18**	21.2	12.6904	24.1546
C19	20.1	20	19.9203	**C20**	19.9	20.2703	17.5439
C21	19.8	19.8675	19.2308	**C22**	18.1	17.341	8.1522
C23	17.8	17.8571	17.8571	**C24**	17.5	15.9574	16.6667
C25	17.1	16.7598	17.2414	**C26**	16.7	16.7598	17.6471
C27	16.1	14.218	27.7778	**C28**	14.9	16.9492	17.4419
C29	12.5	12.0482	12.5	**C30**	12.4	12.1951	12.605
C31	12.1	12.987	12.2951	**C32**	12	11.583	6.9767
C33	8.2	8.0128	8.1235				

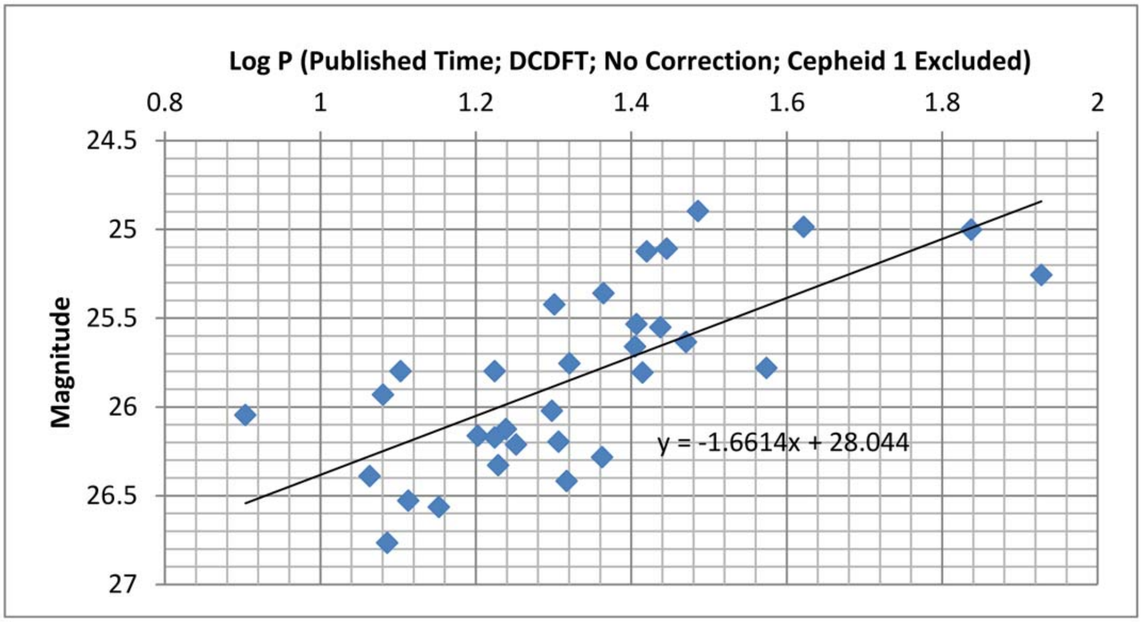

Figure 2.23 The $P-L$ Plot from DCDFT Period Recovery and the Linear Fit for NGC 3319.

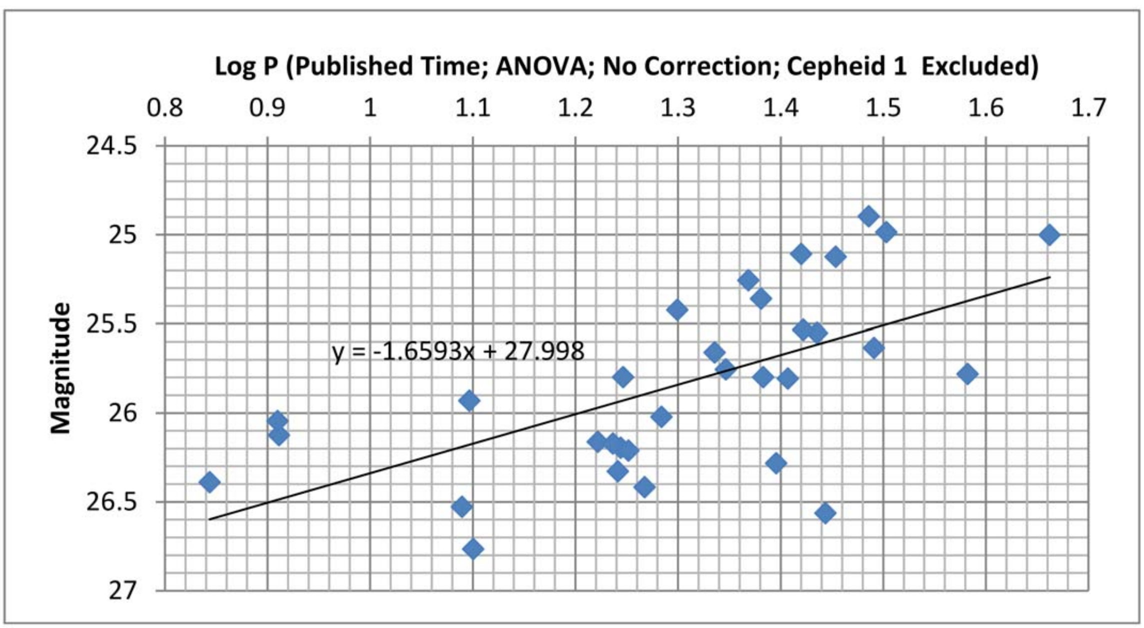

Figure 2.24 The $P-L$ Plot from ANOVA Period Recovery and the Linear Fit for NGC 3319.

2.2.9 NGC 3351

NGC 3351 is another famous galaxy known better by its Messier number. It was first seen by Mechain in 1781 and was included in Messier's list as M95. It is a bright nearby example of a barred spiral galaxy. It is classified as SBb(r) II with magnitude B_T = 10.52 mag by Sandage & Tammann (1981) and as SB(r)b by de Vaucouleurs (1975). Ground-based images have shown that this galaxy has a bright nucleus, broad bar, and two major arms made up of stellar knots interlaced with a complex web of absorbing dust lanes (Graham et al. 1997). It also contains a circum-nuclear structure which is related to a twin-peaked CO distribution (Rubin et al. 1975)(Kenney et al. 1992). While the galaxy has considerable interest in its own right as an evolving stellar system, from the viewpoint of the Key Project, its most significant characteristic is its membership of the Leo I group which includes several other bright galaxies with morphological types ranging from elliptical (NGC 3377, NGC 3379) and lenticular (NGC 3384) to late-type spiral and Magellanic irregular types (Graham et al. 1997). It is one of the earliest spiral types included in the Key Project. Given its relative close distance of 38 million light-years a total of 49 Cepheids have been studied for this galaxy as shown in selected for observation Table 2.10. The relations generated are shown in Figure 2.25, Figure 2.26, and Figure 2.27.

Table 2.10. Recovery of Cepheid Periods in NGC 3351

Cepheid	Published (days)	DCDFT (days)	ANOVA (days)	Cepheid	Published (days)	DCDFT (days)	ANOVA (days)
C1	43	42.169	42.787	**C2**	41	42.169	40.698
C3	37.9	39.474	39.735	**C4**	36.8	39.735	38.710
C5	35	33.149	33.898	**C6**	34.5	36.145	34.682
C7	34.5	35.928	34.483	**C8**	32	30.000	31.579
C9	32	34.682	10.000	**C10**	27	28.305	9.369
C11	25.7	25.569	9.463	**C12**	24.7	24.771	49.481
C13	24.4	24.390	25.164	**C14**	23.9	26.717	25.297
C15	23.4	22.978	23.430	**C16**	21.6	20.864	11.251
C17	21.4	22.227	21.427	**C18**	20.8	20.864	20.956
C19	19.8	19.646	5.664	**C20**	19.5	19.249	19.249
C21	19	18.382	36.430	**C22**	17.5	16.863	16.194
C23	16.9	16.287	17.376	**C24**	16.1	16.103	16.103
C25	16.1	18.034	18.034	**C26**	16	16.194	16.103
C27	15.8	16.194	8.699	**C28**	15.4	15.163	30.912
C29	15.2	14.327	15.004	**C30**	15.2	13.514	14.695
C31	15.1	15.244	14.925	**C32**	14.4	14.771	14.620
C33	14	14.399	14.620	**C34**	14	14.114	14.045
C35	13.5	13.578	13.708	**C36**	13.4	12.618	12.962
C37	13.4	13.643	27.100	**C38**	13.2	12.903	11.884
C39	12.8	12.453	12.674	**C40**	12.5	12.508	12.085
C41	12.3	12.346	6.329	**C42**	12.3	12.453	25.641
C43	11.8	11.689	11.786	**C44**	11.4	11.186	11.455

Table 2.10 (cont'd)

Cepheid	Published (days)	DCDFT (days)	ANOVA (days)	Cepheid	Published (days)	DCDFT (days)	ANOVA (days)
C45	11.2	11.547	5.598	**C46**	11.2	10.971	11.409
C47	10.6	10.724	10.764	**C48**	10.6	10.684	10.764
C49	10	10.225	20.942				

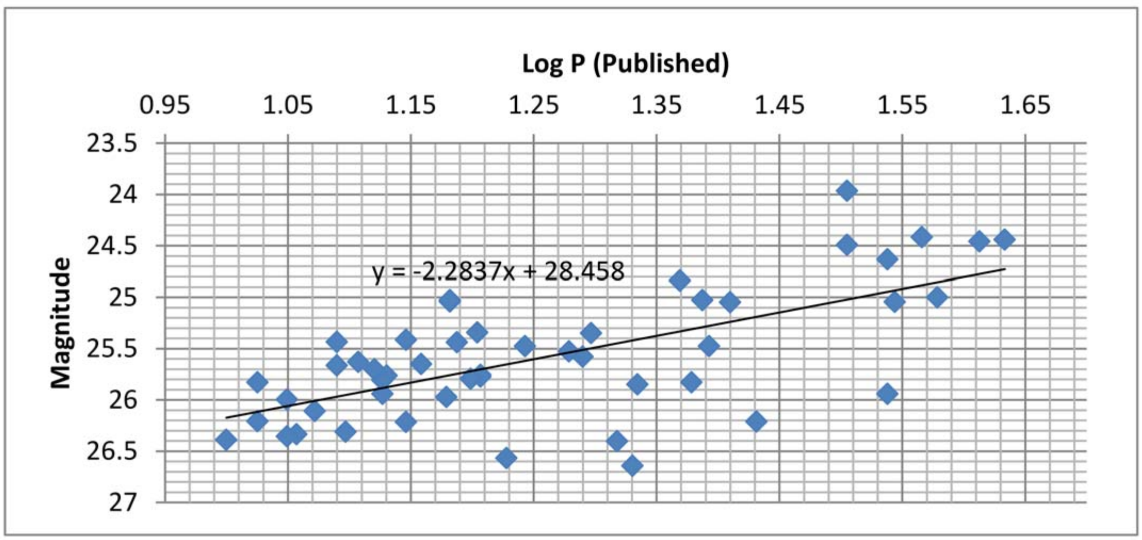

Figure 2.25 The Published $P-L$ Plot and Linear Fit for NGC 3351.

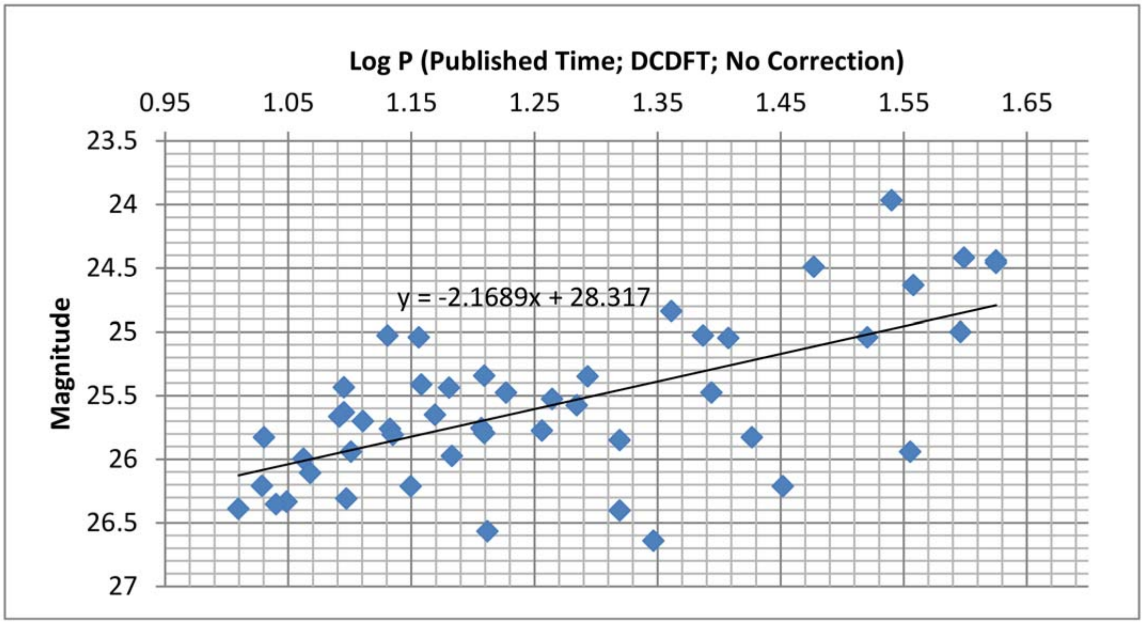

Figure 2.26 The $P-L$ Plot from DCDFT Period Recovery and the Linear Fit for NGC 3351.

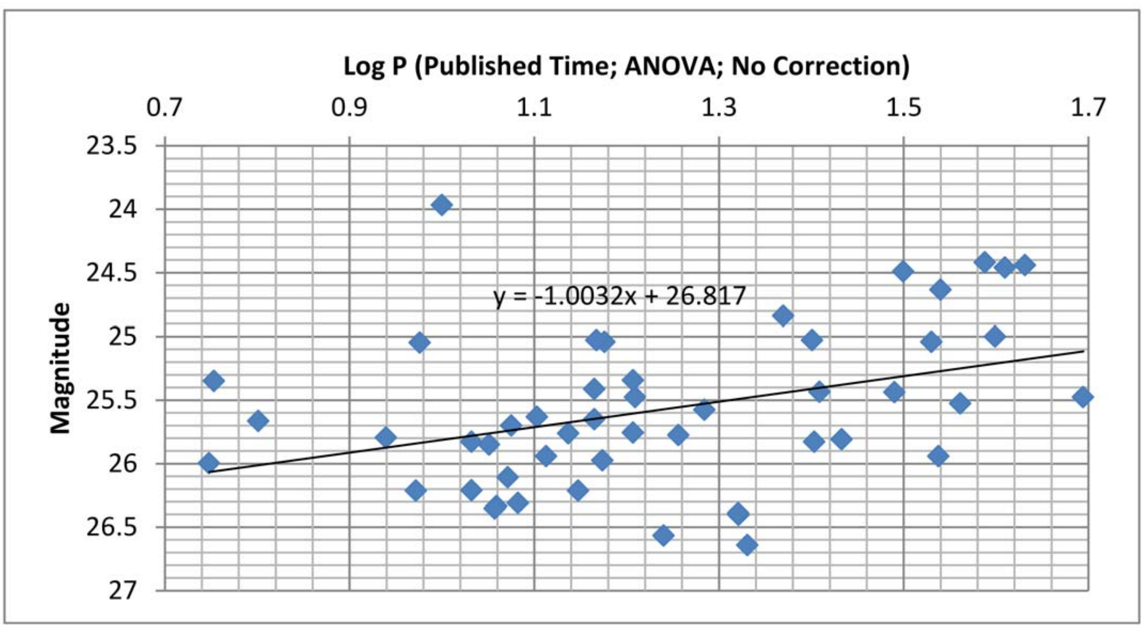

Figure 2.27 The $P-L$ Plot from ANOVA Period Recovery and the Linear Fit for NGC 3351.

2.2.10 NGC 3621

NGC 3612 is a nearby spiral, 22 million light-years, in the constellation of Hydra. It is a relatively isolated spiral with a morphological classification of Sc II.8 (Sandage & Tammann 1981) or Sc III-IV (de Vaucouleurs et al. 1991). Its complex pattern of partially resolved, irregular spiral arms makes it an excellent candidate for the detection of Cepheids. At the same time, its high inclination of 51 degrees makes it an ideal object for the calibration of the Tully-Fisher relation (Rawson et al. 1997). This is a rare galaxy with little evidence of a bulge. The galaxy is also known to have an active nucleus that matches a Seyfert 2 spectrum. The 69 Cepheids studied in this galaxy are given in Table 2.11. The relations generated are shown in Figure 2.28, Figure 2.29, and Figure 2.30.

Table 2.11. Recovery of Cepheid Periods in NGC 3621

Cepheid	Published (days)	DCDFT (days)	ANOVA (days)	Cepheid	Published (days)	DCDFT (days)	ANOVA (days)
C1	60	43.7743	46.4876	**C2**	45.5	43.6047	47.0219
C3	44.7	42.735	41.5512	**C4**	40.9	37.9747	39.1645
C5	40.7	36.1446	38.4615	**C6**	39	37.3134	38.7597
C7	38.3	38.1679	37.6884	**C8**	37.7	63.4518	58.4112
C9	34.5	31.9149	31.3152	**C10**	34	36.6748	33.4076
C11	32.7	47.1698	32.6087	**C12**	32	31.9149	32.8947
C13	31.7	33.1126	34.3249	**C14**	31.5	31.25	31.0559
C15	31.5	32.7511	31.25	**C16**	31.2	31.9149	32.3276
C17	28.3	27.7778	27.9018	**C18**	27.8	27.9018	28.6697
C19	27.7	29.3427	27.533	**C20**	26.4	24.9004	26.7094
C21	26.3	25.1004	25.4065	**C22**	26.2	25.2016	26.3713
C23	25.6	24.8016	49.6032	**C24**	25.4	21.7014	23.4962
C25	25.3	23.2342	23.6742	**C26**	24.7	23.6742	21.7014
C27	24.5	21.5517	23.855	**C28**	24.4	22.242	23.2342
C29	24.4	23.6742	23.855	**C30**	23.8	24.2248	49.2126
C31	23.8	21.7014	22.4014	**C32**	23.5	22.6449	22.482
C33	23.3	24.2248	23.4962	**C34**	23.1	21.9298	22.8102
C35	22.8	22.9779	23.5849	**C36**	22.7	22.242	44.964
C37	22.2	23.4082	23.3209	**C38**	21.5	21.3311	21.4777
C39	21.2	22.3214	21.2585	**C40**	21	21.0438	20.4248
C41	20.7	21.3311	21.5517	**C42**	19.9	20.6612	21.0084
C43	19.9	20.2429	40	**C44**	19.2	16.3934	18.797

Table 2.11 (cont'd)

Cepheid	Published (days)	DCDFT (days)	ANOVA (days)	Cepheid	Published (days)	DCDFT (days)	ANOVA (days)
C45	18.8	17.4216	16.6667	**C46**	18.7	18.8679	10.101
C47	18.5	19.3798	21.5517	**C48**	18.4	18.1818	18.1159
C49	18.2	17.7305	17.3611	**C50**	18	17.5439	34.7222
C51	17.8	17.5439	17.4216	**C52**	17.8	17.0648	17.0068
C53	17.5	17.301	16.5017	**C54**	17.4	17.7305	35.461
C55	17	16.3399	16.3934	**C56**	16.5	16.3934	16.6113
C57	16.3	15.0602	16.340	**C58**	16.2	16.835	16.4474
C59	16.2	16.0772	32.8947	**C60**	14.8	14.7783	14.9254
C61	13.9	14.1509	8.3102	**C62**	13.8	13.3929	13.4529
C63	13	13.1004	13.1004	**C64**	12.2	11.6732	12.931
C65	12.1	12.5523	7.4257	**C66**	11.9	12.0482	24
C67	11.5	11.583	23.4375	**C68**	10	9.9668	9.7403
C69	9.4	9.1743	9.1185				

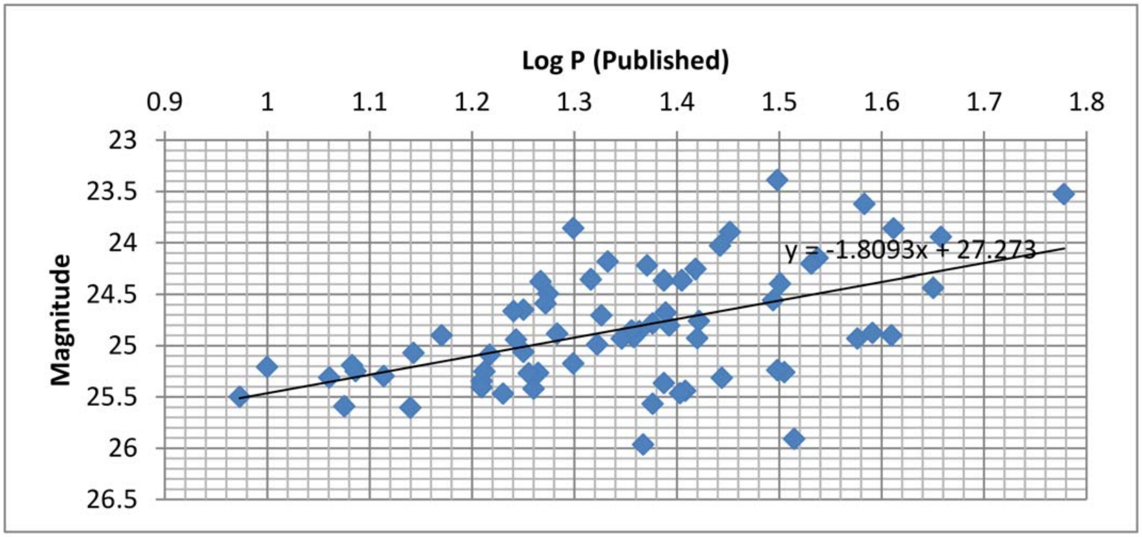

Figure 2.28 The Published $P-L$ Plot and Linear Fit for NGC 3621.

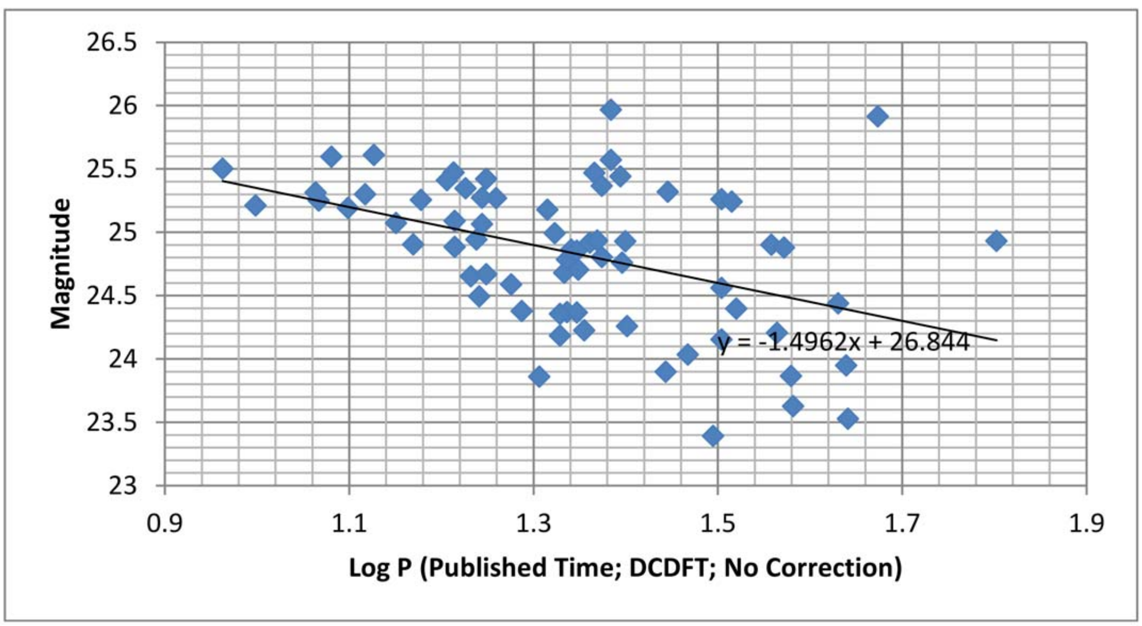

Figure 2.29 The $P-L$ Plot from DCDFT Period Recovery and the Linear Fit for NGC 3621.

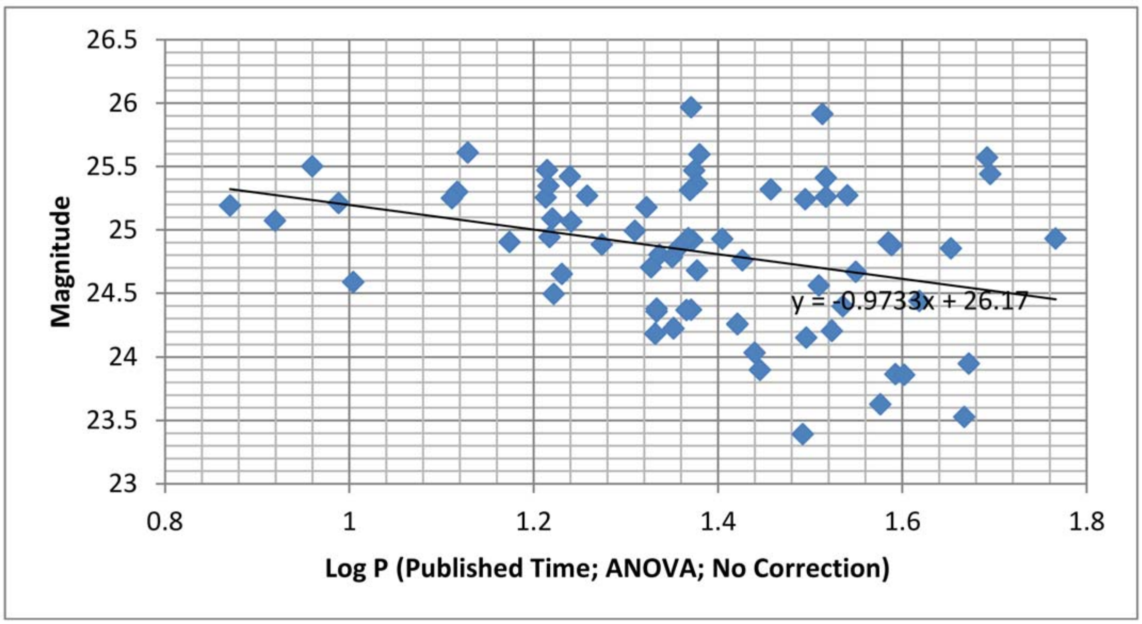

Figure 2.30 The $P-L$ Plot from ANOVA Period Recovery and the Linear Fit for NGC 3621.

2.2.11 NGC 4321

NGC 4321 is an example of a grand design spiral and is another famous Messier object, M100. It is a luminous spiral galaxy in the Virgo cluster that is seen nearly face-on. This galaxy has very well defined symmetric spiral arms. It is classified as Sc(s) I by Sandage & Tammann (1981) and as SAB(s)bc by de Vaucouleurs et al. (1976). From the ground, this galaxy is not well resolved, and little was previously known about its stellar populations (Freedman et al. 1994a). Although the Cepheids for this galaxy were originally numbered to 70, only 52 Cepheids have been studied and are collected in Table 2.12. The relations generated are shown in Figure 2.31, Figure 2.32, and Figure 2.33.

Table 2.12. Recovery of Cepheid Periods in NGC 4321

Cepheid	Published (days)	DCDFT (days)	ANOVA (days)	Cepheid	Published (days)	DCDFT (days)	ANOVA (days)
C1	85	110.701	120.000	**C2**	76.3	54.905	62.788
C3	63.5	82.327	71.839	**C4**	53.1	57.252	100.000
C5	52.8	53.937	47.483	**C6**	52	45.956	46.454
C7	51	45.372	43.796	**C8**	50.3	47.483	52.484
C9	50.3	48.123	47.801	**C10**	50	48.450	47.170
C11	48	56.225	46.667	**C12**			
C13	47	39.548	45.752	**C14**	46.5	49.296	46.205
C15	44	42.945	43.887	**C16**	42.9	44.164	44.164
C17	42.9	37.940	40.816	**C18**	42.3	44.164	43.478
C19	41.7	31.603	62.222	**C20**			
C21	41.5	43.077	42.042	**C22**			
C23	41.1	36.083	39.886	**C24**			
C25	34.7	34.420	34.200	**C26**			
C27	33.9	36.532	35.327	**C28**			
C29				**C30**			
C31	32	30.675	29.738	**C32**	31.7	33.034	33.663
C33	31.6	31.120	32.439	**C34**			
C35	30	29.092	29.251	**C36**			
C37	29.7	30.628	32.258	**C38**			
C39	28.8	28.777	29.155	**C40**	28.2	29.412	28.289
C41	28.2	29.155	28.902	**C42**	26.5	26.702	26.281
C43	26.4	25.773	26.490	**C44**			

Table 2.12 (cont'd)

Cepheid	Published (days)	DCDFT (days)	ANOVA (days)	Cepheid	Published (days)	DCDFT (days)	ANOVA (days)
C45	25.5	24.907	25.873	**C46**	25.3	23.585	24.184
C47	25.3	27.816	11.062	**C48**	25.1	14.225	23.838
C49	24.8	32.103	33.058	**C50**	24.5	23.585	23.838
C51	24	26.385	24.450	**C52**	22.4	21.598	21.459
C53	21.8	22.396	21.459	**C54**			
C55	21	20.921	21.119	**C56**	21	22.472	22.396
C57				**C58**			
C59	19	24.390	20.979	**C60**	18.8	19.355	17.857
C61				**C62**	17.7	18.519	18.072
C63	17.6	18.987	18.072	**C64**	17	16.667	16.854
C65	15.7	16.304	16.216	**C66**	15.5	15.625	30.000
C67				**C68**	10.9	10.870	10.909
C69				**C70**	7.3	7.335	14.778

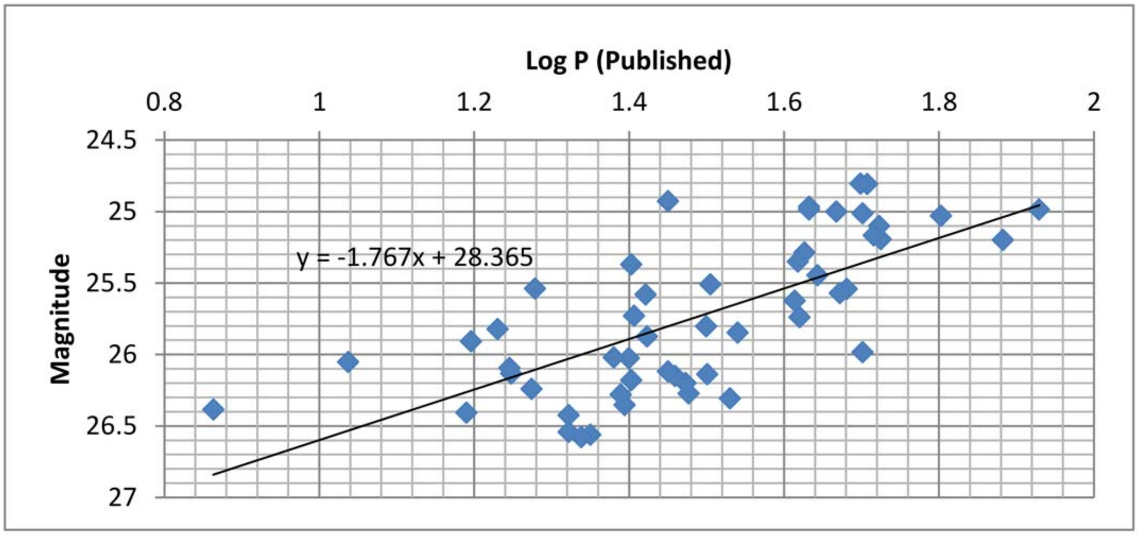

Figure 2.31 The Published $P-L$ Plot and Linear Fit for NGC 4321.

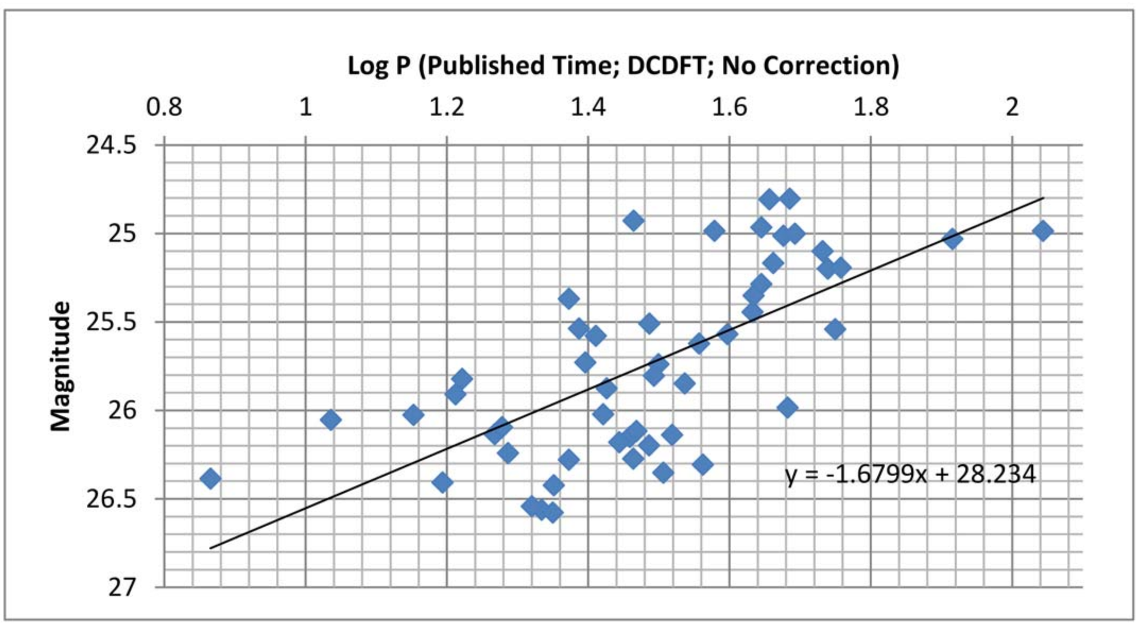

Figure 2.32 The $P-L$ Plot from DCDFT Period Recovery and the Linear Fit for NGC 4321.

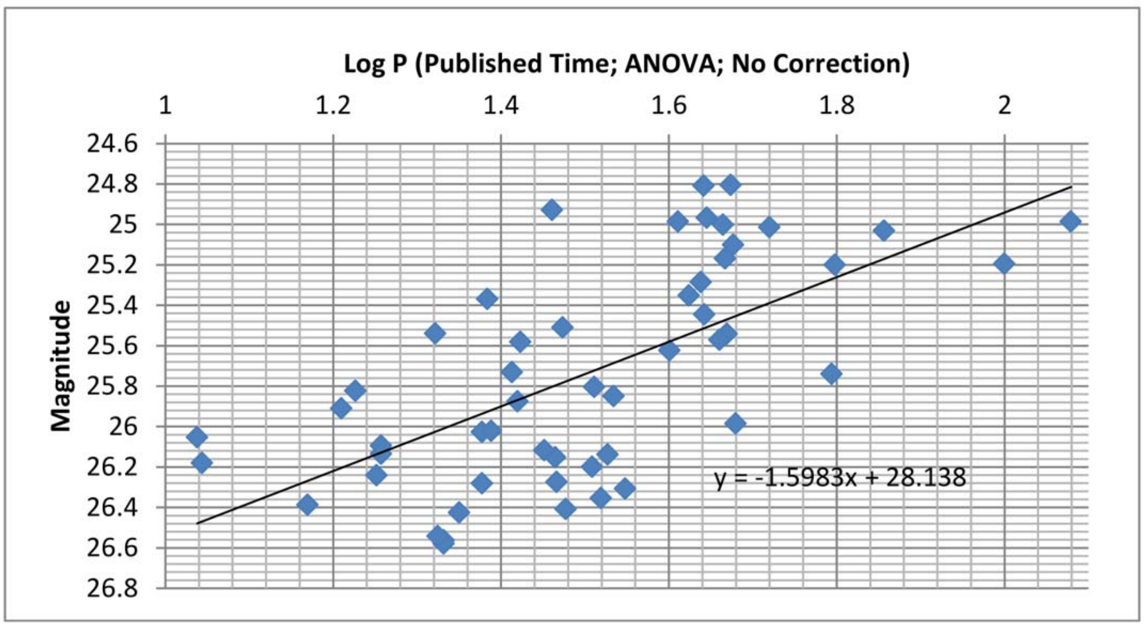

Figure 2.33 The $P - L$ Plot from ANOVA Period Recovery and the Linear Fit for NGC 4321.

Table 2.13. Recovery of Cepheid Periods in NGC 4414

Cepheid	Published (days)	DCDFT (days)	ANOVA (days)	Cepheid	Published (days)	DCDFT (days)	ANOVA (days)
C1	45.5	44.510	36.720	**C2**	20.4	20.921	20.921
C3	33.8	39.308	33.967	**C4**	36.9	37.879	37.651
C5	26.4	25.381	25.381	**C6**	28.8	29.762	28.736
C7	68.2	65.982	67.365	**C8**	19.0	18.450	18.248
C9	40.8	36.842	37.554	**C10**	42.7	41.866	41.568
C11	34	37.879	41.667				

2.2.12 NGC 4414

NGC 4414 was host to the Type Ia supernova 1974G (Ciatti & Rosino 1977). It is described as a Sc(sr) II.2 galaxy by (Sandage & Tammann 1981) and is a calibrator for the Tully-Fisher relation. There are only 11 Cepheids which have been selected for observation in this galaxy. The small sample size is due to the compact size and high surface brightness of NGC 4414. The bright stars are generally crowded and concentrated on the higher surface brightness areas of the galaxy. And the background surface brightness of the galaxy has a steep gradient. In addition, the exposure times are relatively short for a target at the distance of NGC 4414. All these facts make this galaxy one of the most challenging targets in the Key Project (Turner et al. 1998). Only 11 Cepheids were examined from this galaxy (Table 2.13). The relations generated are shown in Figure 2.34, Figure 2.35, and Figure 2.36.

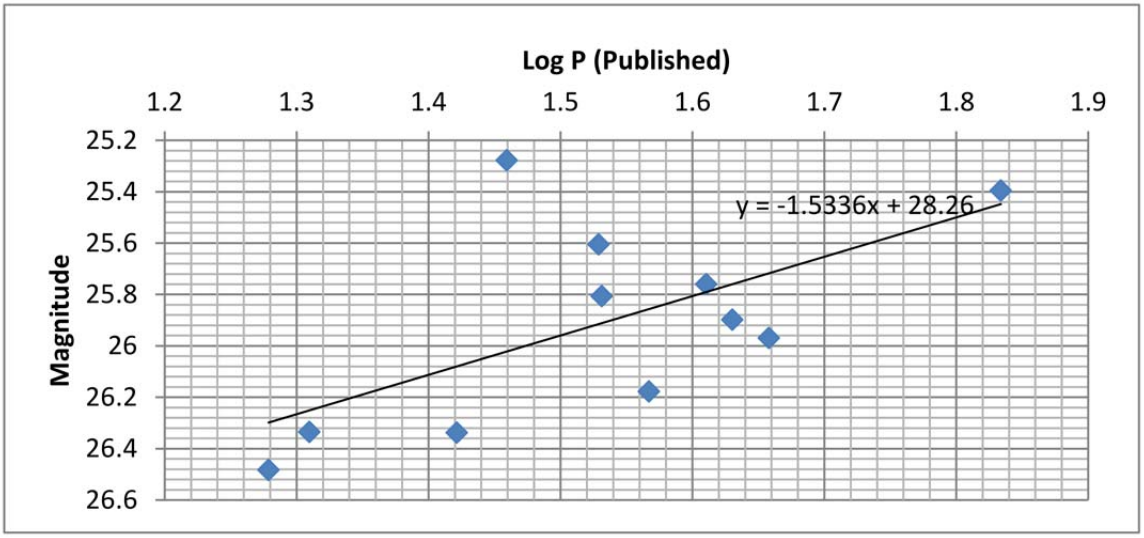

Figure 2.34 The Published $P-L$ Plot and Linear Fit for NGC 4414.

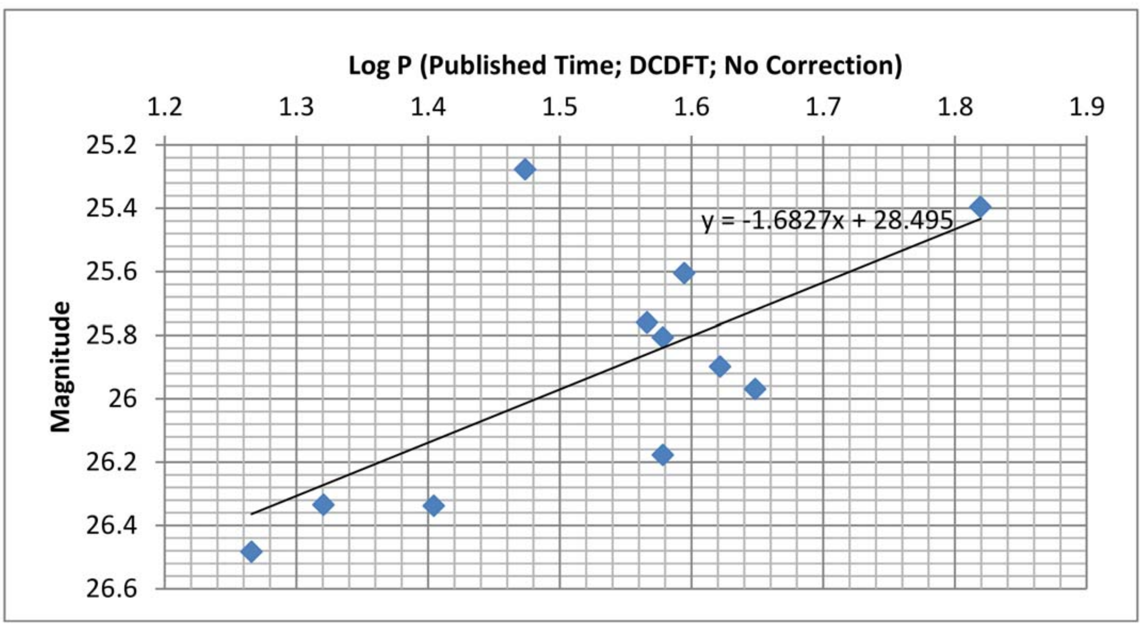

Figure 2.35 The $P-L$ Plot from DCDFT Period Recovery and the Linear Fit for NGC 4414.

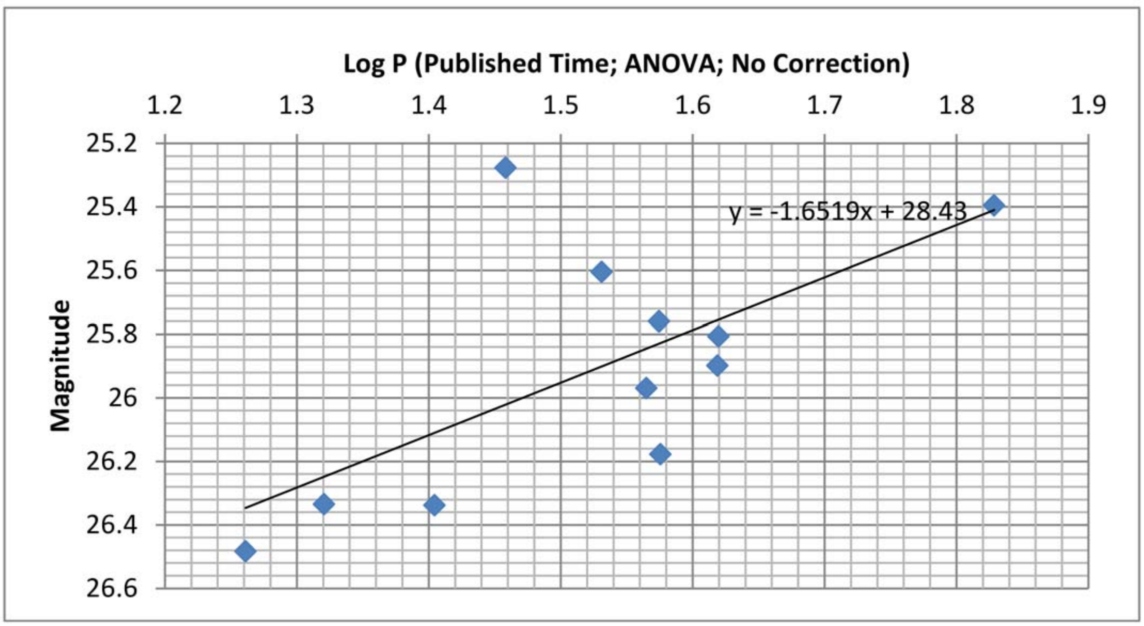

Figure 2.36 The $P - L$ Plot from ANOVA Period Recovery and the Linear Fit for NGC 4414.

2.2.13 NGC 4535

NGC 4535 is a SAb(s)c I/I-II (de Vaucouleurs et al. 1991) or a SB(s)c I.3 (Sandage & Tammann 1981) type of morphology. It has an inclination angle of 47 degrees, which makes it a suitable calibrator of the Tully-Fisher relation (Macri et al. 1999). This galaxy is a member of the Virgo cluster and is located near the more famous M87. Given its face-on nature it provided 50 Cepheids that were examined in the Key Project and this study (Table 2.14). The relations generated are shown in Figure 2.37, Figure 2.38, and Figure 2.39.

Table 2.14. Recovery of Cepheid Periods in NGC 4535

Cepheid	Published (days)	DCDFT (days)	ANOVA (days)	Cepheid	Published (days)	DCDFT (days)	ANOVA (days)
C1	71.5	61.920	65.445	**C2**	66.7	95.694	95.694
C3	59.5	58.680	59.113	**C4**	56.1	56.471	55.944
C5	54.2	57.416	53.452	**C6**	49.8	45.161	44.872
C7	49	48.951	48.951	**C8**	45.6	41.177	42.945
C9	45.1	42.424	45.161	**C10**	41.6	38.997	43.210
C11	40.7	42.814	42.945	**C12**	39.9	40.269	40.000
C13	38.6	40.816	38.462	**C14**	36.7	34.091	33.520
C15	35.4	33.149	37.037	**C16**	34.5	32.787	34.286
C17	34.2	30.303	30.151	**C18**	33.1	35.714	33.149
C19	32.9	32.787	30.151	**C20**	32.5	28.571	28.571
C21	32.2	28.302	35.088	**C22**	32.2	35.088	32.258
C23	31.8	26.316	30.457	**C24**	30.8	28.436	27.523
C25	30.5	26.786	38.621	**C26**	29.8	27.778	8.0386
C27	28.4	28.736	28.736	**C28**	28.2	28.736	28.249
C29	27.8	27.933	26.596	**C30**	27.4	32.895	26.882
C31	27.4	29.940	28.736	**C32**	27.2	28.249	25.381
C33	26.2	27.027	25.510	**C34**	25.2	30.303	25.253
C35	24.6	25.773	26.042	**C36**	24.6	29.586	23.810
C37	24.3	23.474	23.474	**C38**	23.4	25.126	23.810
C39	23.2	22.222	22.523	**C40**	23.2	22.936	22.936
C41	22.4	21.834	9.524	**C42**	21.8	20.325	20.408
C43	21.7	22.222	23.697	**C44**	21.6	21.739	22.222

Table 2.14 (cont'd)

Cepheid	Published (days)	DCDFT (days)	ANOVA (days)	Cepheid	Published (days)	DCDFT (days)	ANOVA (days)
C45	21.1	21.739	12.346	**C46**	19.6	20.202	20.202
C47	18.3	19.249	19.249	**C48**	15.9	15.244	5.297
C49	14.8	14.771	14.620	**C50**	13.9	14.045	13.908

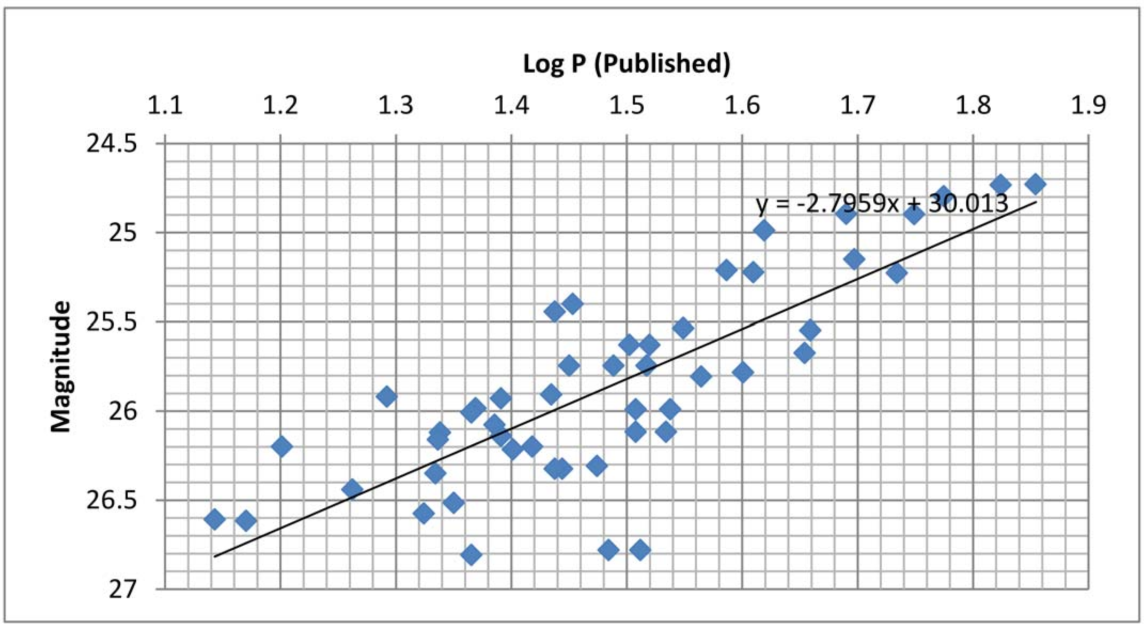

Figure 2.37 The Published $P-L$ Plot and Linear Fit for NGC 4535.

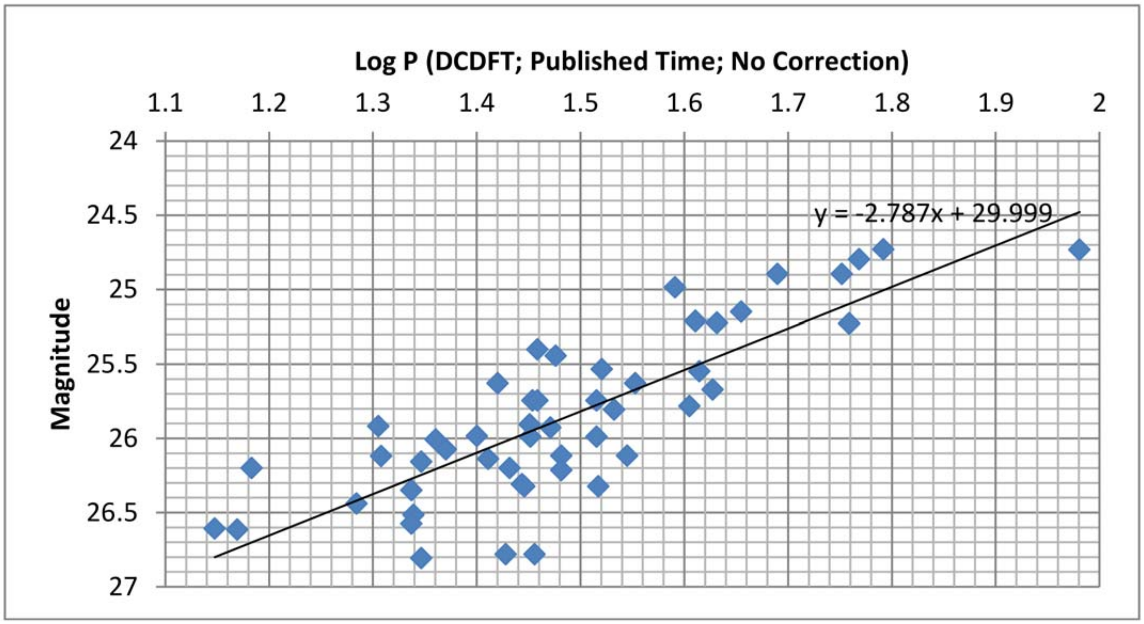

Figure 2.38 The $P-L$ Plot from DCDFT Period Recovery and the Linear Fit for NGC 4535.

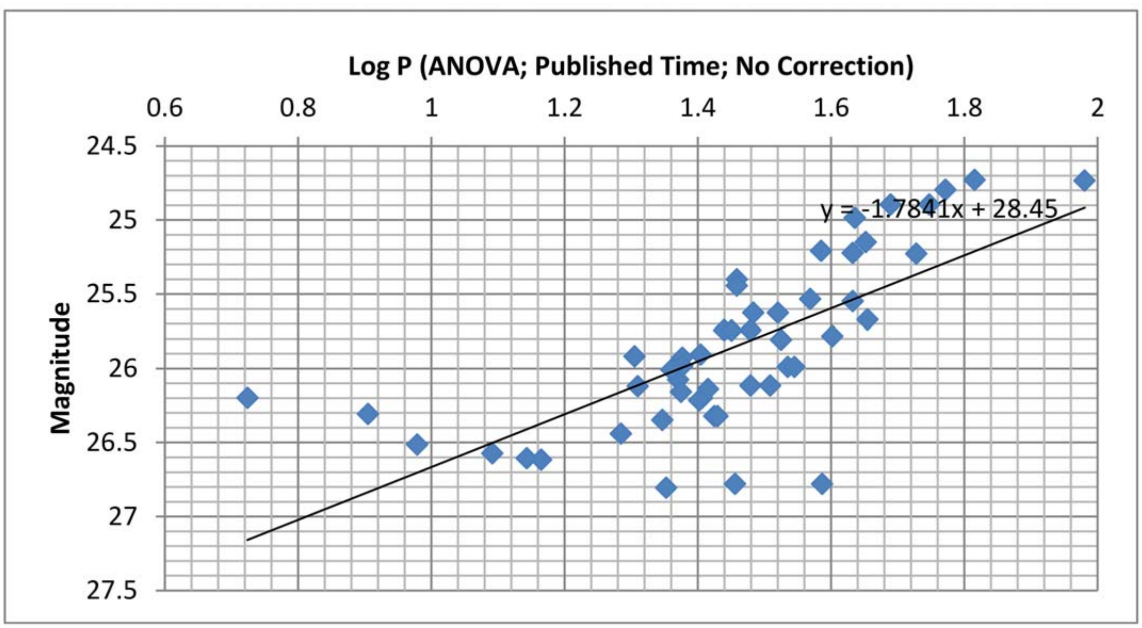

Figure 2.39 The $P-L$ Plot from ANOVA Period Recovery and the Linear Fit for NGC 4535.

2.2.14 NGC 4548

NGC 4548 is a well-resolved spiral galaxy of morphological type SBb(rs) I-II (Sandage & Tammann 1981) or SBb(rs) (de Vaucouleurs 1975). It appears very similar to galaxy NGC 3351 (M95). Van de Bergh refers to it as "a fine example of an anemic spiral" (van den Bergh 1976). NGC 4548 can probably be identified with Messier 91, although some historical uncertainty exists (Mallas & Kreimer 1978), as it was once considered a missing Messier object. This galaxy is a member of the Virgo cluster. The Virgo galaxies are playing a significant part in providing the calibration for the secondary distance indicators that bridge local flow perturbations and enlarge the volume over which a global Hubble constant can be derived (Graham et al. 1999). Besides NGC 4548, two other members of the Virgo cluster (NGC 4321 and NGC 4535) are also included in the Key Project as well as in our selection. The 24 Cepheids used in this study are given in Table 2.15. The relations generated are shown in Figure 2.40, Figure 2.41, and Figure 2.42.

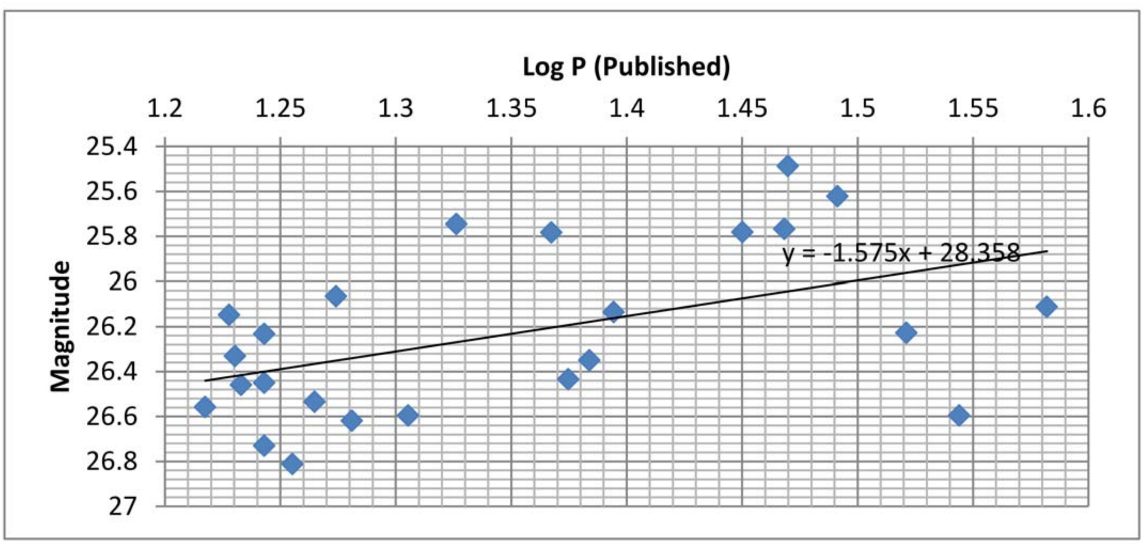

Figure 2.40 The Published $P-L$ Plot and Linear Fit for NGC 4548.

Table 2.15. Recovery of Cepheid Periods in NGC 4548

Cepheid	Published (days)	DCDFT (days)	ANOVA (days)	Cepheid	Published (days)	DCDFT (days)	ANOVA (days)
C1	33.2	33.2447	33.24477	**C2**	18.4	19.6464	38.9105
C3	24.8	24.8756	24.8756	**C4**	29.5	28.0899	29.411832
C5	24.2	25.7732	25.9067	**C6**	19.1	22.779	19.9203
C7	17.1	17.8094	35.9712	**C8**	38.2	42.517	38.5802
C9	18.8	18.1488	18.7441	**C10**	23.7	16.8919	13.1926
C11	29.4	29.4118	29.2398	**C12**	18	18.0343	37.8788
C13	31	30.4878	30.6373	**C14**	17.5	17.4825	17.3762
C15	17.5	18.1488	18.149	**C16**	35	32.2165	35.1124
C17	16.5	16.38	16.0128	**C18**	17.5	18.2648	18.2648
C19	28.2	33.3333	30.303	**C20**	16.9	16.4745	32.3102
C21	21.2	19.9203	19.8413	**C22**	20.2	32.0513	34.965
C23	23.3	23.0415	23.2558	**C24**	17	17.9211	17.6991

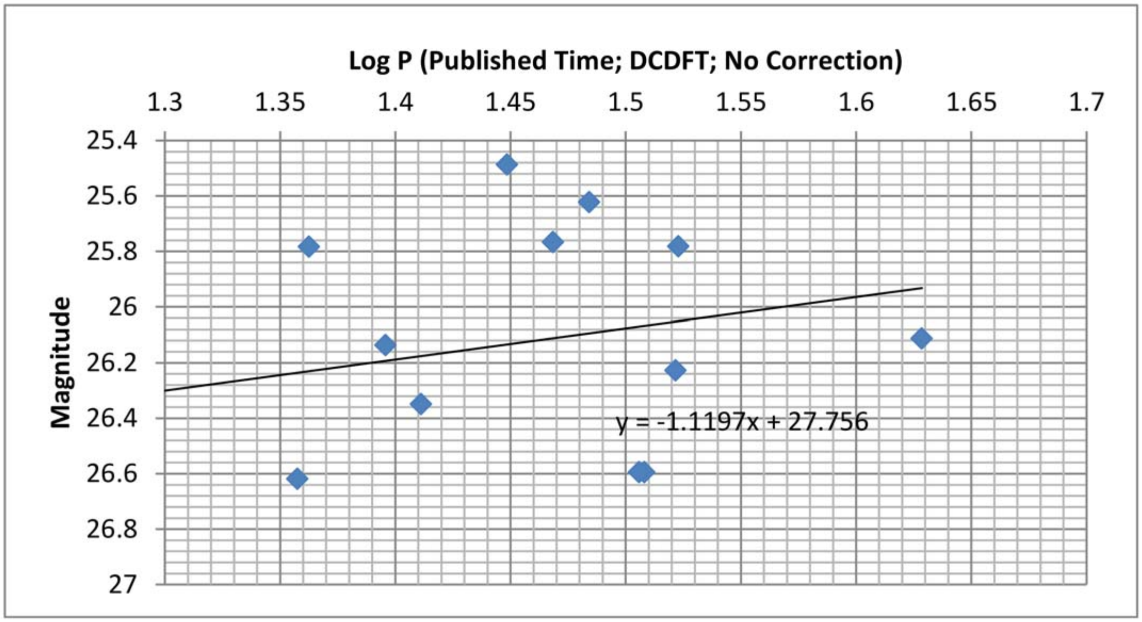

Figure 2.41 The $P - L$ Plot from DCDFT Period Recovery and the Linear Fit for NGC 4548.

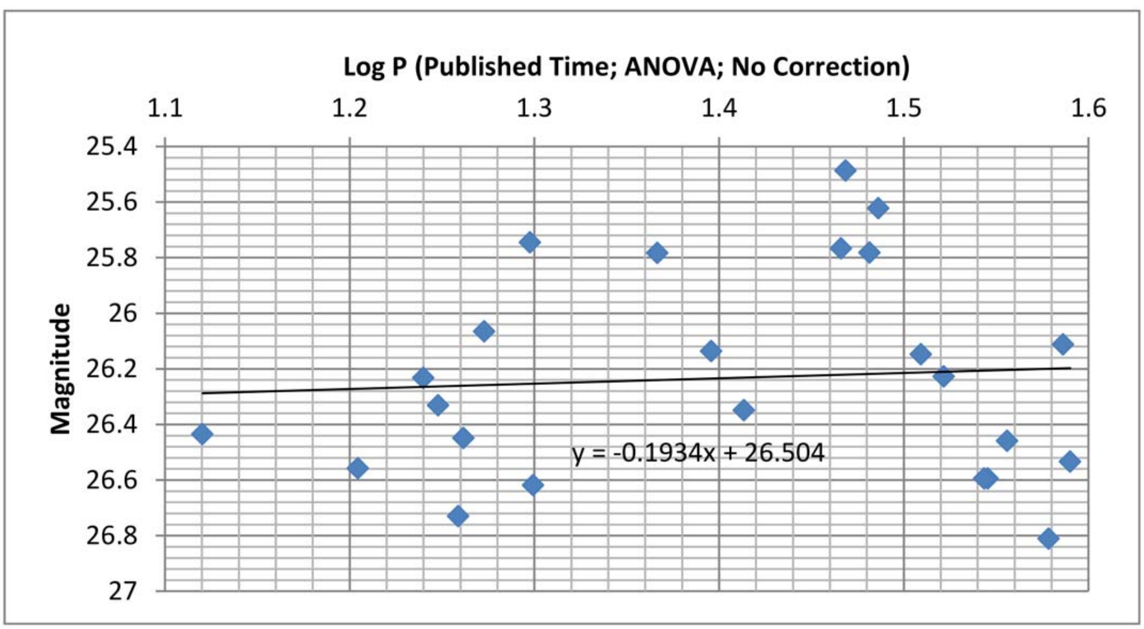

Figure 2.42 The $P - L$ Plot from ANOVA Period Recovery and the Linear Fit for NGC 4548.

2.2.15 NGC 4725

This galaxy is a Sb/SB(r)II barred spiral (Sandage 1996). It is assigned to be part of the Coma-Sculptor cloud, although it is relatively isolated dynamically from the remainder of the cloud (Zaritsky et al. 1997). It also belongs to the Coma II Group of galaxies (Tully 1988). This galaxy is one of the Key Project's primary calibrators for the infrared Tully-Fisher relation. Because of the assumed association of the Coma II Group with that of the neighboring (larger) Coma I Group and to some degree, the Coma-Sculptor cloud as a whole, it was hoped that NGC 4725 would indirectly provide calibration for the surface brightness fluctuation, planetary nebula luminosity function, and globular cluster luminosity function (Gibson et al. 1999). This galaxy is host of supernova 1940B, a typical example of the regular class of "plateau" Type II events (Patat et al. 1994). However, no data of that event was accessible for the purpose of the Key Project (Gibson et al. 1999). The 20 Cepheids are listed in Table 2.16. The relations generated are shown in Figure 2.43, Figure 2.44, and Figure 2.45.

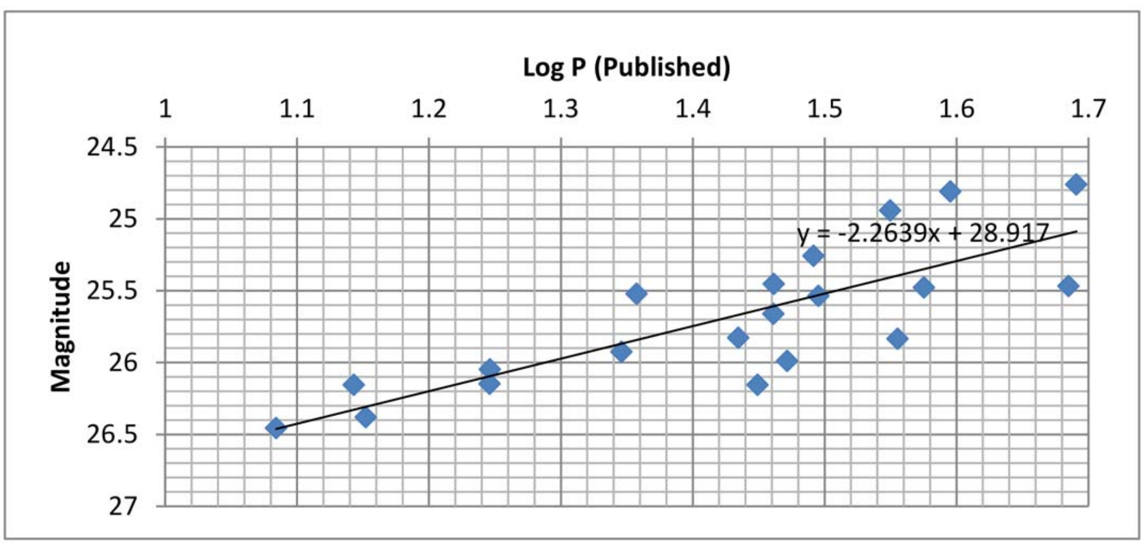

Figure 2.43 The Published $P-L$ Plot and Linear Fit for NGC 4725.

Table 2.16. Recovery of Cepheid Periods in NGC 4725

Cepheid	Published (days)	DCDFT (days)	ANOVA (days)	Cepheid	Published (days)	DCDFT (days)	ANOVA (days)
C1	28.95	26.455	26.738	**C2**	12.14	12.605	11.9522
C3	17.63	18.2927	18.2927	**C4**	22.19	9.8619	10.2041
C5	28.13	29.2398	30.1205	**C6**	49.09	56.8182	57.2519
C7	29.63	27.3224	27.3224	**C8**	31.29	31.25	28.4091
C9	39.39	39.0625	39.3082	**C10**	35.46	38.3436	38.1098
C11	22.78	22.3214	22.4215	**C12**	27.2	18.1159	35.7143
C13	37.63	37.2024	37.6506	**C14**	17.62	15.3061	7.5949
C15	14.2	14.218	14.218	**C16**	35.93	40.3226	35.9195
C17	31.03	11.0035	22.007	**C18**	28.93	29.4118	31.6456
C19	48.41	49.6689	47.9233	**C20**	13.9	13.453	14.085

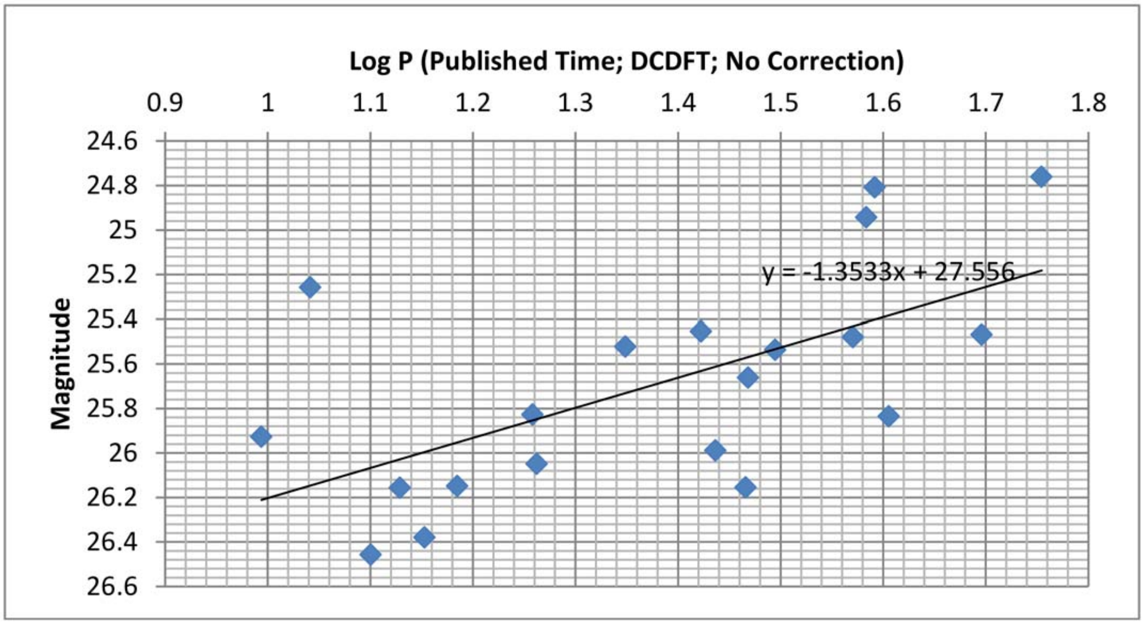

Figure 2.44 The $P-L$ Plot from DCDFT Period Recovery and the Linear Fit for NGC 4725.

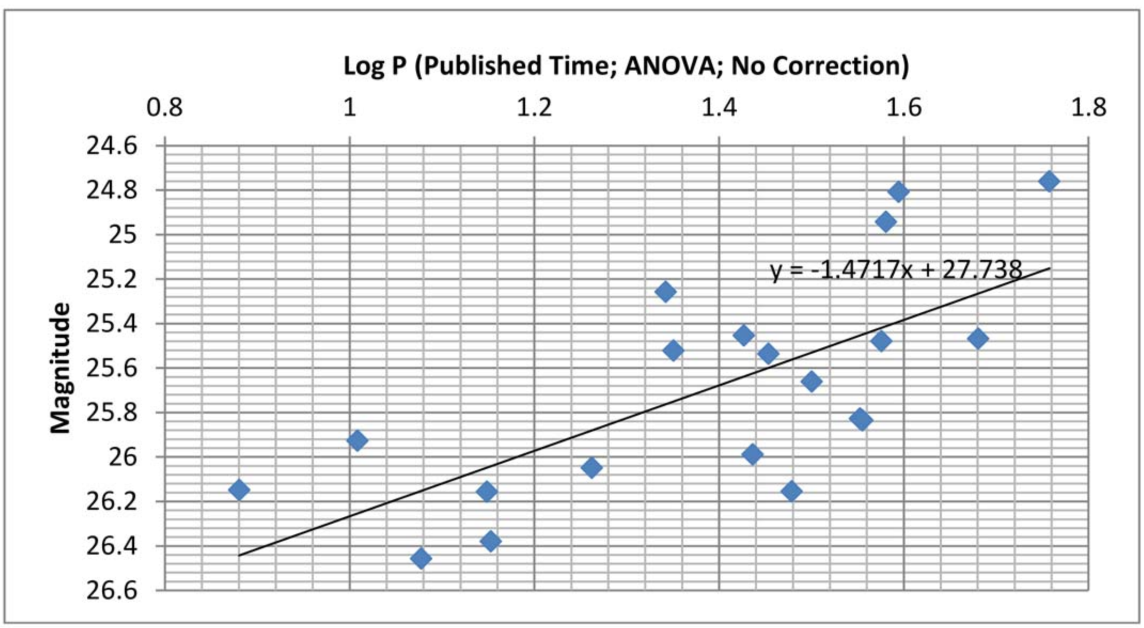

Figure 2.45 The $P-L$ Plot from ANOVA Period Recovery and the Linear Fit for NGC 4725.

Table 2.17. Recovery of Cepheid Periods in NGC 5457

Cepheid	Published (days)	DCDFT (days)	ANOVA (days)	Cepheid	Published (days)	DCDFT (days)	ANOVA (days)
C1	58.54	58.5023	58.4053	**C2**	18.2	18.0879	18.0879
C3	16.67	14.7493	16.6389	**C4**	14.27	14.3541	14.2857
C5	47.1	46.7122	47.1698	**C6**	45.8	45.1613	57.377
C7	43	42.8135	42.1687	**C8**	41	41.2979	41.1765
C9	38	37.9747	38.1679	**C10**	37.6	37.6884	37.4251
C11	23.7	23.5849	11.5808	**C12**	33.5	33.7838	33.7838
C13	32	31.6067	31.6706	**C14**	25	24.6063	38.8199
C15	23.4	19.7161	23.2342	**C16**	22.8	22.242	22.242
C17	16.45	16.4042	32.7225	**C18**	13	12.931	12.931
C19	43	29.8507	43.0571	**C20**	42.5	41.3618	41.2437
C21	33.5	33.1126	33.4076	**C22**	27.3	26.2812	27.248
C23	25.6	25.8732	25.8732	**C24**	23.5	23.4192	23.4192
C25	19.35	19.1466	9.2789	**C26**	17.7	17.7485	22.2081
C27	17.2	17.4303	5.6379	**C28**	16.7	6.9225	6.2411
C29	14	11.9522	13.1579				

2.2.16 NGC 5457

This galaxy is often referred to as *the Pinwheel Galaxy* or M101 from the Messier catalog. It is a luminous Sc spiral of morphological type SAB(re)cd (de Vaucouleurs et al. 1991). As a face-on, grand-design spiral, M101 has been widely used for the study of spiral structures (Kelson et al. 1996). This galaxy contained 29 Cepheids that were used as part of the Key Project (Table 2.17. The relations generated are shown in Figure 2.46, Figure 2.47, and Figure 2.48.

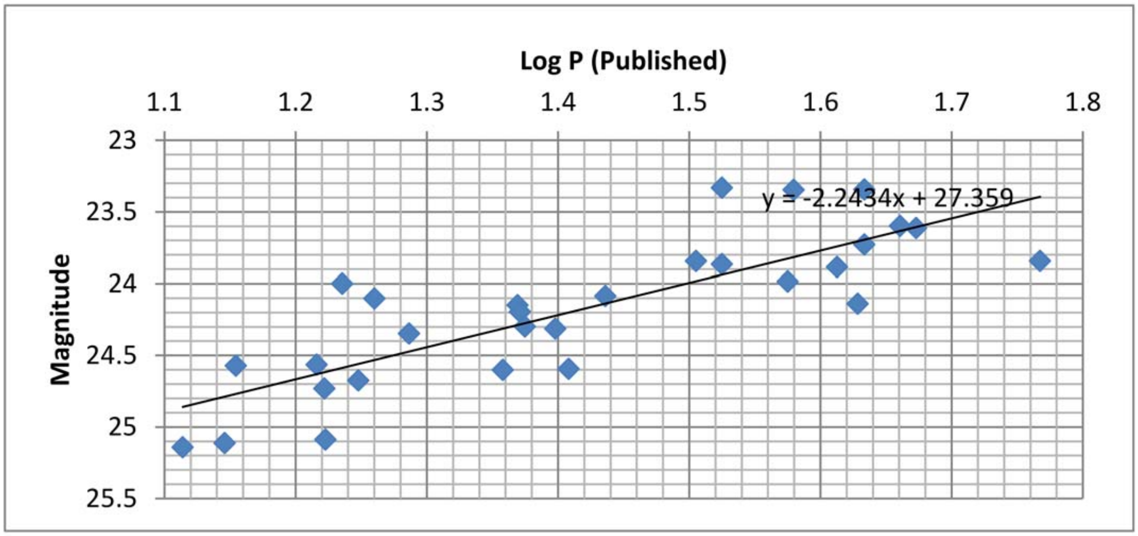

Figure 2.46 The Published $P - L$ Plot and Linear Fit for NGC 5457.

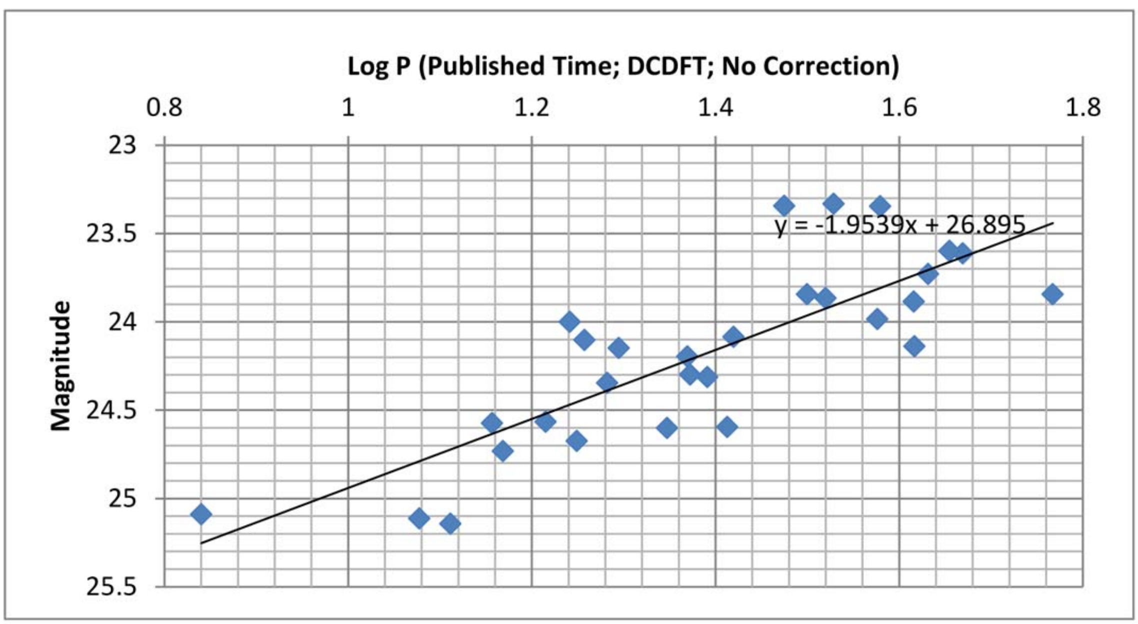

Figure 2.47 The $P - L$ Plot from DCDFT Period Recovery and the Linear Fit for NGC 5457.

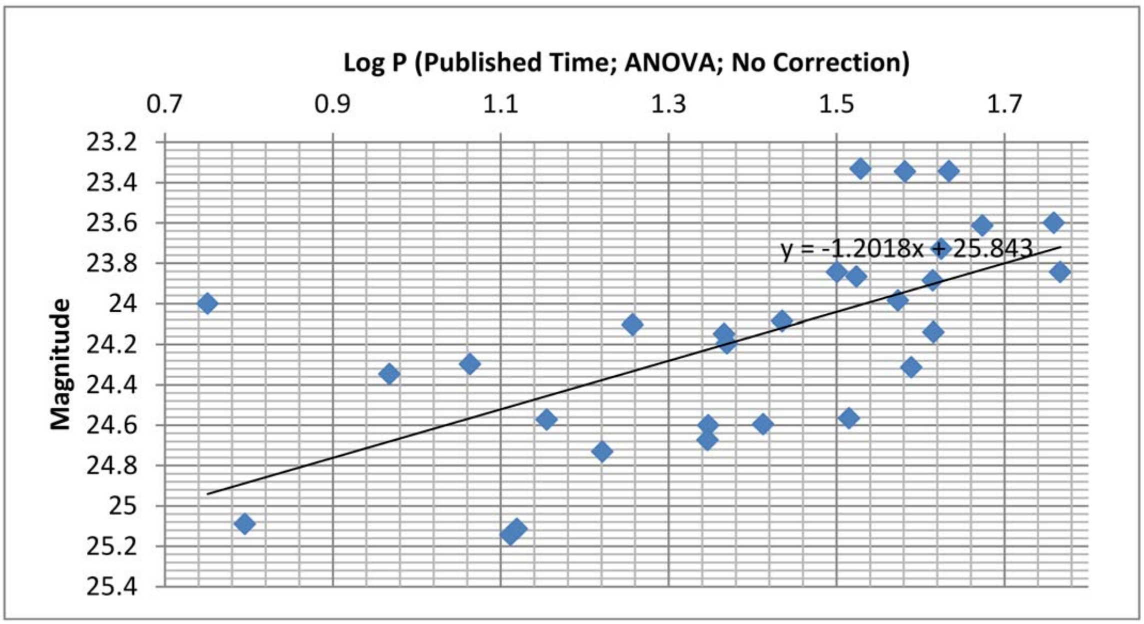

Figure 2.48 The $P-L$ Plot from ANOVA Period Recovery and the Linear Fit for NGC 5457.

Table 2.18. Recovery of Cepheid Periods in NGC 7331

Cepheid	Published (days)	DCDFT (days)	ANOVA (days)	Cepheid	Published (days)	DCDFT (days)	ANOVA (days)
C1	42.59	42.827	42.827	**C2**	21.19	21.277	42.373
C3	13.91	13.419	14.008	**C4**	22.6	22.852	24.248
C5	33.94	37.554	31.139	**C6**	29.05	29.377	29.691
C7	39.9	45.455	45.455	**C8**	11.13	11.166	12.378
C9	24.41	26.069	24.462	**C10**	11.61	12.029	11.610
C11	19.82	19.721	21.020	**C12**	24.82	24.900	24.900
C13	41.2	41.280	41.280				

2.2.17 NGC 7331

NGC 7331 is a LINER-type AGN galaxy and is often imaged due to its own beautiful structure and other nearby galaxies. It lies in the constellation of Pegasus and has an early-type spiral classification of Sb(rs) I-II (Sandage & Tammann 1981). It has an inclination angle of 75 degrees, which makes it an ideal calibrator for the Tully-Fisher relation (Hughes et al. 1998). Only 13 Cepheids have been selected for observation in this galaxy. As with previous sections three $P-L$ relation are presented in Figures 2.49, 2.50, and 2.51. For this galaxy we find that both the DCDFT and ANOVA methods recover the $P-L$ relation quite well. The 13 Cepheids from the Key Project are collected in Table 2.18.

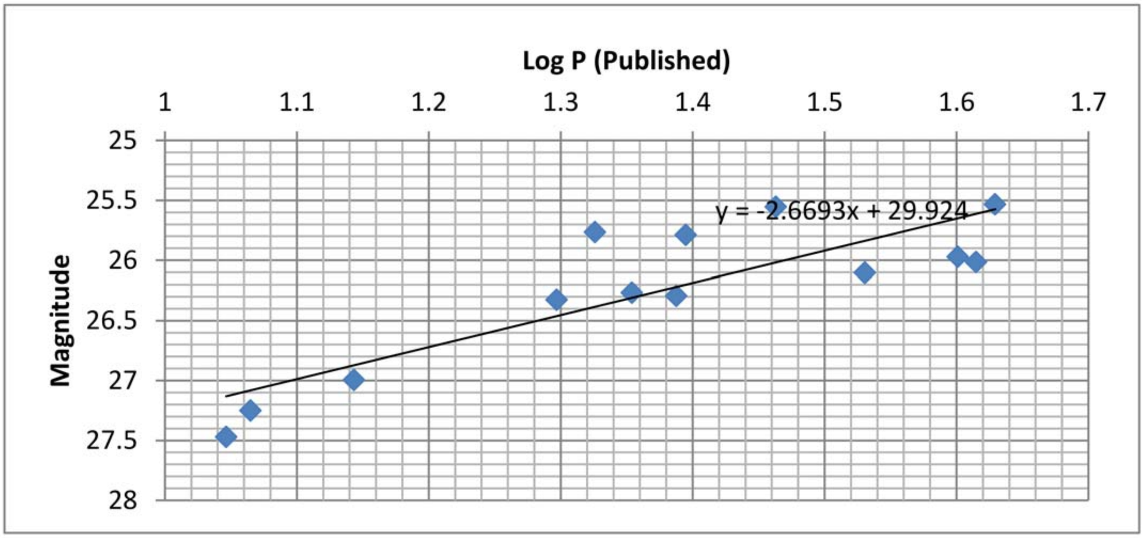

Figure 2.49 The Published $P-L$ Plot and Linear Fit for NGC 7331.

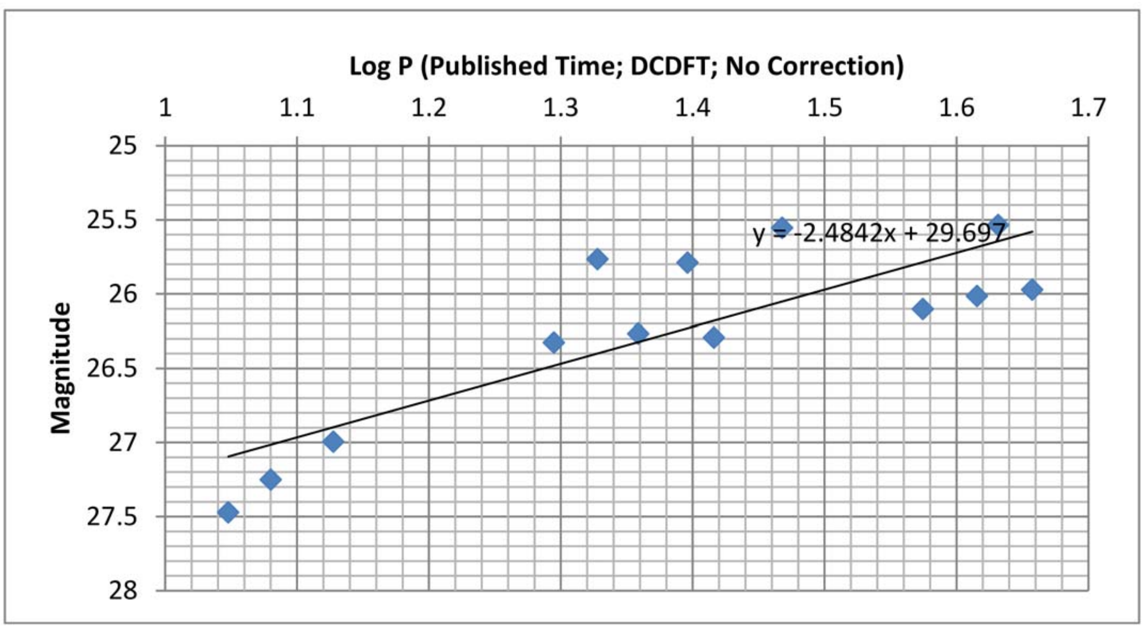

Figure 2.50 The $P-L$ Plot from DCDFT Period Recovery and the Linear Fit for NGC 7331.

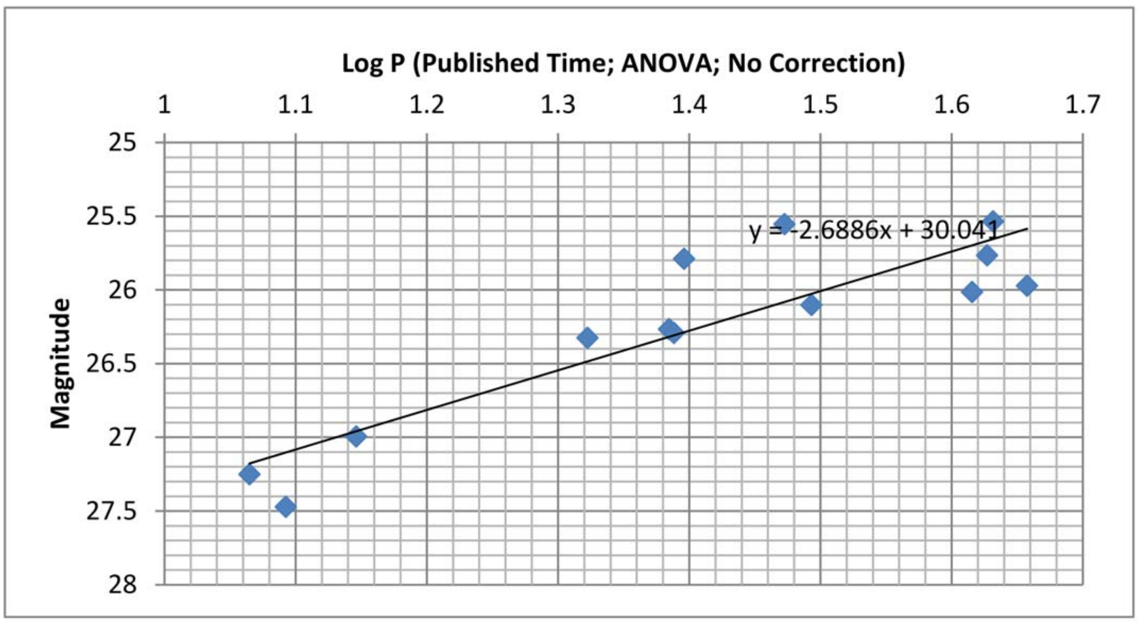

Figure 2.51 The $P-L$ Plot from ANOVA Period Recovery and the Linear Fit for NGC 7331.

2.3 Stage Two: The Time Correction

2.3.1 The Corrected Times

The second stage of our project is to perform a time correction using the recessional velocity of each galaxy. Clearly the total change in distance might include a tangential component and the rotation of the galaxy. However, for this study only the recessional velocity was used. According to the basic principles discussed in Section 1.3, light from a galaxy with a positive recessional velocity takes a longer time to reach us, whereas light from a galaxy with a negative recessional velocity takes a shorter time to reach us. In our selection of galaxies, NGC 3031 (M81) is the only one that has a negative recessional velocity.

The method we use for time correction is based on the most fundamental Newtonian kinematics, which implies that we are neglecting any non-linear effects such as relativity. In a time set where time of measurement (in HJD) is marked as T_0, T_1, T_2, etc., the mathematical form of times correction is

$$T_0 = T_0 \tag{2.1}$$

$$T_1 = T_1 + \frac{(T_1 - T_0) \times v_{recessional}}{c} \tag{2.2}$$

$$\vdots$$

$$T_n = T_n + \frac{(T_n - T_{n-1}) \times v_{recessional}}{c}, \tag{2.3}$$

where T_n is the n^{th} point in the time set, $v_{recessional}$ is the recessional velocity of the galaxy in km/s, and c is the speed of light, which is $3 \times 10^5 km/s$. Here we present the comparison of the original time and the corrected time for each galaxy. Note that NGC 3031 was observed in two different time sets.

For each galaxy the published HJD values were used as a starting point and then corrected. The values of the published HJD, corrected HJD and the difference are shown in Figures 2.52 to 2.69.

Original HJD (T_0)	Corrected HJD (T_{crr})	T_{crr}-T_0
2449573.402	2449573.402	0
2449582.043	2449582.059	0.01589944
2449591.472	2449591.489	0.01734936
2449594.53	2449594.536	0.00562672
2449597.339	2449597.344	0.00516856
2449604.382	2449604.395	0.01295912
2449608.609	2449608.617	0.00777768
2449613.362	2449613.371	0.00874552
2449618.925	2449618.935	0.01023592
2449625.359	2449625.371	0.01183856
2449633.335	2449633.35	0.01467584
2449643.187	2449643.205	0.01812768

Figure 2.52 Comparison of the original time and the corrected time for NGC 925.

Original HJD (T_0)	Corrected HJD (T_{crr})	T_{crr}-T_0
2450667.095	2450667.095	0
2450670.12	2450670.137	0.017319158
2450673.008	2450673.025	0.016540904
2450675.906	2450675.923	0.016597598
2450679.2	2450679.219	0.018861922
2450684.371	2450684.401	0.029612021
2450687.743	2450687.763	0.019313183
2450693.317	2450693.349	0.03192044
2450697.293	2450697.315	0.022764073
2450704.275	2450704.314	0.039983587
2450709.382	2450709.411	0.029249523
2450716.17	2450716.209	0.038872041

Figure 2.53 Comparison of the original time and the corrected time for NGC 1326A.

Original HJD (T_0)	Corrected HJD (T_{crr})	T_{crr}-T_0
2449936.164	2449936.164	0
2449943.937	2449943.98	0.04314015
2449951.31	2449951.351	0.04092015
2449953.659	2449953.672	0.01303695
2449956.204	2449956.218	0.01412475
2449959.223	2449959.24	0.01675545
2449962.309	2449962.326	0.0171273
2449965.728	2449965.747	0.01897545
2449969.414	2449969.434	0.0204573
2449974.238	2449974.265	0.0267732
2449980.27	2449980.303	0.0334776
2449985.295	2449985.323	0.02788875

Figure 2.54 Comparison of the original time and the corrected time for NGC 1365.

Original HJD (T_0)	Corrected HJD (T_{crr})	T_{crr}-T_0
2449763.25	2449763.25	0
2450100.25	2450101.287	1.036836667
2450107.5	2450107.522	0.022305833
2450115.75	2450115.775	0.0253825
2450117.75	2450117.756	0.006153333
2450120.5	2450120.508	0.008460833
2450123	2450123.008	0.007691666
2450126.5	2450126.511	0.010768333
2450129.75	2450129.76	0.009999167
2450133.5	2450133.512	0.0115375
2450138.75	2450138.766	0.0161525
2450145.25	2450145.27	0.019998333
2450150.5	2450150.516	0.0161525

Figure 2.55 Comparison of the original time and the corrected time for NGC 2090.

Original HJD (T_0)	Corrected HJD (T_{crr})	T_{crr}-T_0
2449714.728	2449714.728	0
2450020.588	2450021.156	0.567880067
2450027.23	2450027.242	0.01233198
2450035.006	2450035.02	0.01443744
2450037.018	2450037.022	0.003735613
2450038.962	2450038.966	0.00360936
2450041.915	2450041.92	0.005482737
2450044.323	2450044.327	0.004470854
2450047.405	2450047.411	0.005722247
2450051.224	2450051.231	0.00709061
2450055.11	2450055.117	0.007215007
2450060.339	2450060.349	0.00970851
2450067.103	2450067.116	0.012558493

Figure 2.56 Comparison of the original time and the corrected time for NGC 2541.

Original HJD (T_0)	Corrected HJD (T_{crr})	T_{crr}-T_0
2448620.6	2448620.6	0
2448620.612	2448620.612	-1.68011E-06
2448621.536	2448621.536	-0.00012936
2448630.493	2448630.492	-0.00125398
2448641.213	2448641.211	-0.0015008
2448641.956	2448641.956	-0.00010402
2448643.224	2448643.224	-0.00017752
2448644.567	2448644.567	-0.00018802
2448646.365	2448646.365	-0.00025172
2448646.377	2448646.377	-1.68011E-06
2448649.188	2448649.188	-0.00039354
2448653.136	2448653.135	-0.00055272
2448653.148	2448653.148	-1.68011E-06
2448657.704	2448657.703	-0.00063784
2448662.852	2448662.851	-0.00072072
2448662.864	2448662.864	-1.68011E-06
2448984.166	2448984.121	-0.04498228
2448987.246	2448987.246	-0.0004312
2448992.272	2448992.271	-0.00070364
2449000.029	2449000.028	-0.00108598
2449012.208	2449012.206	-0.00170506
2449029.177	2449029.175	-0.00237566

Figure 2.57 Comparison of the original time and the corrected time for NGC 3031 (time set 1).

Original HJD (T_0)	Corrected HJD (T_{crr})	T_{crr}-T_0
2448620.867	2448620.867	0
2448620.879	2448620.879	-1.68011E-06
2448621.803	2448621.803	-0.00012936
2448630.759	2448630.758	-0.00125384
2448641.15	2448641.149	-0.00145474
2448642.025	2448642.025	-0.0001225
2448643.098	2448643.098	-0.00015022
2448644.633	2448644.633	-0.0002149
2448646.231	2448646.231	-0.00022372
2448646.243	2448646.243	-1.68011E-06
2448649.062	2448649.062	-0.00039466
2448653.002	2448653.001	-0.0005516
2448653.014	2448653.014	-1.68011E-06
2448658.106	2448658.105	-0.00071288
2448663.053	2448663.052	-0.00069258
2448663.065	2448663.065	-1.68011E-06
2448984.101	2448984.056	-0.04494504
2448987.38	2448987.38	-0.00045906
2448992.334	2448992.333	-0.00069356
2449000.162	2449000.161	-0.00109592
2449012.273	2449012.271	-0.00169554
2449029.241	2449029.239	-0.00237552

Figure 2.58 Comparison of the original time and the corrected time for NGC 3031 (time set 2).

Original HJD (T_0)	Corrected HJD (T_{crr})	T_{crr}-T_0
2449049.033	2449049.033	0
2449049.094	2449049.094	0.00013829
2449057.46	2449057.479	0.018935047
2449064.083	2449064.098	0.014990057
2449064.114	2449064.114	6.97109E-05
2449069.266	2449069.278	0.011661825
2449069.329	2449069.329	0.000143043
2449131.659	2449131.8	0.141072661
2449131.723	2449131.723	0.000144627
2449141.626	2449141.649	0.022414921
2449141.694	2449141.694	0.000152322
2449146.11	2449146.12	0.00999488
2449146.177	2449146.177	0.000152548
2449156.886	2449156.91	0.024238037
2449156.95	2449156.95	0.000144627
2449160.766	2449160.774	0.008636653
2449160.83	2449160.831	0.000146212
2449163.245	2449163.25	0.005465045
2449163.305	2449163.306	0.000136706
2449251.613	2449251.813	0.199869535
2449251.675	2449251.675	0.000139874
2449295.263	2449295.362	0.098655305
2449295.32	2449295.32	0.000127199
2449307.704	2449307.732	0.028029346
2449307.766	2449307.766	0.000141458
2449429.602	2449429.877	0.275754348

Figure 2.59 Comparison of the original time and the corrected time for NGC 3198.

Original HJD (T_0)	Corrected HJD (T_{crr})	T_{crr}-T_0
2450083.39	2450083.39	0
2450083.4	2450083.4	2.50665E-05
2450769.47	2450771.19	1.7197488
2450769.48	2450769.48	2.50665E-05
2450776.39	2450776.407	0.017321066
2450776.41	2450776.41	5.01331E-05
2450784.18	2450784.199	0.0194768
2450784.2	2450784.2	5.01331E-05
2450785.59	2450785.593	0.003484267
2450785.61	2450785.61	5.01336E-05
2450788.15	2450788.156	0.006366933
2450788.16	2450788.16	2.50665E-05
2450790.37	2450790.376	0.005539733
2450790.37	2450790.37	0
2450793.19	2450793.197	0.0070688
2450793.2	2450793.2	2.50665E-05
2450796.41	2450796.418	0.0080464
2450796.43	2450796.43	5.01331E-05
2450800.44	2450800.45	0.010051733
2450800.46	2450800.46	5.01336E-05
2450804.48	2450804.49	0.0100768
2450804.49	2450804.49	2.50665E-05
2450809.33	2450809.342	0.012132267
2450809.35	2450809.35	5.01331E-05
2450816.32	2450816.337	0.017471467
2450816.33	2450816.33	2.50665E-05

Figure 2.60 Comparison of the original time and the corrected time for NGC 3319.

Original HJD (T_0)	Corrected HJD (T_{crr})	T_{crr}-T_0
2449686.375	2449686.375	0
2449694.492	2449694.513	0.02102303
2449703.471	2449703.494	0.02325561
2449705.815	2449705.821	0.00607096
2449708.567	2449708.574	0.00712768
2449711.311	2449711.318	0.00710696
2449714.931	2449714.94	0.0093758
2449718.617	2449718.627	0.00954674
2449723.106	2449723.118	0.01162651
2449728.135	2449728.148	0.01302511
2449734.099	2449734.114	0.01544676
2449741.333	2449741.352	0.01873606

Figure 2.61 Comparison of the original time and the corrected time for NGC 3351.

Original HJD (T_0)	Corrected HJD (T_{crr})	T_{crr}-T_0
2449714.37	2449714.37	0
2449722.28	2449722.299	0.019168566
2449733.4	2449733.427	0.026947467
2449735.48	2449735.485	0.005040533
2449738.43	2449738.437	0.007148833
2449742.18	2449742.189	0.0090875
2449746.01	2449746.019	0.009281367
2449750.09	2449750.1	0.0098872
2449755.25	2449755.263	0.0125044
2449761.16	2449761.174	0.0143219
2449767.39	2449767.405	0.015097367
2449773.69	2449773.705	0.015267

Figure 2.62 Comparison of the original time and the corrected time for NGC 3621.

Original HJD (T_0)	Corrected HJD (T_{crr})	T_{crr}-T_0
2449465.78	2449465.78	0
2449476.71	2449476.767	0.057200334
2449478.99	2449479.002	0.011932
2449482.4	2449482.418	0.017845667
2449485.22	2449485.235	0.014758
2449489.04	2449489.06	0.019991333
2449493.53	2449493.553	0.023497667
2449498.82	2449498.848	0.027684333
2449503.85	2449503.876	0.026323667
2449510.82	2449510.856	0.036476334
2449520.95	2449521.003	0.053013667
2449522.96	2449522.971	0.010519

Figure 2.63 Comparison of the original time and the corrected time for NGC 4321.

Original HJD (T_0)	Corrected HJD (T_{crr})	T_{crr}-T_0
2449814.28	2449814.28	0
2449816.16	2449816.164	0.0044932
2449817.9	2449817.904	0.0041586
2449820.31	2449820.316	0.0057599
2449823.26	2449823.267	0.0070505
2449827.35	2449827.36	0.0097751
2449831.76	2449831.771	0.0105399
2449837.26	2449837.273	0.013145
2449843.76	2449843.776	0.015535
2449852.88	2449852.902	0.0217968
2449864.28	2449864.307	0.027246
2449878.62	2449878.654	0.0342726
2450189.08	2450189.822	0.7419994

Figure 2.64 Comparison of the original time and the corrected time for NGC 4414.

Original HJD (T_0)	Corrected HJD (T_{crr})	T_{crr}-T_0
2449512.47	2449512.47	0
2450227.55	2450232.215	4.6647052
2450235.59	2450235.642	0.0524476
2450246.32	2450246.39	0.069995367
2450249.14	2450249.158	0.0183958
2450252.08	2450252.099	0.0191786
2450255.31	2450255.331	0.021070367
2450259.05	2450259.074	0.024397267
2450263.08	2450263.106	0.026289033
2450267.49	2450267.519	0.0287679
2450274.34	2450274.385	0.044684833
2450287.26	2450287.344	0.084281466
2450302.14	2450302.237	0.0970672

Figure 2.65 Comparison of the original time and the corrected time for NGC 4535.

Original HJD (T_0)	Corrected HJD (T_{crr})	T_{crr}-T_0
2450189.847	2450189.847	0
2450198.024	2450198.037	0.01341028
2450208.947	2450208.965	0.01791372
2450211.106	2450211.11	0.00354076
2450213.64	2450213.644	0.00415576
2450217.94	2450217.947	0.007052
2450221.077	2450221.082	0.00514468
2450225.313	2450225.32	0.00694704
2450229.922	2450229.93	0.00755876
2450235.162	2450235.171	0.0085936
2450241.986	2450241.997	0.01119136
2450249.763	2450249.776	0.01275428
2450574.203	2450574.735	0.5320816

Figure 2.66 Comparison of the original time and the corrected time for NGC 4548.

Original HJD (T_0)	Corrected HJD (T_{crr})	T_{crr}-T_0
2449819.813	2449819.813	0
2449819.867	2449819.867	0.00021726
2449828.528	2449828.563	0.03484609
2449828.579	2449828.579	0.00020519
2449839.777	2449839.822	0.045053286
2449839.836	2449839.836	0.000237377
2449842.722	2449842.734	0.01161134
2449842.785	2449842.785	0.00025347
2449845.269	2449845.279	0.00999396
2449845.288	2449845.288	7.64434E-05
2449848.756	2449848.77	0.01395292
2449848.819	2449848.819	0.00025347
2449852.993	2449853.01	0.016793394
2449853.044	2449853.044	0.00020519
2449856.946	2449856.962	0.015699047
2449856.999	2449856.999	0.000213237
2449857.082	2449857.082	0.000333937
2449862.174	2449862.194	0.020486814
2449862.233	2449862.233	0.000237377
2449868.206	2449868.23	0.02403137
2449868.264	2449868.264	0.000233353
2449874.974	2449875.001	0.026996566
2449875.025	2449875.025	0.00020519
2449883.417	2449883.451	0.033763813
2449883.468	2449883.468	0.00020519
2450203.095	2450204.381	1.285965963
2450203.109	2450203.109	5.63269E-05

Figure 2.67 Comparison of the original time and the corrected time for NGC 4725.

Original HJD (T_0)	Corrected HJD (T_{crr})	T_{crr}-T_0
2449049.033	2449049.033	-0.0003
2449049.094	2449049.094	5.42901E-05
2449057.46	2449057.467	0.00744574
2449064.083	2449064.089	0.00589447
2449064.114	2449064.114	2.759E-05
2449069.266	2449069.271	0.00458528
2449069.329	2449069.329	5.60698E-05
2449131.659	2449131.714	0.0554737
2449131.723	2449131.723	5.69602E-05
2449141.694	2449141.703	0.00887419
2449146.11	2449146.114	0.00393024
2449146.177	2449146.177	5.96298E-05
2449156.886	2449156.896	0.00953101
2449156.95	2449156.95	5.69602E-05
2449160.766	2449160.769	0.00339624
2449160.83	2449160.83	5.69602E-05
2449163.245	2449163.247	0.00214935
2449163.305	2449163.305	5.34002E-05
2449251.613	2449251.692	0.07859412
2449251.675	2449251.675	5.51799E-05
2449295.263	2449295.302	0.03879332
2449295.32	2449295.32	5.07301E-05
2449307.704	2449307.715	0.01102176
2449307.766	2449307.766	5.51799E-05
2449429.602	2449429.71	0.108

Figure 2.68 Comparison of the original time and the corrected time for NGC 5457.

Original HJD (T_0)	Corrected HJD (T_{crr})	T_{crr}-T_0
2449521.832	2449521.832	0
2449530.612	2449530.636	0.023940133
2449543.952	2449543.988	0.036373734
2449545.762	2449545.767	0.004935266
2449549.586	2449549.596	0.010426773
2449552.806	2449552.815	0.008779867
2449557.044	2449557.056	0.011555613
2449561.927	2449561.94	0.013314313
2449573.584	2449573.616	0.031784753
2449573.861	2449573.862	0.000755287
2449581.226	2449581.246	0.0200819
2449887.615	2449888.45	0.835420673
2449902.628	2449902.669	0.040935447
2449921.593	2449921.645	0.051711233
2449946.395	2449946.463	0.067626787

Figure 2.69 Comparison of the original time and the corrected time for NGC 7331.

2.3.2 $P-L$ Plots after the Time Correction to Published Times

In a previous section we presented the $P-L$ relation for each galaxy. This included a $P-L$ relation for each of the following; the published periods, the periods recovered from the DCDFT method, and the periods recovered from the ANOVA method. Here we present the $P-L$ relation for each galaxy using the HJD values time corrected from the published values. For each galaxy the DCDFT and ANOVA $P-L$ relations are given.

It should be noted at this point that the time corrections shown in the previous section were made to the HJDs published for each galaxy in the final paper for each galaxy. As can be seen the majority of those times were reported to only the third decimal place, and in some cases the second decimal place. In many instances our time corrected were in the fourth or fifth decimal place. This will be addressed in the next section.

NGC 925

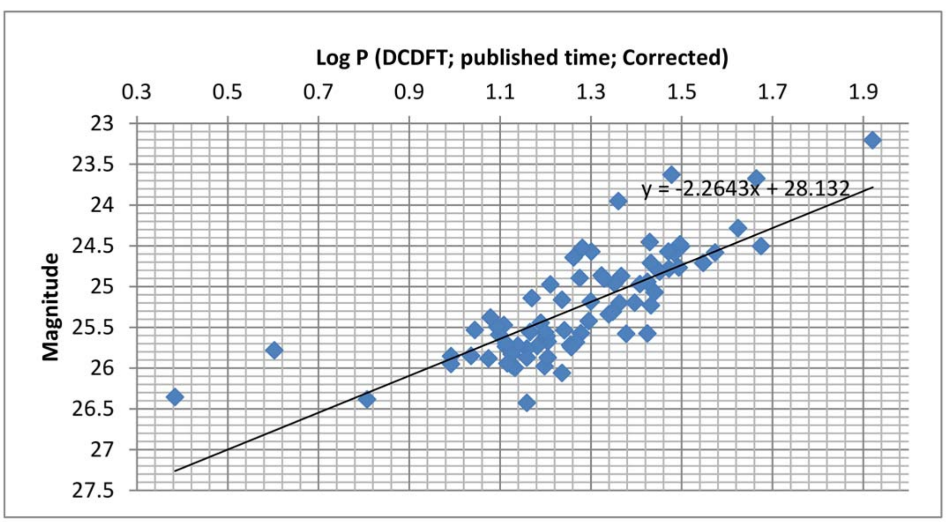

Figure 2.70 The $P-L$ Plot from DCDFT Data after Time Correction and the Linear Fit for NGC 925.

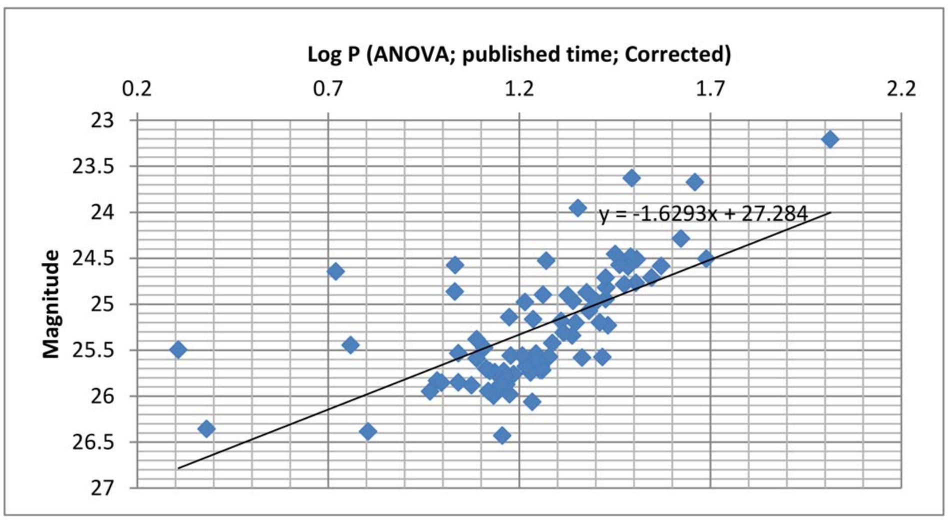

Figure 2.71 The $P-L$ Plot from ANOVA Data after Time Correction and the Linear Fit for NGC 925.

NGC 1326A

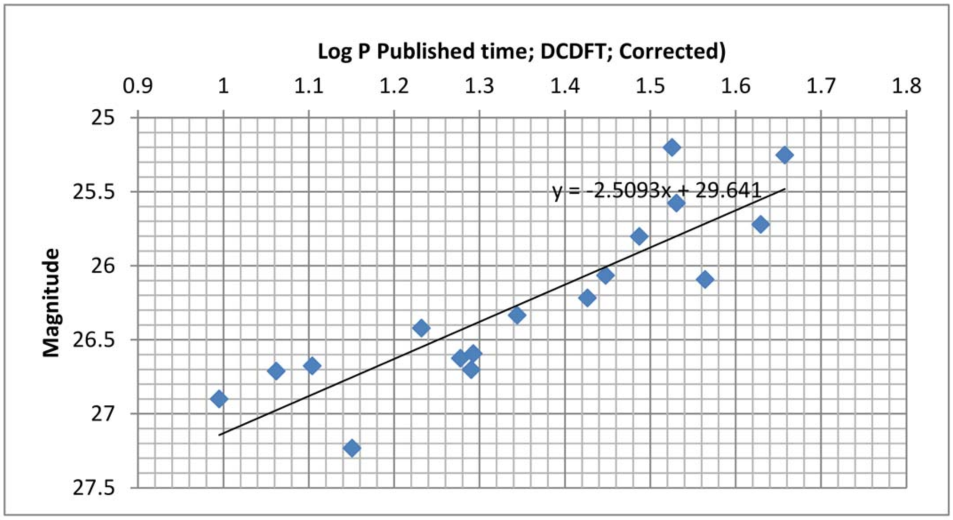

Figure 2.72 The $P-L$ Plot from DCDFT Data after Time Correction and the Linear Fit for NGC 1326A.

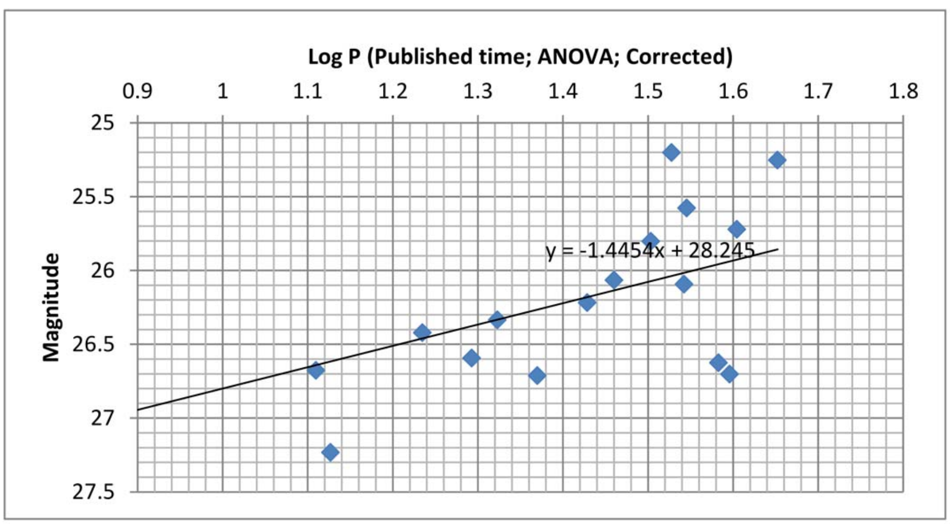

Figure 2.73 The $P-L$ Plot from ANOVA Data after Time Correction and the Linear Fit for NGC 1326A.

NGC 1365

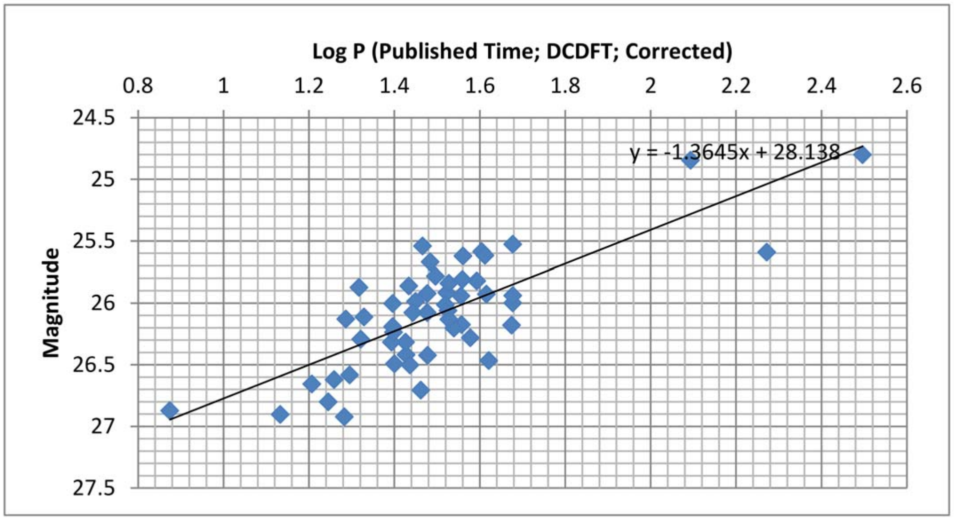

Figure 2.74 The $P-L$ Plot from DCDFT Data after Time Correction and the Linear Fit for NGC 1365.

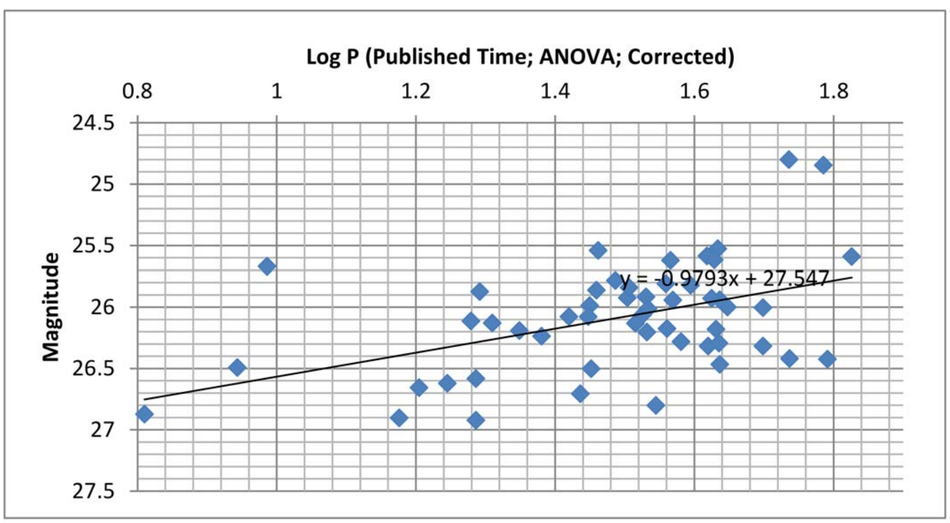

Figure 2.75 The $P-L$ Plot from ANOVA Data after Time Correction and the Linear Fit for NGC 1365.

NGC 2090

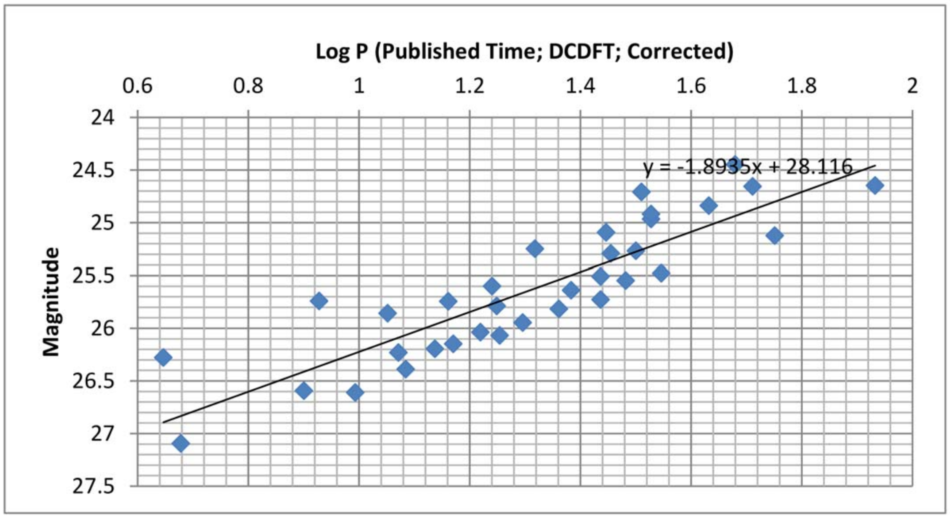

Figure 2.76 The $P-L$ Plot from DCDFT Data after Time Correction and the Linear Fit for NGC 2090.

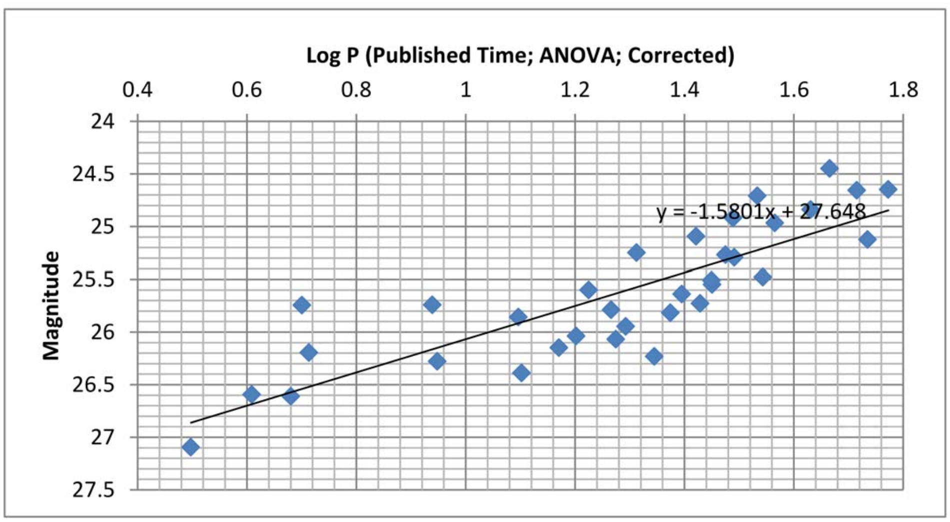

Figure 2.77 The $P-L$ Plot from ANOVA Data after Time Correction and the Linear Fit for NGC 2090.

NGC 2541

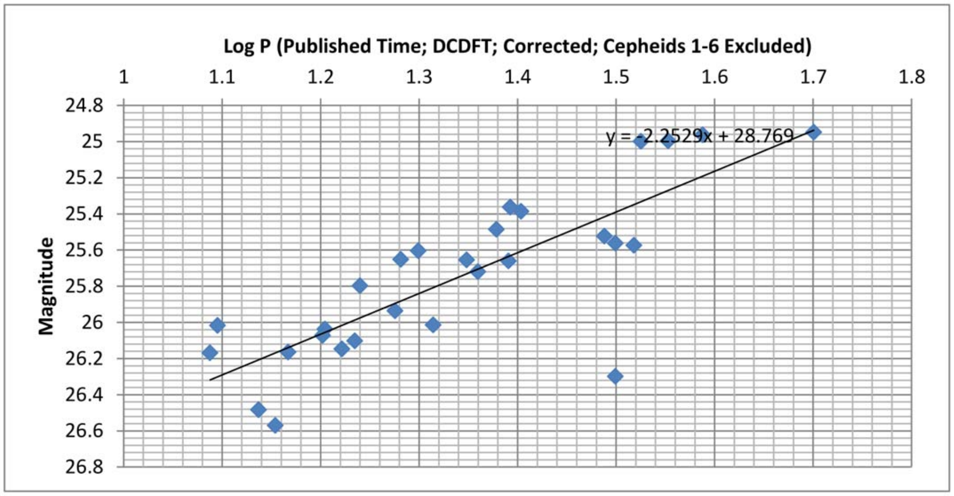

Figure 2.78 The $P-L$ Plot from DCDFT Data after Time Correction and the Linear Fit for NGC 2541.

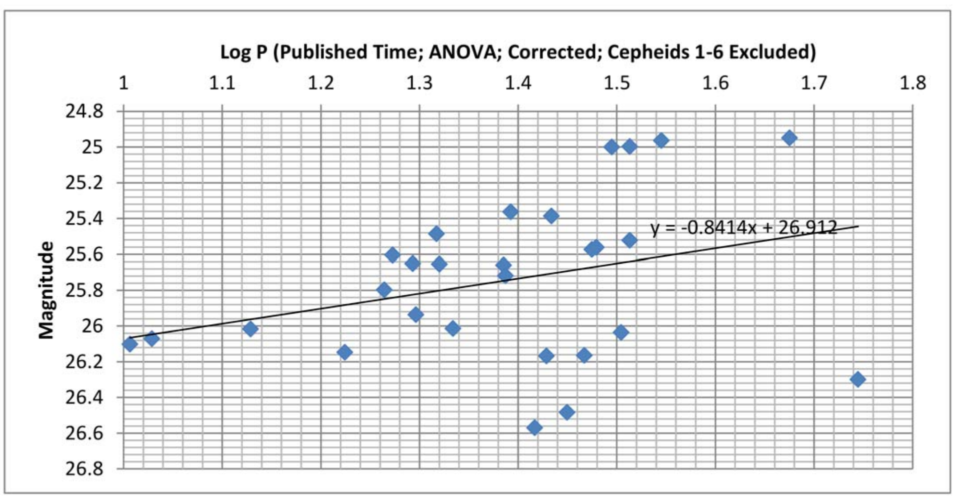

Figure 2.79 The $P-L$ Plot from ANOVA Data after Time Correction and the Linear Fit for NGC 2541.

NGC 3031

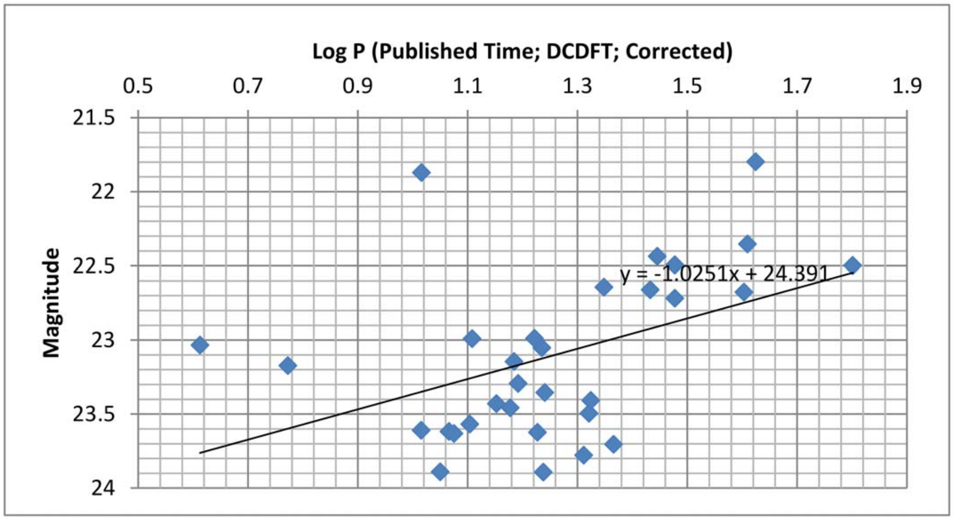

Figure 2.80 The $P-L$ Plot from DCDFT Data after Time Correction and the Linear Fit for NGC 3031.

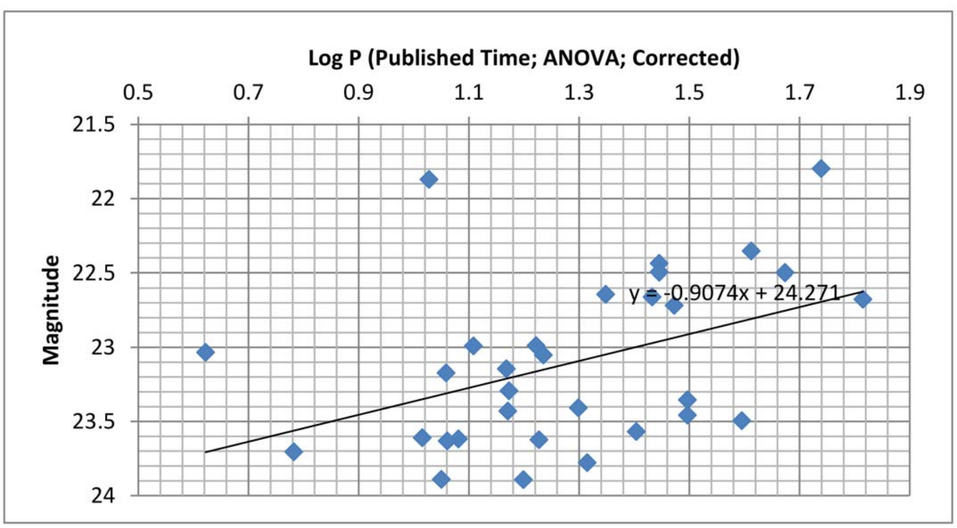

Figure 2.81 The $P-L$ Plot from ANOVA Data after Time Correction and the Linear Fit for NGC 3031.

NGC 3198

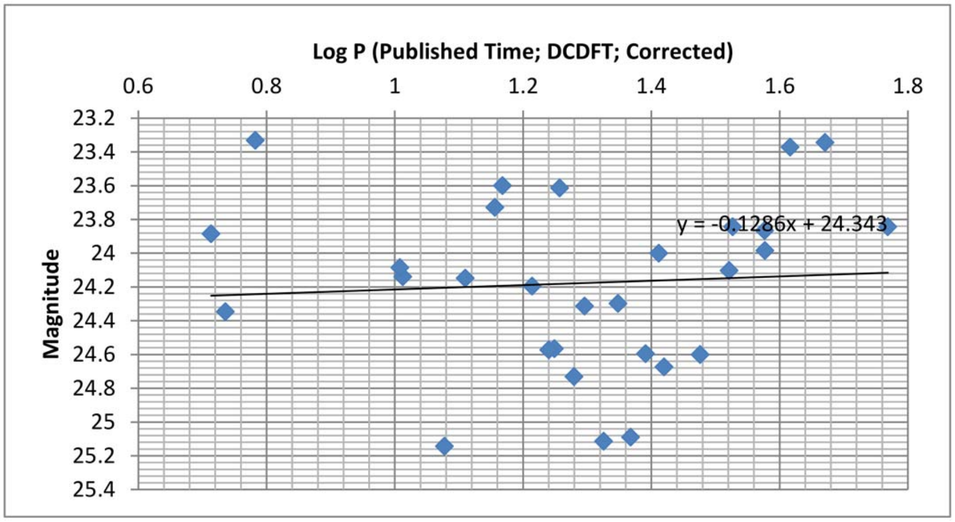

Figure 2.82 The $P-L$ Plot from DCDFT Data after Time Correction and the Linear Fit for NGC 3198.

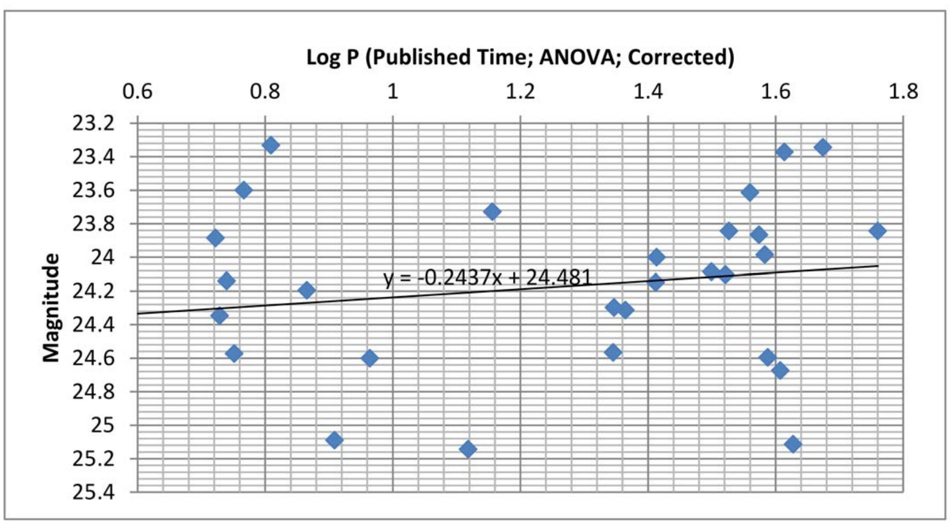

Figure 2.83 The $P-L$ Plot from ANOVA Data after Time Correction and the Linear Fit for NGC 3198.

NGC 3319

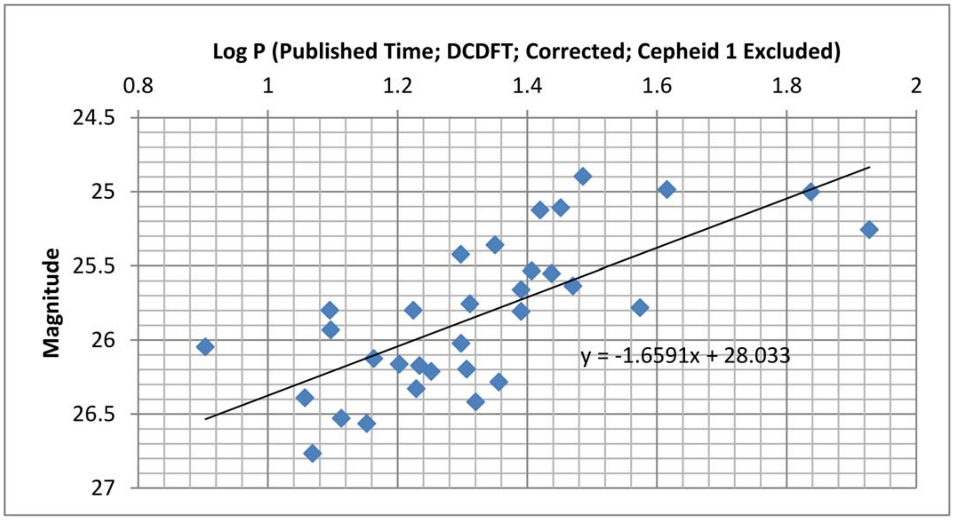

Figure 2.84 The $P-L$ Plot from DCDFT Data after Time Correction and the Linear Fit for NGC 3319.

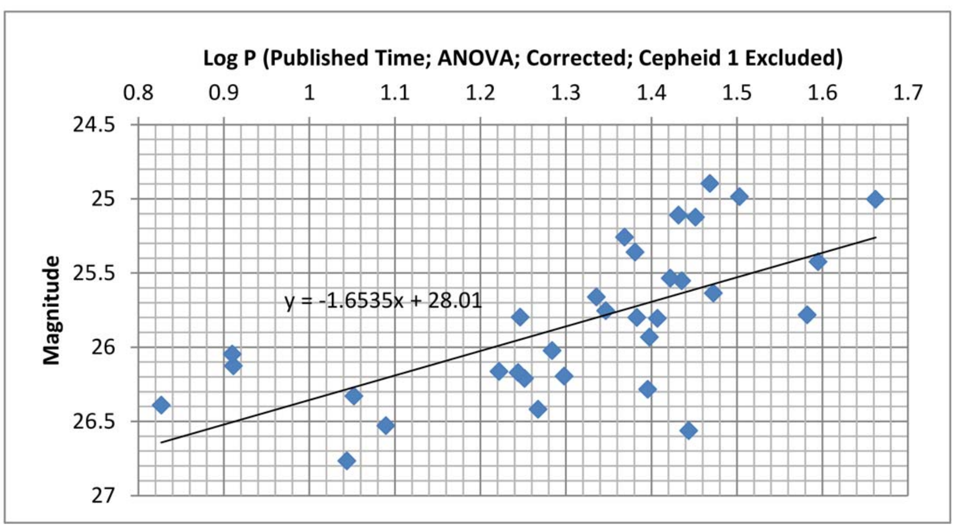

Figure 2.85 The $P-L$ Plot from ANOVA Data after Time Correction and the Linear Fit for NGC 3319.

NGC 3351

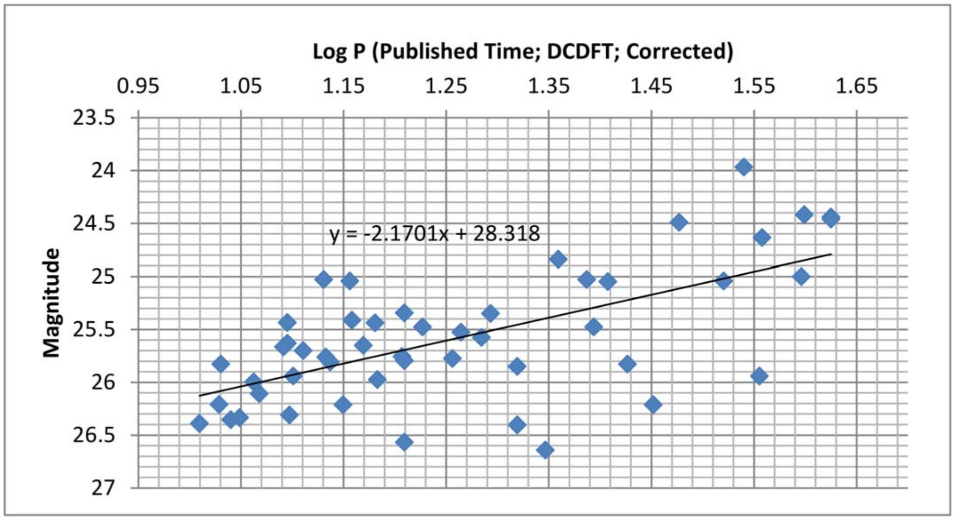

Figure 2.86 The $P-L$ Plot from DCDFT Data after Time Correction and the Linear Fit for NGC 3351.

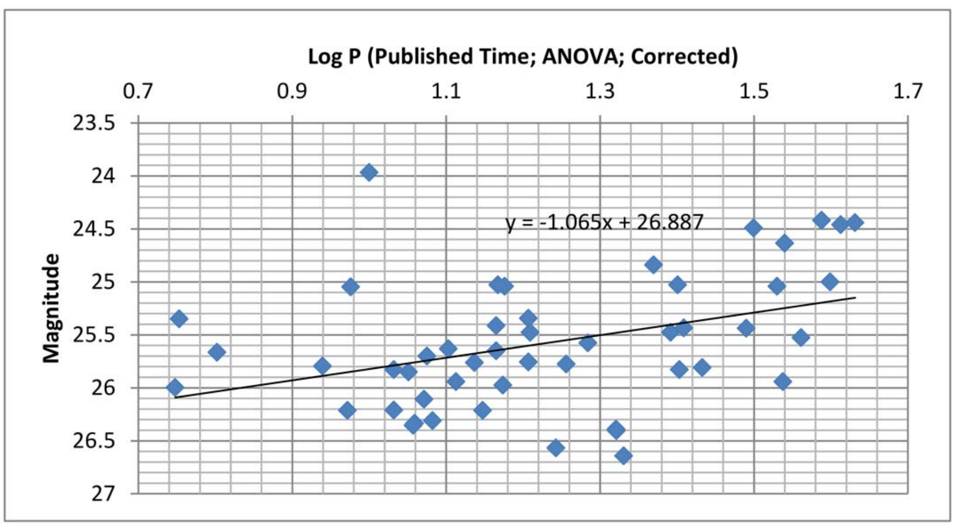

Figure 2.87 The $P-L$ Plot from ANOVA Data after Time Correction and the Linear Fit for NGC 3351.

NGC 3621

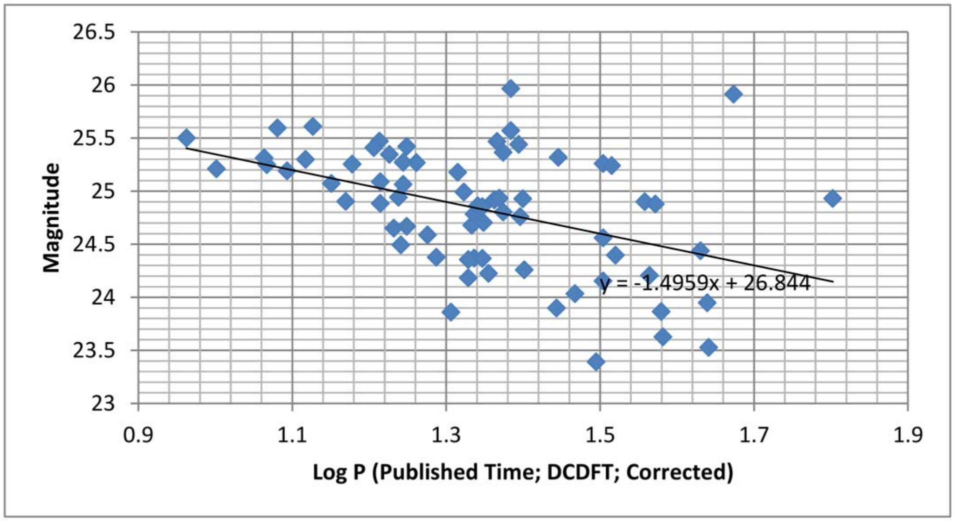

Figure 2.88 The $P-L$ Plot from DCDFT Data after Time Correction and the Linear Fit for NGC 3621.

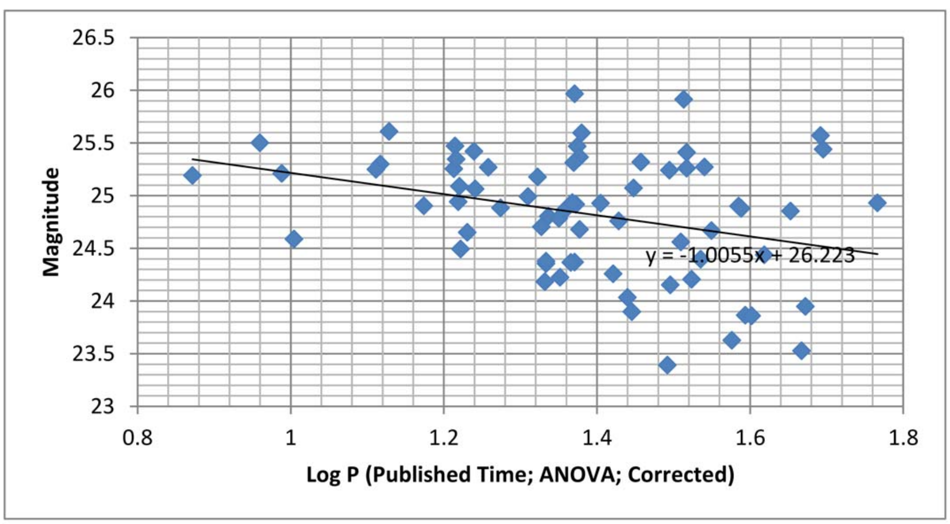

Figure 2.89 The $P-L$ Plot from ANOVA Data after Time Correction and the Linear Fit for NGC 3621.

NGC 4321

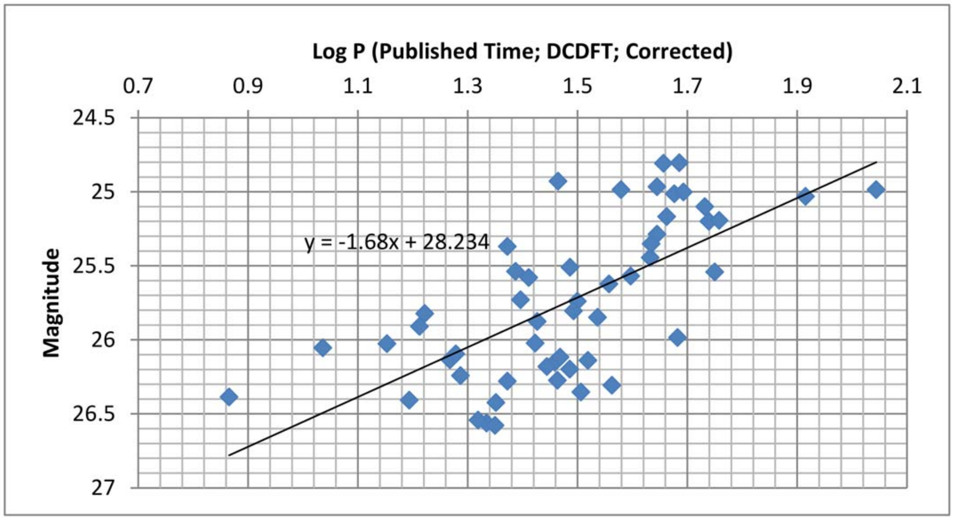

Figure 2.90 The $P - L$ Plot from DCDFT Data after Time Correction and the Linear Fit for NGC 4321.

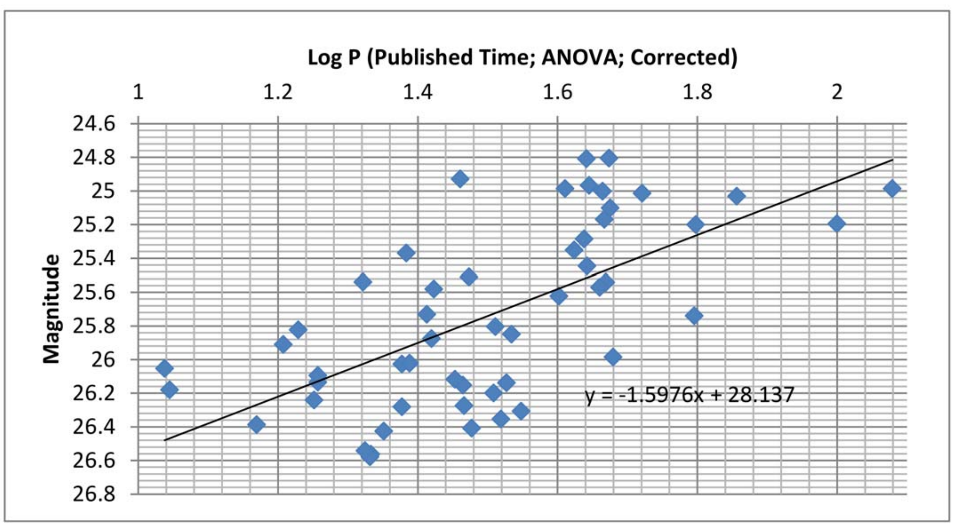

Figure 2.91 The $P - L$ Plot from ANOVA Data after Time Correction and the Linear Fit for NGC 4321.

NGC 4414

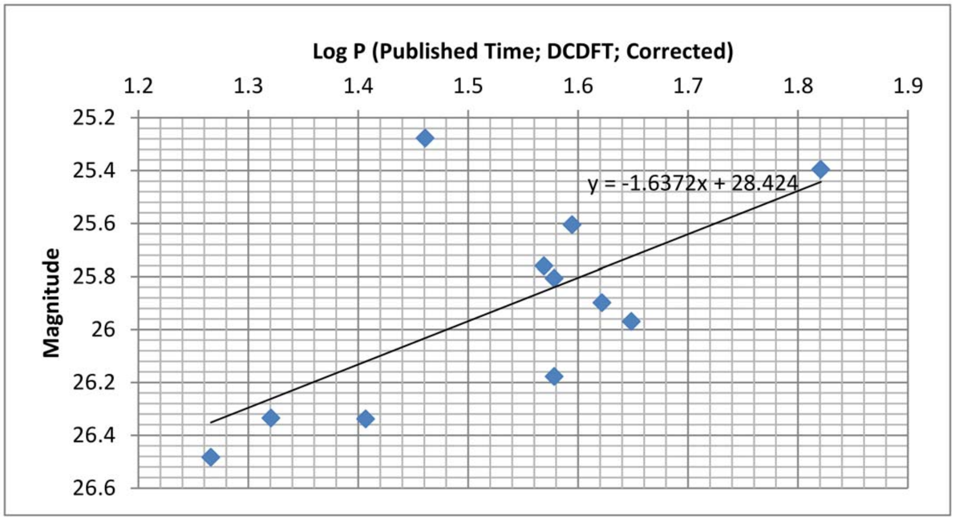

Figure 2.92 The $P-L$ Plot from DCDFT Data after Time Correction and the Linear Fit for NGC 4414.

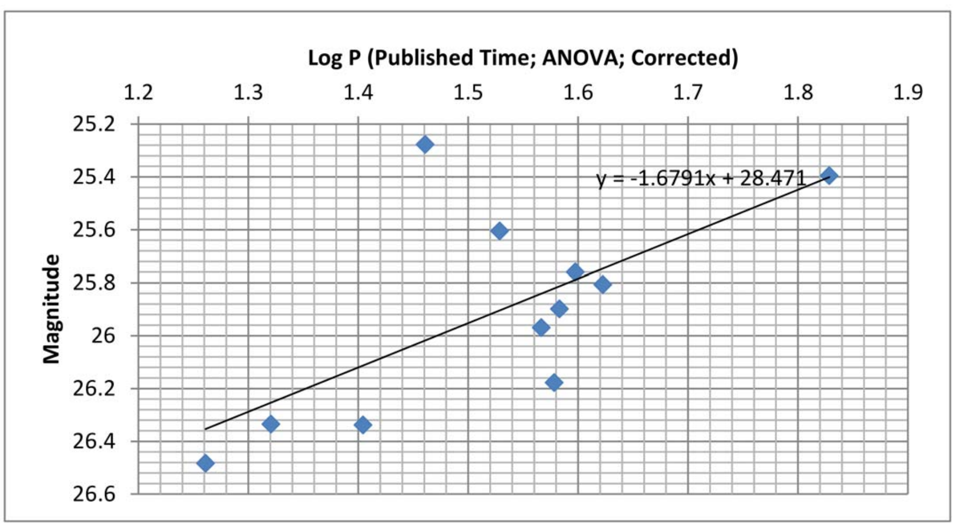

Figure 2.93 The $P-L$ Plot from ANOVA Data after Time Correction and the Linear Fit for NGC 4414.

NGC 4535

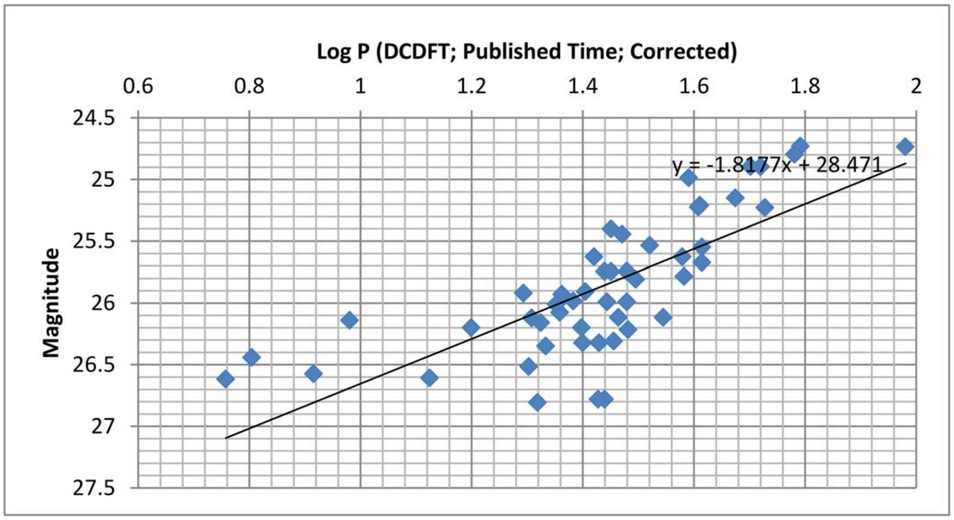

Figure 2.94 The $P-L$ Plot from DCDFT Data after Time Correction and the Linear Fit for NGC 4535.

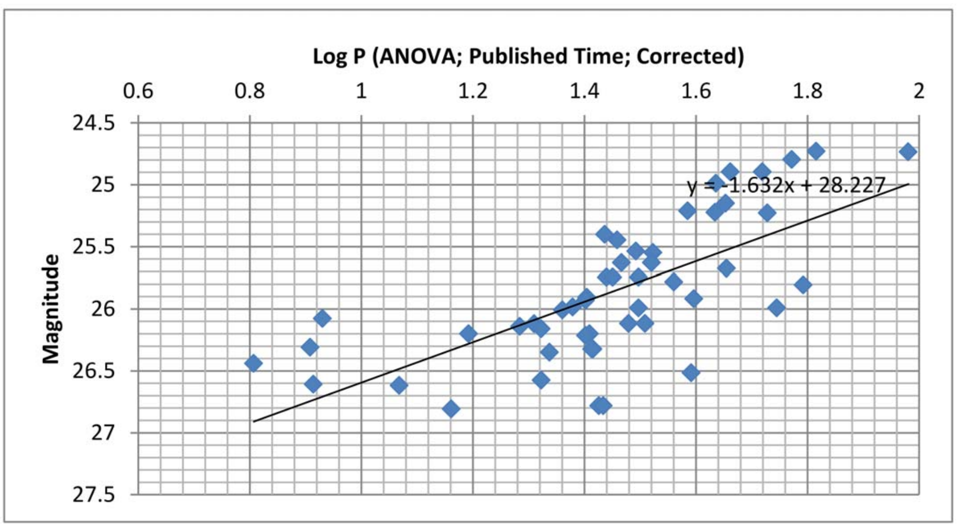

Figure 2.95 The $P-L$ Plot from ANOVA Data after Time Correction and the Linear Fit for NGC 4535.

NGC 4548

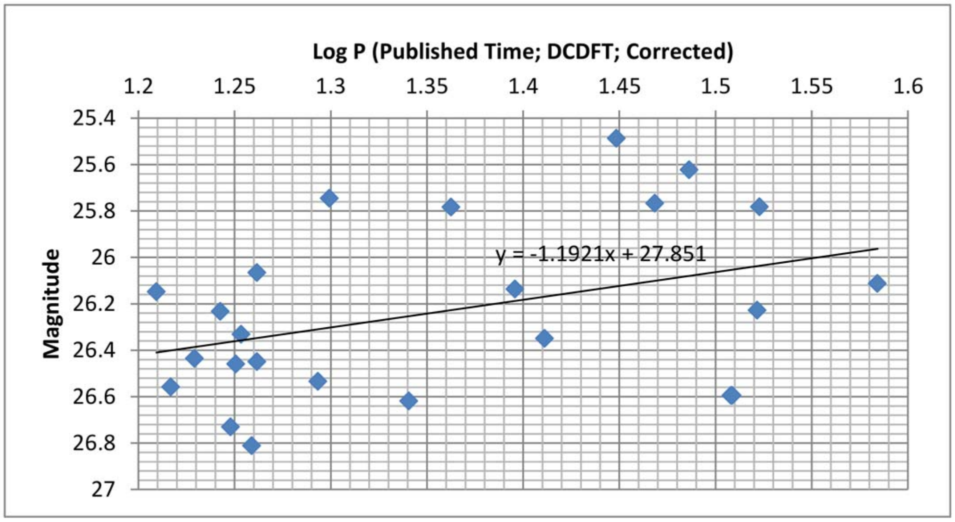

Figure 2.96 The $P-L$ Plot from DCDFT Data after Time Correction and the Linear Fit for NGC 4548.

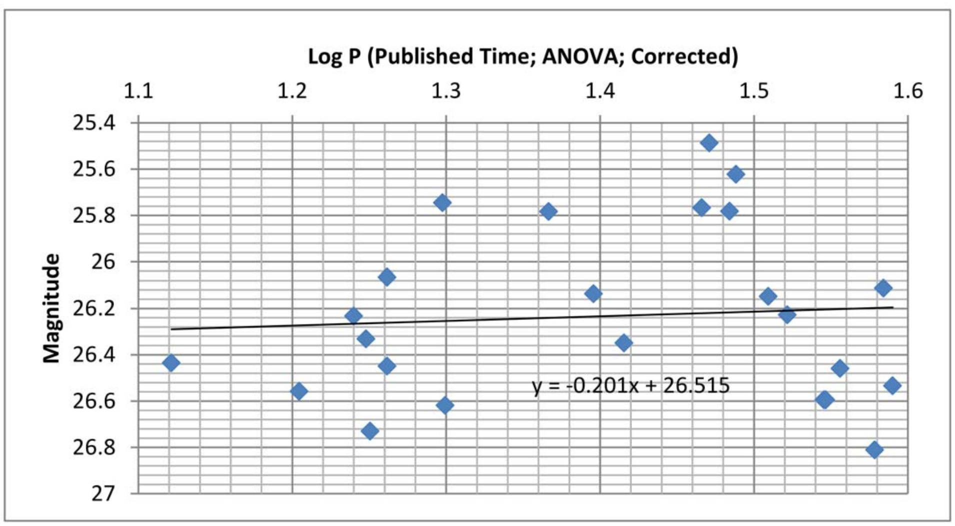

Figure 2.97 The $P-L$ Plot from ANOVA Data after Time Correction and the Linear Fit for NGC 4548.

NGC 4725

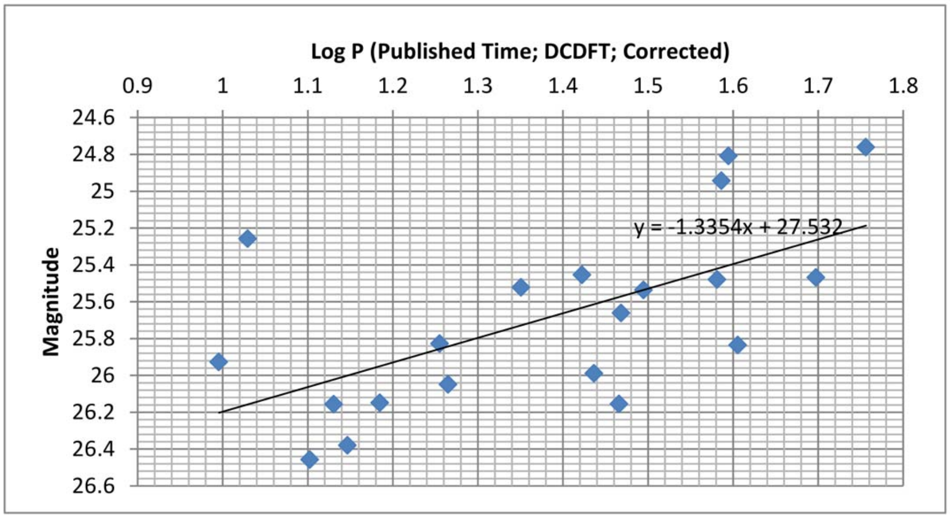

Figure 2.98 The $P-L$ Plot from DCDFT Data after Time Correction and the Linear Fit for NGC 4725.

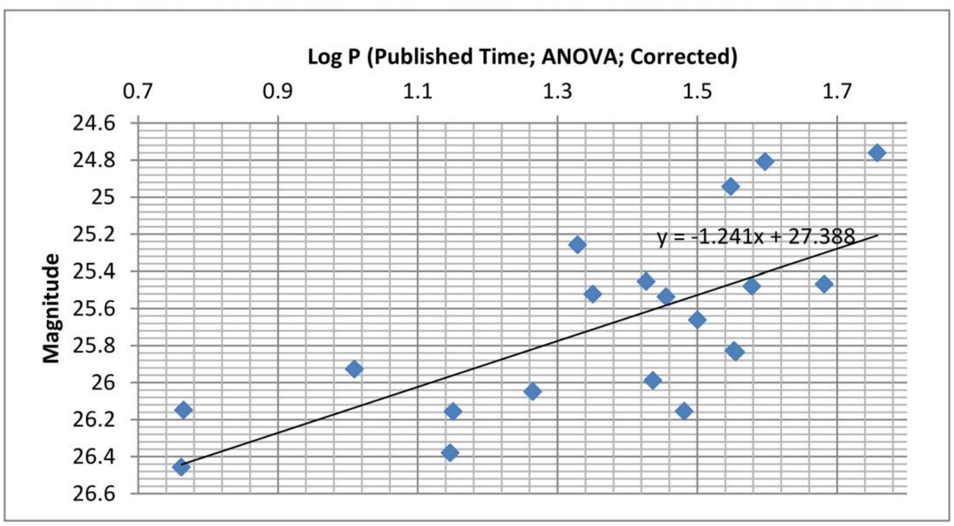

Figure 2.99 The $P-L$ Plot from ANOVA Data after Time Correction and the Linear Fit for NGC 4725.

NGC 5457

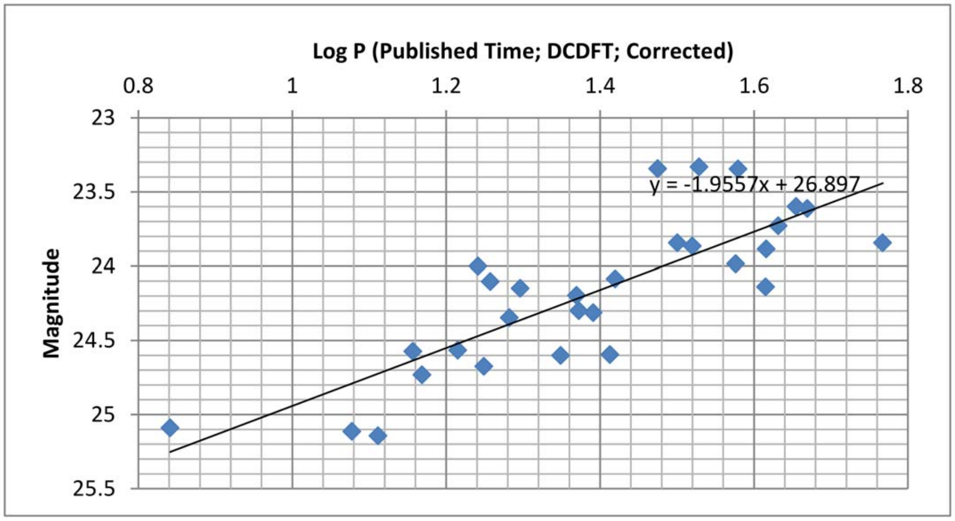

Figure 2.100 The $P-L$ Plot from DCDFT Data after Time Correction and the Linear Fit for NGC 5457.

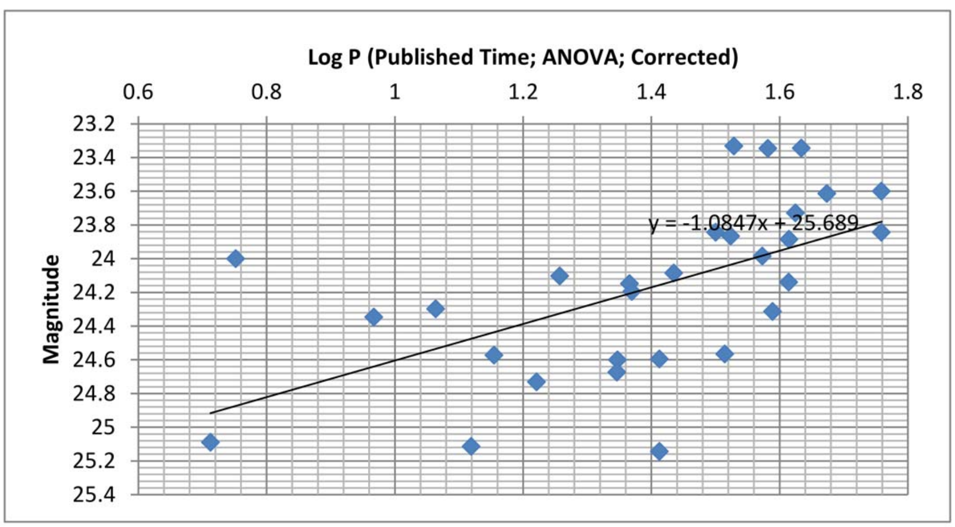

Figure 2.101 The $P-L$ Plot from ANOVA Data after Time Correction and the Linear Fit for NGC 5457.

NGC 7331

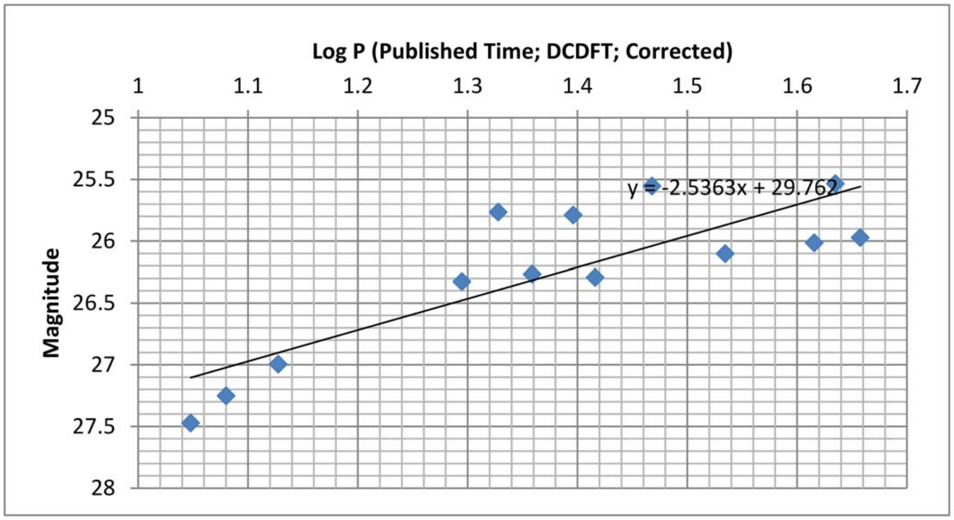

Figure 2.102 The $P-L$ Plot from DCDFT Data after Time Correction and the Linear Fit for NGC 7331.

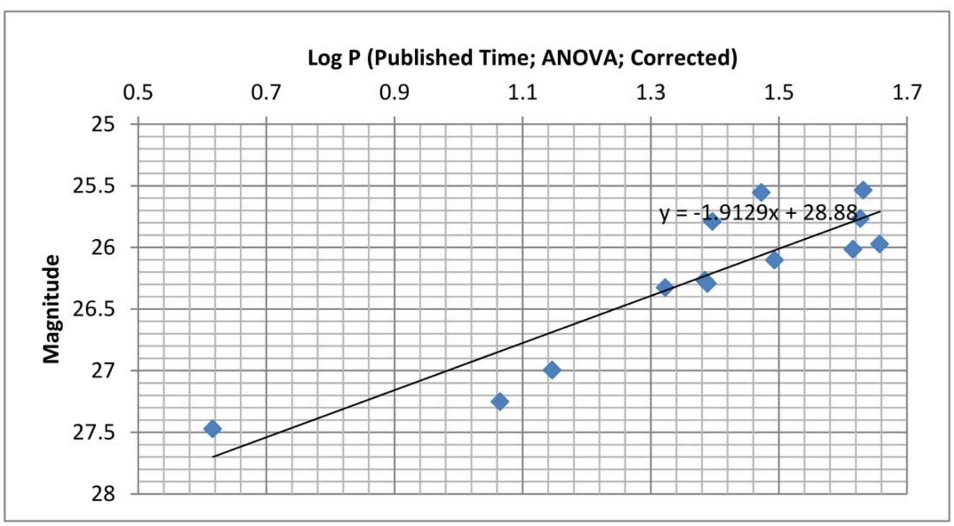

Figure 2.103 The $P-L$ Plot from ANOVA Data after Time Correction and the Linear Fit for NGC 7331.

2.4 Stage Three: Recovery and Time Correction Using More Accurate Time Inputs

2.4.1 Time from HST Headers

By comparing the slopes presented in Table 3.1, we observe that time correction does not seem to have a significant influence on the $P-L$ relation of our sample galaxies, even those with relatively large recessional velocities such as NGC 1365 ($v_{recessional} = 1665$ km/s) and NGC 4535 ($v_{recessional} = 1957$ km/s). At the same time, the effect is almost negligible (one part in 10^8) for galaxies with smaller recessional velocities, such as NGC 3031 ($v_{recessional} = -42$ km/s). However, as expressed in the last section there was a concern about the number of decimal places reported in the published results. For the entire sample of galaxies the most accurate times given were to 3 decimal places. This means the precision of these number is on the order of 2 minutes. We are making some time corrections on the order of a few seconds.

We wanted to see if using a more precise original time, before time correction, would have any impact on the results for the time corrected data. To do this we need to obtain the original HST frames from the archives. Using these files we could extract the time from the header of each file. However, for HST frames the time used in the header is the MJD mentioned earlier, not the traditional HJD. The difference in these two number is 0.5 days to adjust for the fact that the HJD system is based on the time of noon, not midnight. In the tables that follow this 0.5 days difference is clear, but so is the improvement in the number of decimal places in the time. Using the better MJD times from the HST headers we re-examined the slopes.

This process was done on only 4 galaxies from our data set: NGC 925, NGC 1365, NGC 3031, and NGC 4535. In the following figures we show the comparision of the published time to the time from the HST headers. Then the next figure shows the time corrected data for the same list of times for each galaxy.

Less Accurate Time Before Correction	More Accurate Time Before Correction
24490573.402	24490572.92919
24490582.043	24490581.62855
24490591.472	24490591.97195
24490594.530	24490594.94996
24490597.339	24490596.83075
24490604.382	24490603.87311
24490608.609	24490608.09950
24490613.362	24490612.85227
24490618.925	24490618.41443
24490625.359	24490624.88144
24490633.335	24490632.82380
24490643.187	24490642.74973

Figure 2.104 Comparison of The Published Time and The HST Header Time before Correction for NGC 925, After Correction.

Less Accurate Time After Correction	More Accurate Time After Correction
24490573.402	24490572.92919
24490582.059	24490581.64456
24490591.489	24490591.99098
24490594.536	24490594.95544
24490597.344	24490596.83421
24490604.395	24490603.88607
24490608.617	24490608.10728
24490613.371	24490612.86102
24490618.935	24490618.42466
24490625.371	24490624.89334
24490633.350	24490632.83841
24490643.205	24490642.76799

Figure 2.105 Comparison of The Published Time and HST Header Time before Correction for NGC 925, After Correction.

Less Accurate Time Before Correction	More Accurate Time Before Correction
2449936.164	2449936.16322
2449943.937	2449943.93579
2449951.31	2449951.30836
2449953.659	2449953.65766
2449956.204	2449956.20280
2449959.223	2449959.21310
2449962.309	2449962.30732
2449965.728	2449965.72641
2449969.414	2449969.41183
2449974.238	2449974.23544
2449980.27	2449980.26704
2449985.295	2449985.29204

Figure 2.106 Comparison of The Published Time and HST Header Time before Correction for NGC 1365, Before Correction.

Less Accurate Time After Correction	More Accurate Time After Correction
2449936.164	2449936.16322
2449943.98	2449943.97893
2449951.351	2449951.34927
2449953.672	2449953.67070
2449956.218	2449956.21693
2449959.24	2449959.22981
2449962.326	2449962.32449
2449965.747	2449965.74539
2449969.434	2449969.43228
2449974.265	2449974.26221
2449980.303	2449980.30051
2449985.323	2449985.31993

Figure 2.107 Comparison of The Published Time and HST Header Time before Correction for NGC 1365, After Correction.

Less Accurate Time Before Correction	More Accurate Time Before Correction
2448620.6	2448620.60472
2448620.612	2448620.61722
2448621.536	2448621.54257
2448630.493	2448630.49951
2448641.213	2448641.22034
2448641.956	2448641.96270
2448643.224	2448643.23076
2448644.567	2448644.57382
2448646.365	2448646.37000
2448646.377	2448646.38250
2448649.188	2448649.19534
2448653.136	2448653.14083
2448653.148	2448653.15333
2448657.704	2448657.71131
2448662.852	2448662.85680
2448662.864	2448662.86930
2448984.166	2448984.17313
2448987.246	2448987.25299
2448992.272	2448992.27938
2449000.029	2449000.03632
2449012.208	2449012.21479
2449029.177	2449029.18424

Figure 2.108 Comparison of The Published Time and HST Header Time before Correction for NGC 3031, Before Correction.

Less Accurate Time After Correction	More Accurate Time After Correction
2448620.6	2448620.60472
2448620.612	2448620.61722
2448621.536	2448621.54244
2448630.492	2448630.49826
2448641.211	2448641.21884
2448641.956	2448641.96260
2448643.224	2448643.23058
2448644.567	2448644.57363
2448646.365	2448646.36974
2448646.377	2448646.38249
2448649.188	2448649.19495
2448653.135	2448653.14028
2448653.148	2448653.15333
2448657.703	2448657.71068
2448662.851	2448662.85608
2448662.864	2448662.86930
2448984.121	2448984.12814
2448987.246	2448987.25256
2448992.271	2448992.27867
2449000.028	2449000.03523
2449012.206	2449012.21309
2449029.175	2449029.18186

Figure 2.109 Comparison of The Published Time and HST Header Time before Correction for NGC 3031, After Correction.

Less Accurate Time Before Correction	More Accurate Time Before Correction
2449512.47	2449512.53631
2450227.55	2450227.59296
2450235.59	2450235.63462
2450246.32	2450246.35916
2450249.14	2450249.14128
2450252.08	2450252.12282
2450255.31	2450255.30621
2450259.05	2450259.09157
2450263.08	2450263.07913
2450267.49	2450267.53555
2450274.34	2450274.33815
2450287.26	2450287.33639
2450302.14	2450302.18324

Figure 2.110 Comparison of The Published Time and HST Header Time before Correction for NGC 4535, Before Correction.

Less Accurate Time After Correction	More Accurate TimeAfter Correction
2449512.47	2449512.53631
2450232.22	2450232.25751
2450235.64	2450235.68708
2450246.39	2450246.42912
2450249.16	2450249.15943
2450252.10	2450252.14227
2450255.33	2450255.32698
2450259.07	2450259.11626
2450263.11	2450263.10514
2450267.52	2450267.56462
2450274.39	2450274.38253
2450287.34	2450287.42118
2450302.24	2450302.28009

Figure 2.111 Comparison of The Published Time and HST Header Time before Correction for NGC 4535, After Correction.

2.4.2 Comparison of $P-L$ Relation for HST Header Times

In this section we will explore the impact of using the higher precision times taken directly from the HST headers. This will be a comparision of the non-time correct $P-L$ relation vs. the time correct $P-L$ relation. This was done for only the 4 galaxies detailed in the last section, NGC 925, NGC 1365, NGC 3031, and NGC 4535. On each of the following pages we will display two graphs. First will be the $P-L$ relation for the the non-time corrected data using the HST header times. Then we will show the $P-L$ relation for the same data with the time correction included. Each galaxy will be represented on two consecutive pages. First we will show the impact of the time correction when we use the DCDFT period solution package. The following page would then show the same results from the ANOVA period solutions.

It is interesting to note that in the case of the DCDFT results for NGC 925 the curve is much tighter for the time corrected data. For NGC 4535 we see a smoothing out of the ANOVA results for the correction of those stars below $\log P = 1.2$, but almost the oppostie effect on the DCDFT results. In other cases it is not as clear that the relation is tighter, but the slope is clearly changed in many cases. This pattern doesn't hold for all the galaxies and in some case is reversed, but given the large data set for NGC 925 it might be interesting to follow up on this portion of the project for a number of other galaxies with large numbers of Cepheids.

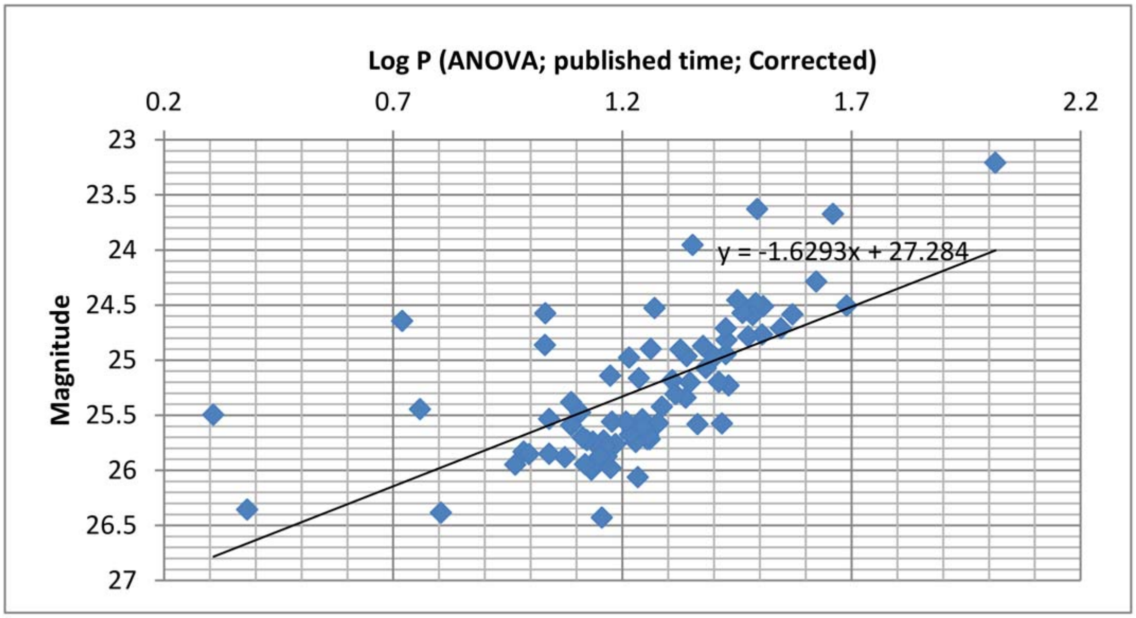

Figure 2.112 The $P-L$ plot from DCDFT data with more accurate time input before time correction for NGC 925.

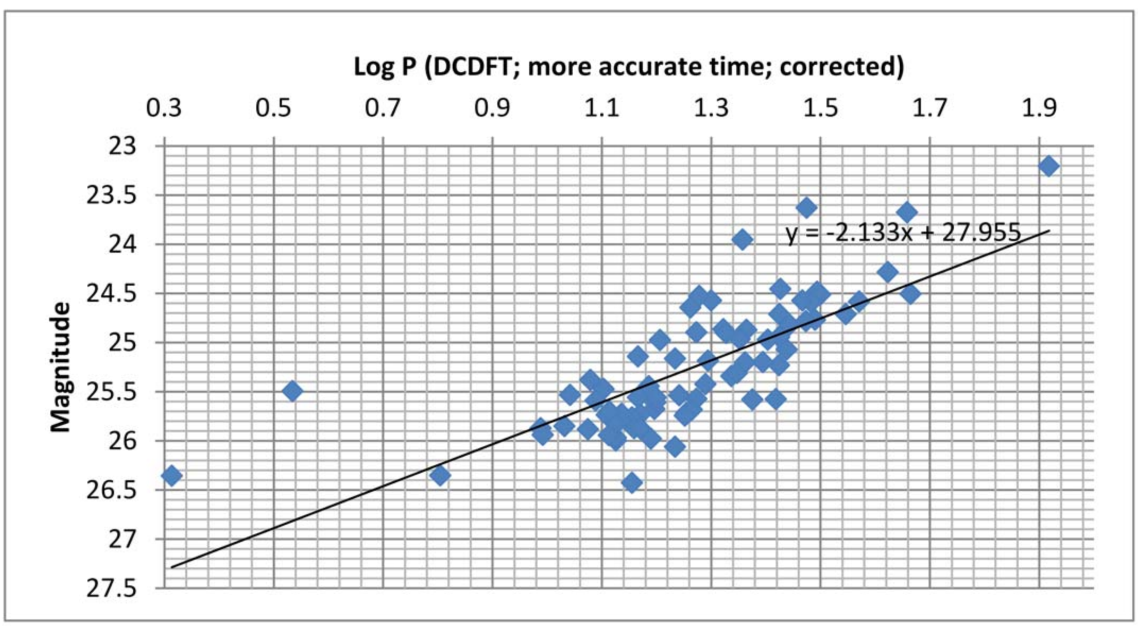

Figure 2.113 The $P-L$ plot from DCDFT data with more accurate time input after time correction and for NGC 925.

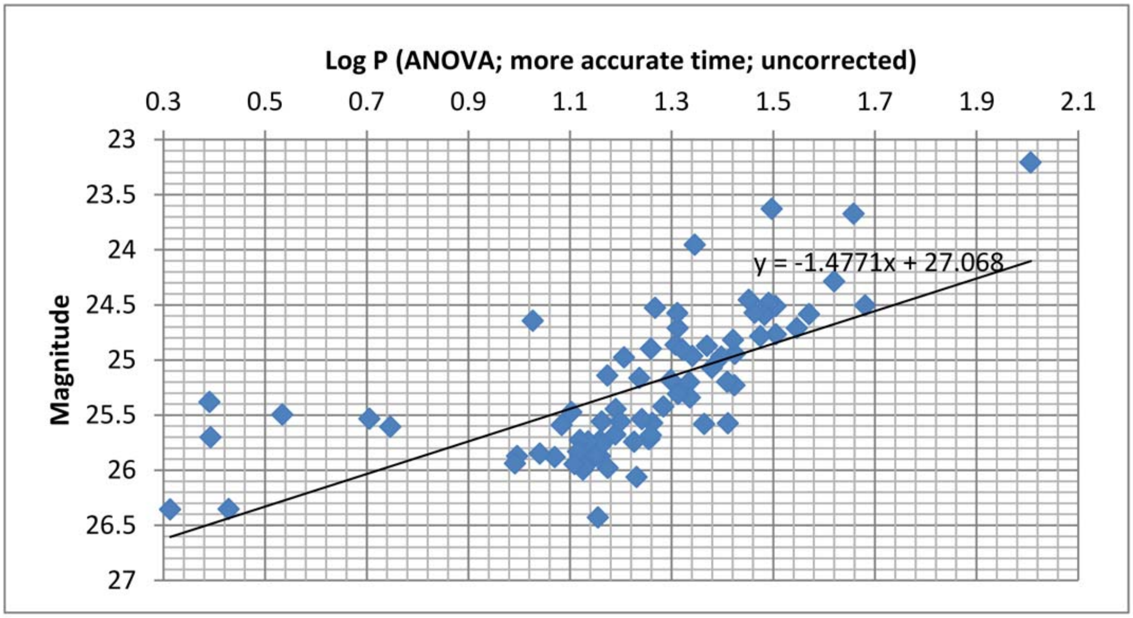

Figure 2.114 The $P-L$ plot from ANOVA data with more accurate time input before time correction for NGC 925.

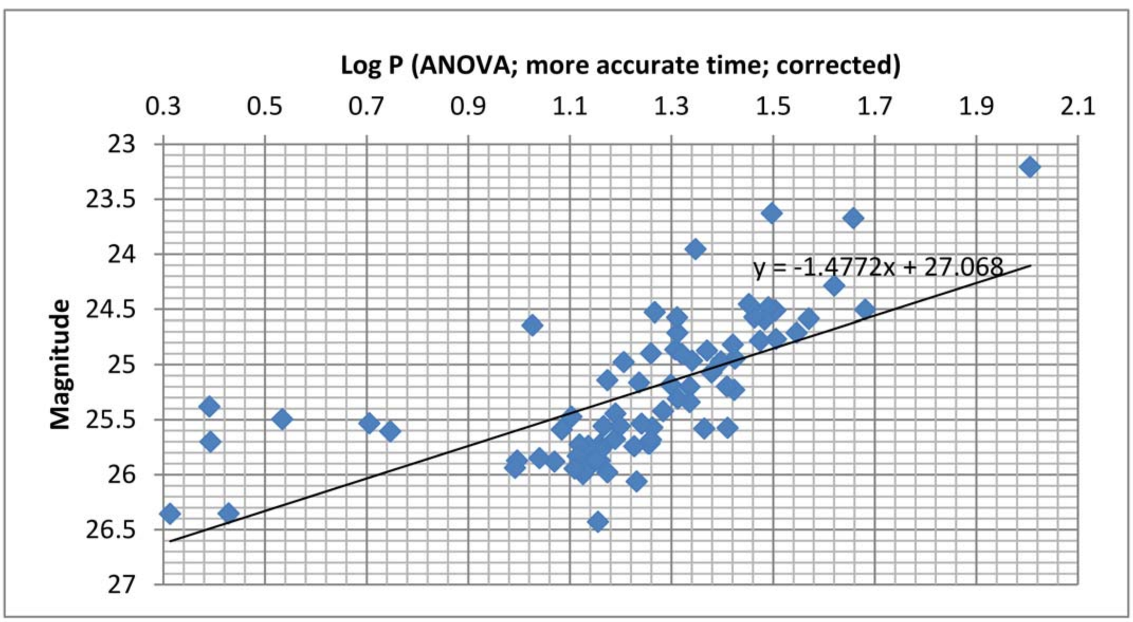

Figure 2.115 The $P-L$ plot from ANOVA data with more accurate time input after time correction for NGC 925.

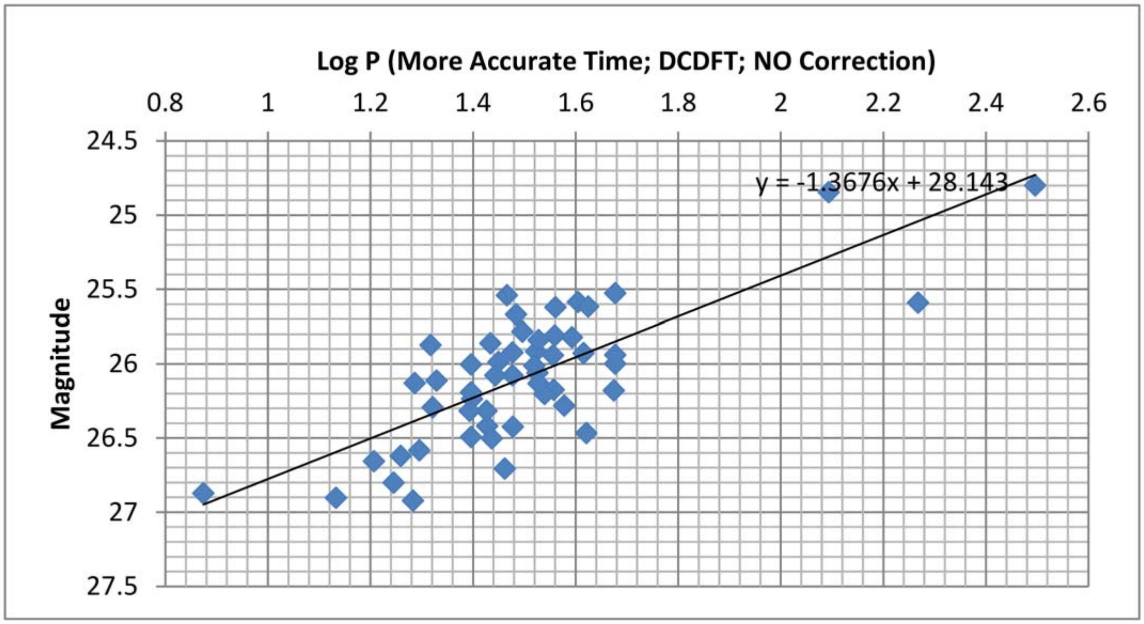

Figure 2.116 The $P-L$ plot from DCDFT data with more accurate time input before time correction and the linear fit for NGC 1365.

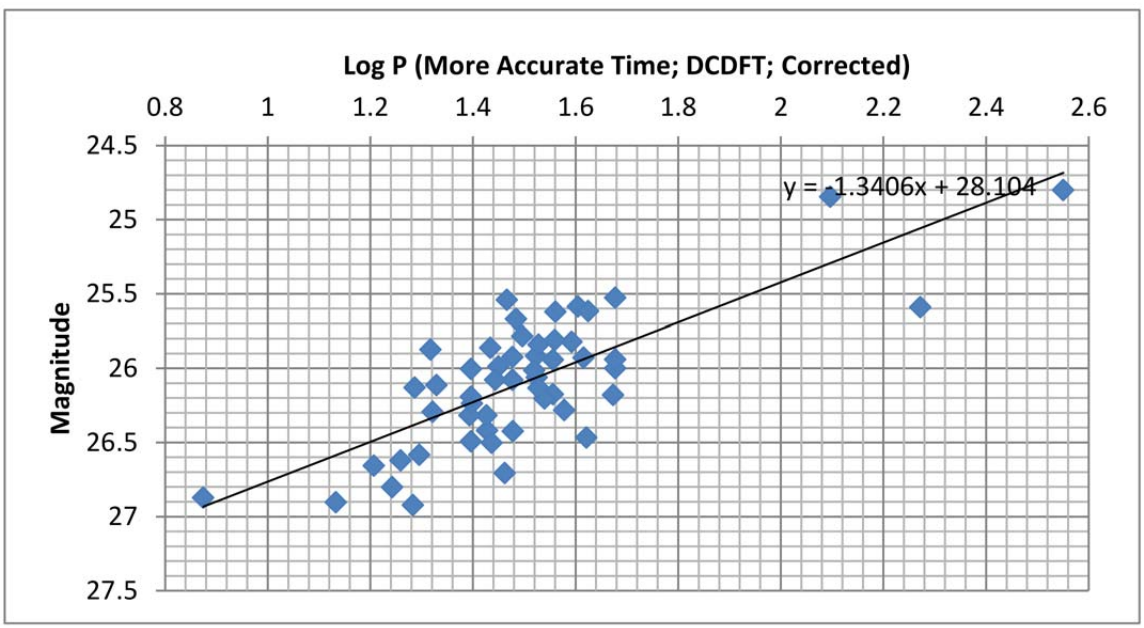

Figure 2.117 The $P-L$ plot from DCDFT data with more accurate time input after time correction and the linear fit for NGC 1365.

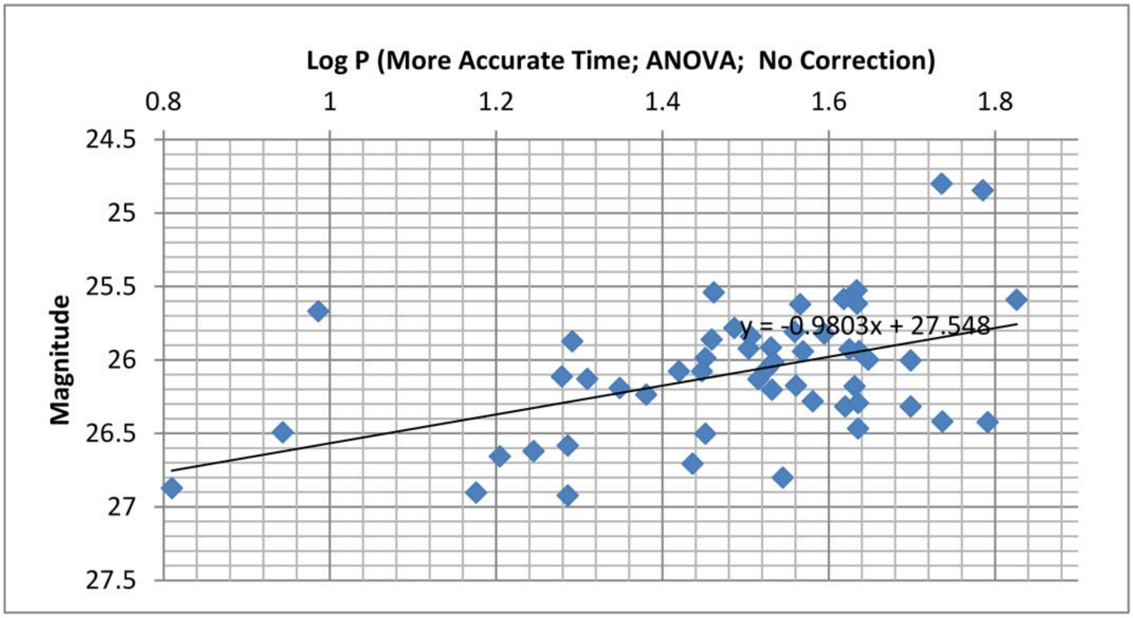

Figure 2.118 The $P-L$ plot from ANOVA data with more accurate time input before time correction and the linear fit for NGC 1365.

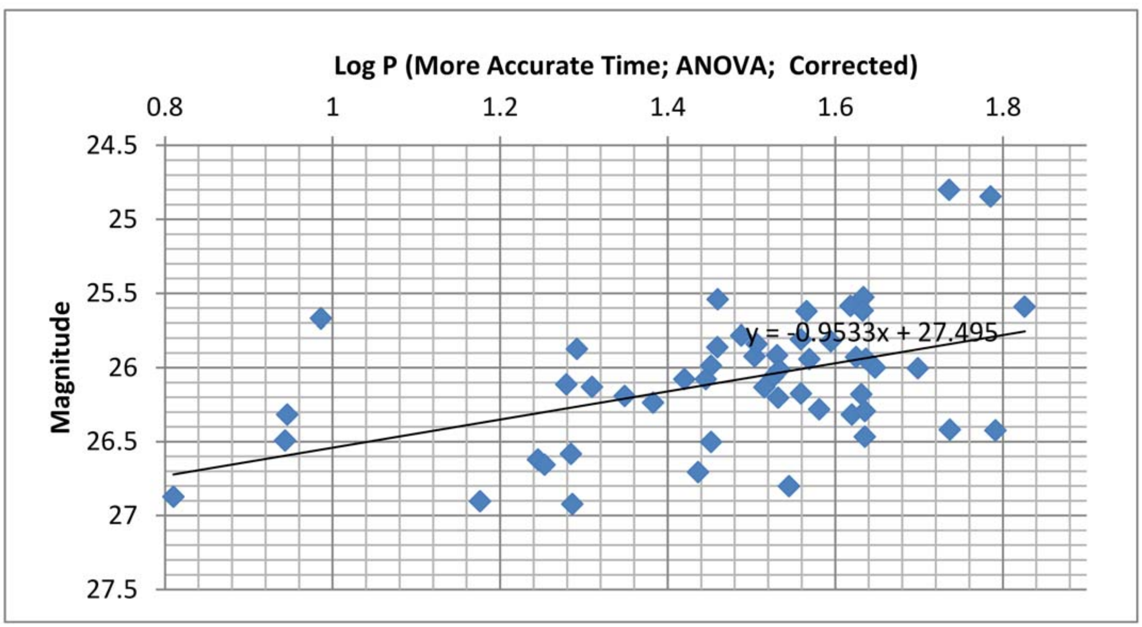

Figure 2.119 The $P-L$ plot from ANOVA data with more accurate time input after time correction and the linear fit for NGC 1365.

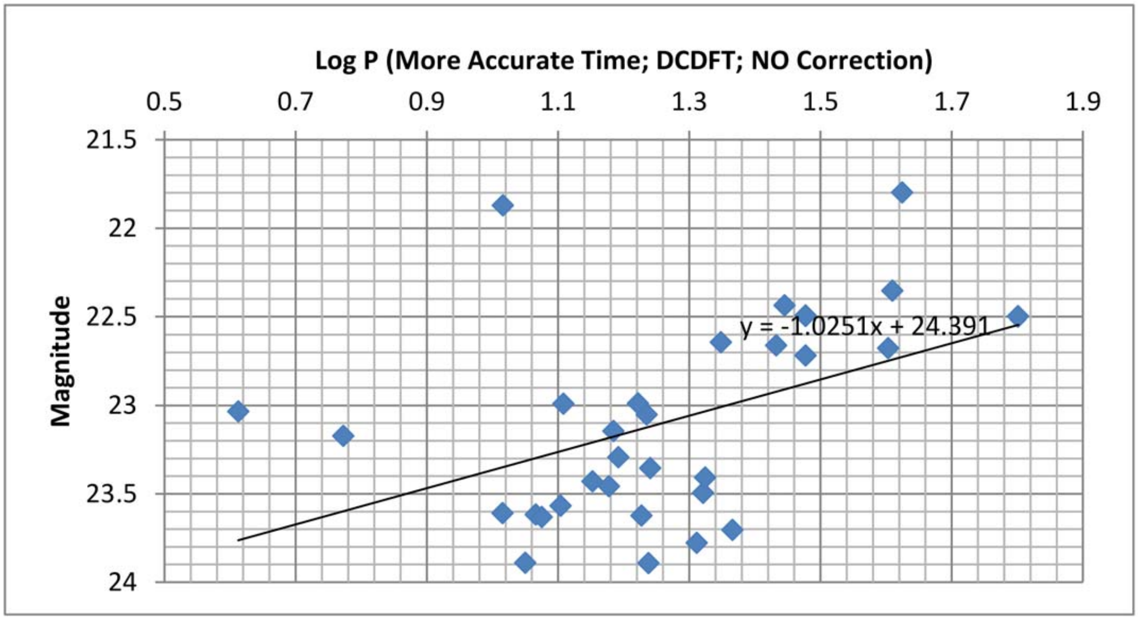

Figure 2.120 The $P-L$ plot from DCDFT data with more accurate time input before time correction and the linear fit for NGC 3031.

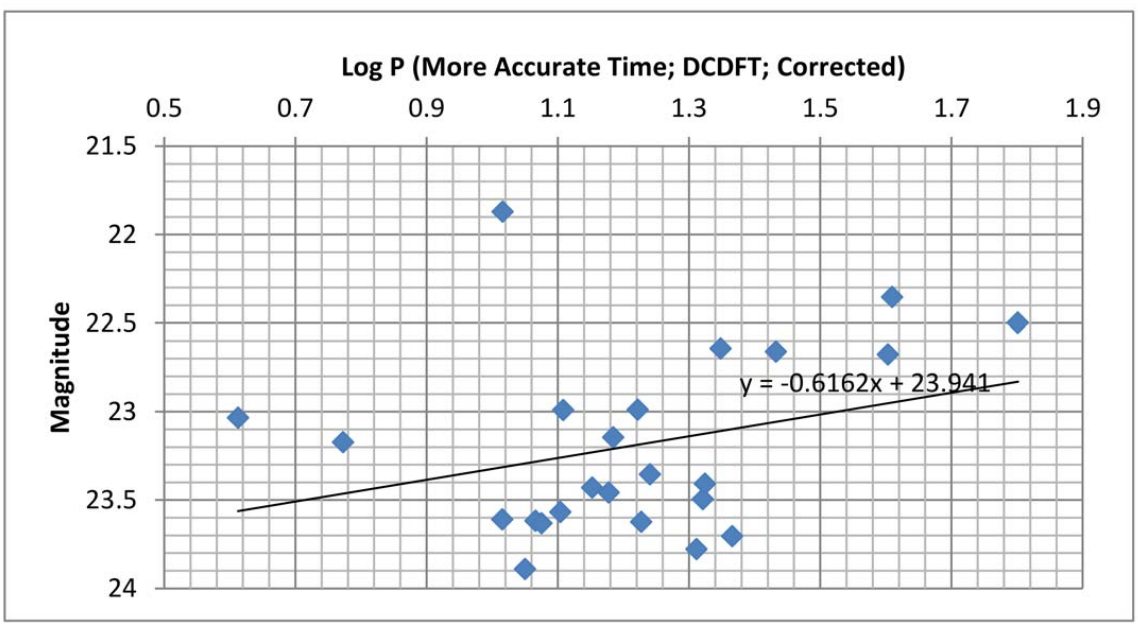

Figure 2.121 The $P-L$ plot from DCDFT data with more accurate time input after time correction and the linear fit for NGC 3031.

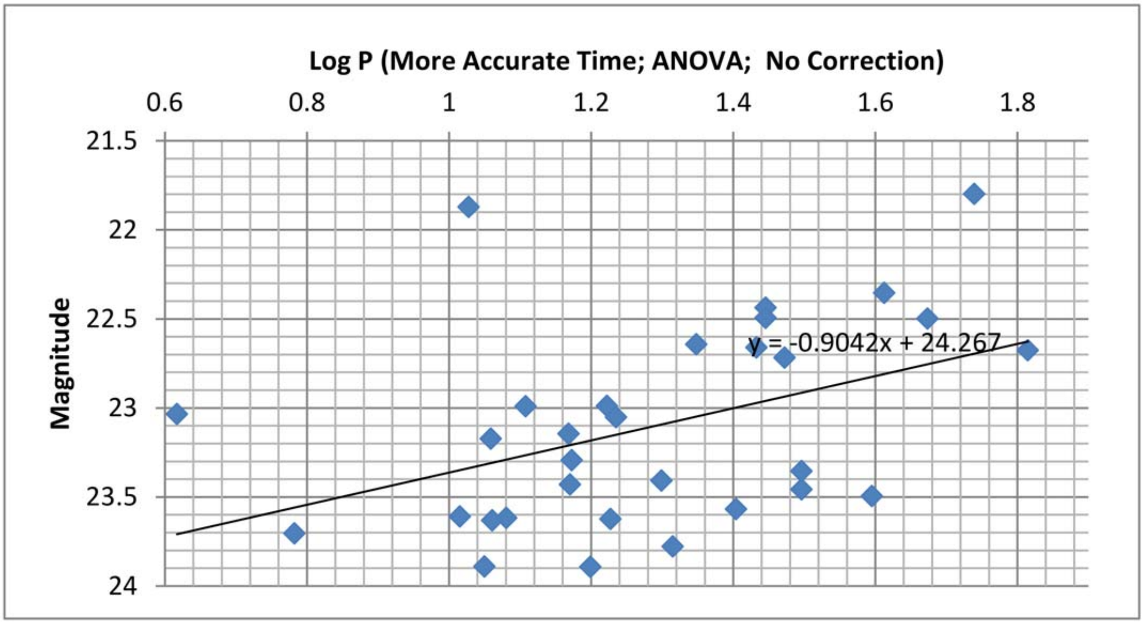

Figure 2.122 The $P-L$ plot from ANOVA data with more accurate time input before time correction and the linear fit for NGC 3031.

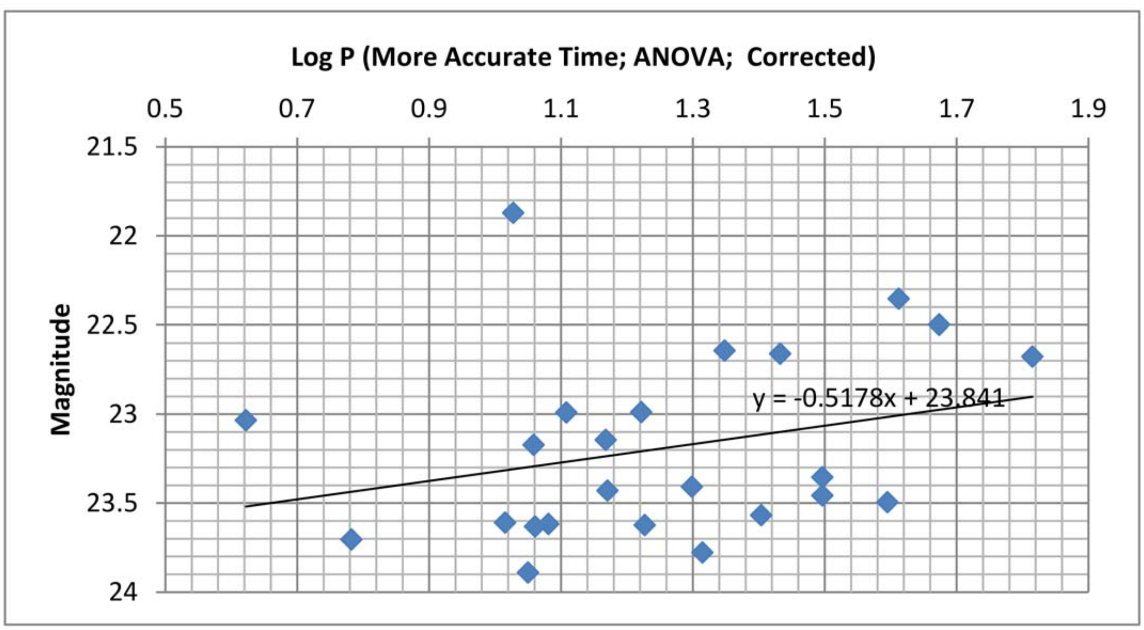

Figure 2.123 The $P-L$ plot from ANOVA data with more accurate time input after time correction and the linear fit for NGC 3031.

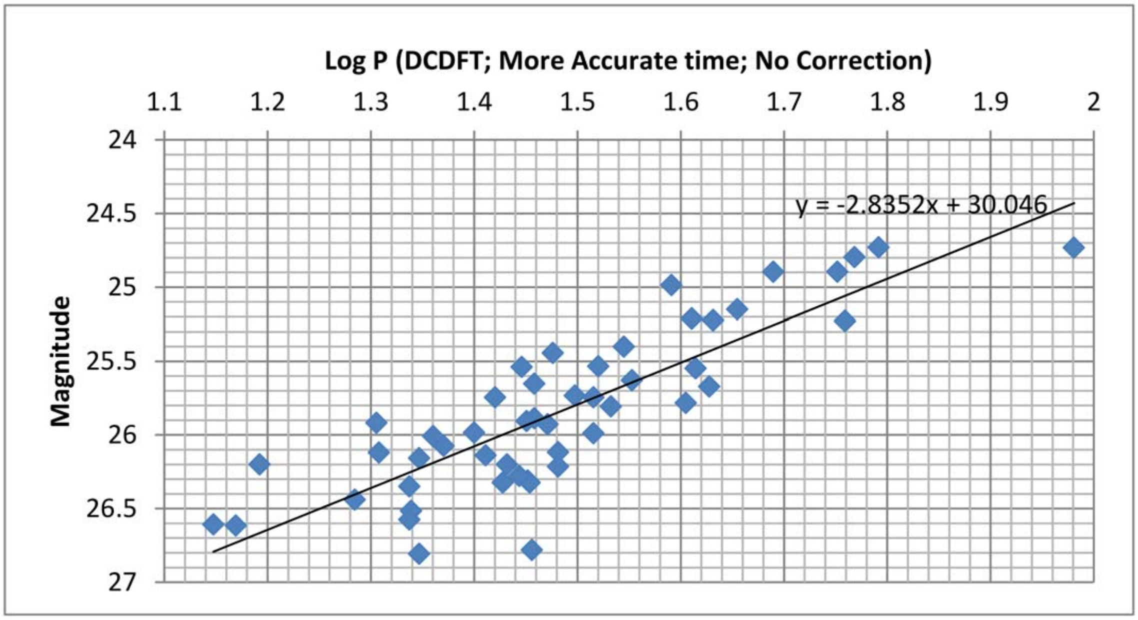

Figure 2.124 The $P-L$ plot from DCDFT data with more accurate time input before time correction and the linear fit for NGC 4535.

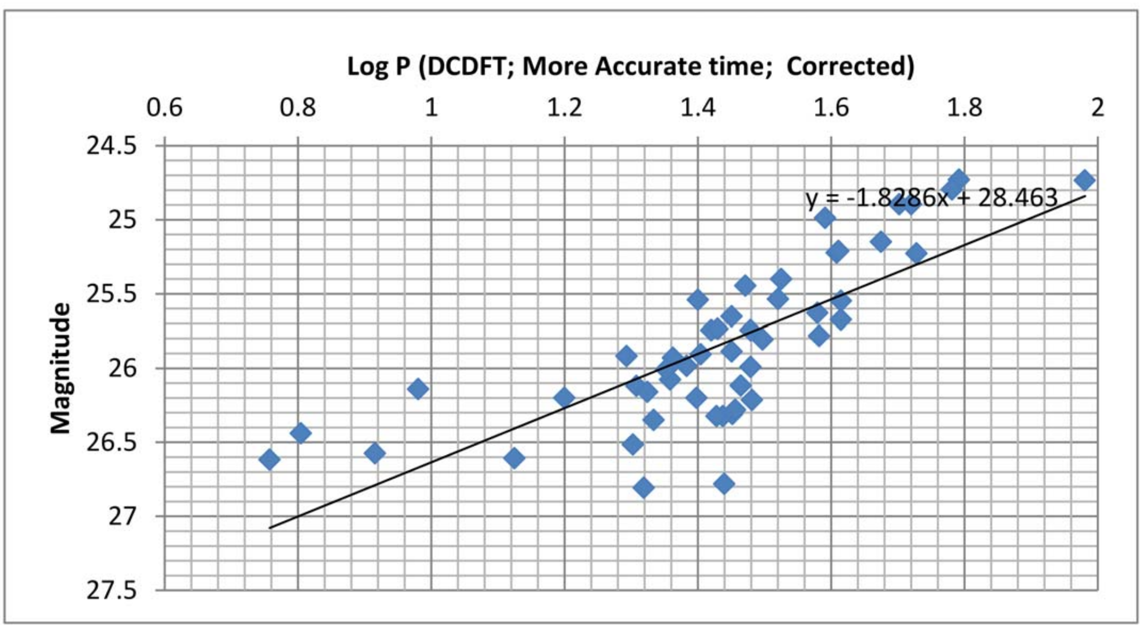

Figure 2.125 The $P-L$ plot from DCDFT data with more accurate time input after time correction and the linear fit for NGC 4535.

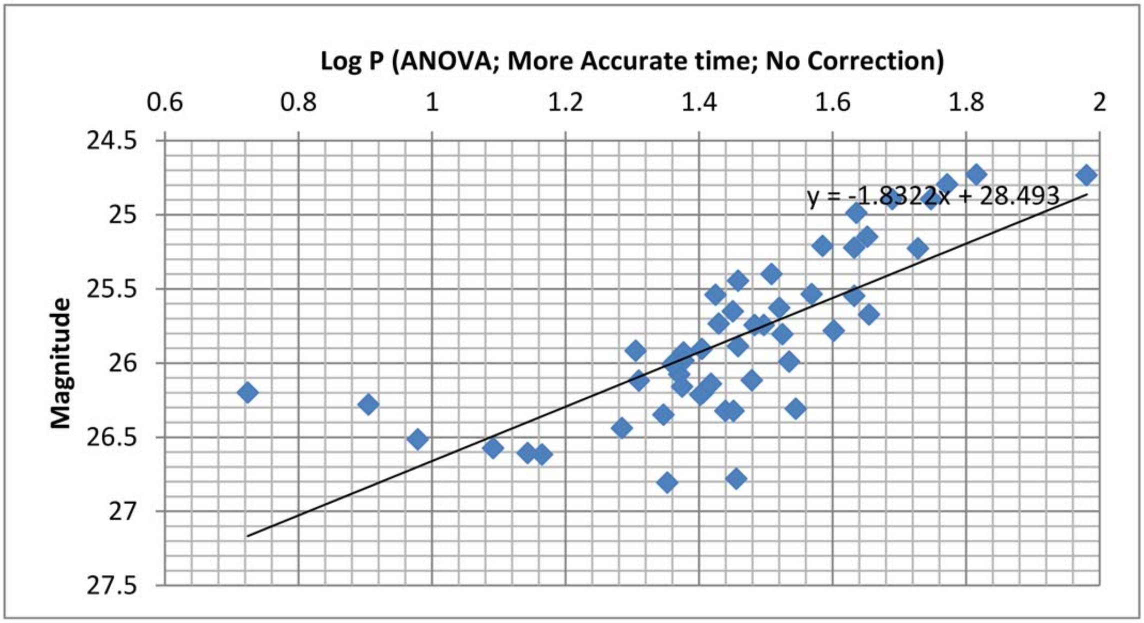

Figure 2.126 The $P-L$ plot from ANOVA data with more accurate time input before time correction and the linear fit for NGC 4535.

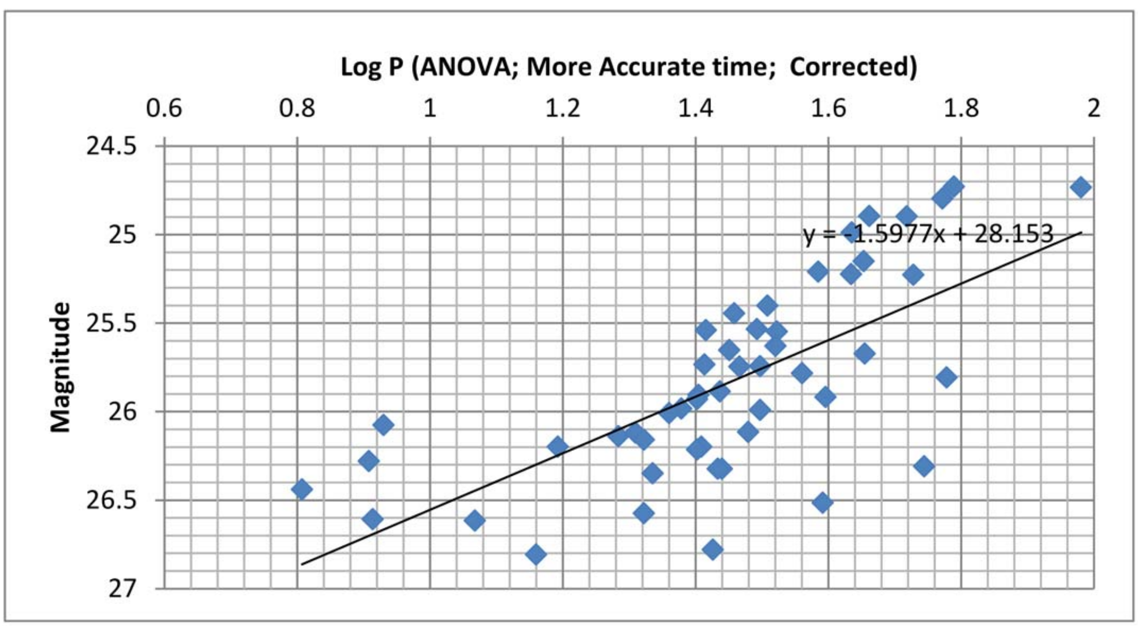

Figure 2.127 The $P-L$ plot from ANOVA data with more accurate time input after time correction and the linear fit for NGC 4535.

2.5 Summary of Potential Errors

A lot of different sources can go into the photometic errors published from the Cepheid portion of the Key Project. As each galaxy was published the authors of the paper would report on which considerations were taken into account. Some of the contributing sources are summarized here:

1. LMC true distance modulus;
2. Filter calibration;
3. Cepheid intrinsic widths (in both V and I);
4. Long vs. short exposure-time correction;
5. P-L zero point (in both V and I);
6. Metallicity of the galaxy;
7. Systematic uncertainty.

These total error (random and systematic) in magnitudes for each galaxy are listed in Table 2.19, which are quoted directly from the publications. Note that for NGC 4321 there is no total error reported. Instead, the authors calculated the errors on each chip for the AllFrame and DoPhot methods separately and did a comparison between those values (Freedman et al. 1994a).

The errors in the periods ($LogP$) are calculated using the standard deviation method

$$\sigma = \sqrt{\frac{1}{N} \times [(LogP_1 - \mu) + (LogP_2 - \mu) + ... + (LogP_N - \mu)]}, \tag{2.4}$$

where

$$\mu = \frac{1}{N} \times (LogP_1 + ... + LogP_N). \tag{2.5}$$

Tables 2.20 and 2.21 present the errors in time (σ) calculated using the published and HST header time inputs respectively.

Table 2.19. The Total Photometric Errors of Each Galaxy

Galaxy	Total Error
NGC 925	± 0.16 (Silbermann et al. 1996)
NGC 1326A	± 0.17 (Random), ± 0.13 (Systematic) (Prosser et al. 1999)
NGC 1365	± 0.20 (Random), ± 0.18 (Systematic) (Silbermann et al. 1999)
NGC 2090	± 0.16 (Phelps et al. 1998)
NGC 2541	± 0.11 (Random), ± 0.12 (Systematic) (Ferrarese et al. 1998)
NGC 3031	± 0.20 (Freedman et al. 1994b)
NGC 3198	± 0.16 (Random), ± 0.12 (Systematic) (Kelson et al. 1999)
NGC 3319	± 0.14 (Random), ± 0.10 (Systematic) (Sakai et al. 1999)
NGC 3351	± 0.19 (Graham et al. 1997)
NGC 3621	± 0.18 (Random), ± 0.16 (Systematic) (Rawson et al. 1997)
NGC 4321	N/A
NGC 4414	± 0.17 (Random), ± 0.16 (Systematic) (Turner et al. 1998)
NGC 4535	± 0.05 (Random), ± 0.26 (Systematic) (Macri et al. 1999)
NGC 4548	± 0.28 (Graham et al. 1999)
NGC 4725	± 0.16 (Random), ± 0.17 (Systematic) (Gibson et al. 1999)
NGC 5457	± 0.17 (Kelson et al. 1996)
NGC 7331	± 0.14 (Random), +0.05 ± 0.13 (Systematic) (Hughes et al. 1998)

Table 2.20. The Errors of $\log_{10} P$ Using Less Accurate Time

Galaxy	σ published	σ DCDFT Recovered	σ DCDFT Time-Corrected	σ ANOVA Recovered	σ ANOVA Time-Corrected
NGC 925	0.183	0.226	0.261	0.223	0.258
NGC 1326	0.204	0.202	0.204	0.202	0.254
NGC 1365	0.148	0.255	0.209	0.250	0.210
NGC 2090	0.249	0.275	0.258	0.293	0.338
NGC 2541	0.153	0.161	0.171	0.161	0.166
NGC 3031	0.204	0.247	0.270	0.247	0.269
NGC 3198	0.222	0.275	0.327	0.278	0.372
NGC 3319	0.174	0.215	0.190	0.216	0.201
NGC 3351	0.179	0.184	0.238	0.184	0.230
NGC 3621	0.166	0.170	0.194	0.170	0.186
NGC 4321	0.210	0.213	0.215	0.213	0.215
NGC 4414	0.160	0.158	0.157	0.158	0.156
NGC 4535	0.161	0.164	0.226	0.233	0.241
NGC 4548	0.116	0.124	0.142	0.121	0.142
NGC 4725	0.175	0.226	0.235	0.228	0.277
NGC 5457	0.186	0.213	0.271	0.213	0.272
NGC 7331	0.198	0.208	0.206	0.205	0.291

Table 2.21. The Errors of $\log_{10} P$ Using More Accurate Time

Galaxy	σ published	σ DCDFT Recovered	σ DCDFT Time-Corrected	σ ANOVA Recovered	σ ANOVA Time-Corrected
NGC 3031	0.183	0.229	0.292	0.229	0.292
NGC 1365	0.148	0.250	0.210	0.255	0.220
NGC 3031	0.204	0.247	0.270	0.256	0.283
NGC 4535	0.161	0.164	0.226	0.233	0.240

The errors in the $P-L$ slopes are calculated using the same standard deviation method as in the calculation of time-domain errors. Table 2.22 and 2.23 present the errors of the slopes using the published times and more-accurate times from the HST headers inputs respectively.

Table 2.22. The Errors of the $P-L$ Slopes before and after Time Correction Using Published Times

Galaxy	Published	DCDFT Recovered	DCDFT Time-Corrected	ANOVA Recovered	ANOVA Time-Corrected
NGC 925	0.195	0.184	0.184	0.195	0.198
NGC 1326A	0.35	0.360	0.360	0.535	0.456
NGC 1365	0.296	0.159	0.162	0.269	0.267
NGC 2090	0.184	0.184	0.186	0.266	0.179
NGC 2541	0.333	0.234	0.321	0.467	0.501
NGC 3031	0.323	0.383	0.383	0.353	0.353
NGC 3198	0.399	0.369	0.366	0.292	0.260
NGC 3319	0.375	0.306	0.303	0.381	0.348
NGC 3351	0.386	0.383	0.383	0.355	0.366
NGC 3621	0.362	0.370	0.370	0.342	0.358
NGC 4321	0.254	0.258	0.258	0.264	0.265
NGC 4414	0.646	0.618	0.627	0.631	0.628
NGC 4535	0.301	0.287	0.229	0.250	0.242
NGC 4548	0.601	0.597	0.609	0.561	0.557
NGC 4725	0.394	0.402	0.400	0.351	0.299
NGC 5457	0.307	0.270	0.270	0.281	0.296
NGC 7331	0.498	0.507	0.503	0.418	0.289

Table 2.23. The Errors of the $P - L$ Slopes before and after Time Correction Using Times from HST Headers

Galaxy	Published	DCDFT Recovered	DCDFT Time-Corrected	ANOVA Recovered	ANOVA Time-Corrected
NGC 925	0.195	0.188	0.187	0.174	0.174
NGC 1365	0.296	0.162	0.159	0.266	0.253
NGC 3031	0.323	0.390	0.405	0.353	0.374
NGC 4535	0.289	0.259	0.216	0.233	0.238

Chapter 3

Conclusion

3.1 Key Project Data Insufficient to Test Time Correction

Table 3.1 presents the slopes of the $P-L$ linear fits using the published data, the DCDFT- and ANOVA- recovered data, and the DCDFT- and ANOVA- time-corrected data for each galaxy using the less accurate time inputs. It is obvious that the time correction does not have a significant influence on the slopes.

In statistics, the Pearson correlation coefficient R^2 is used to describe the quality of a functional fit. The value of R^2 is between 0 and 1. A value close to one means the correlation is strong; otherwise the correlation is weak. We can examine the R^2 values of our $P-L$ fits in Table 3.2 and Table 3.5. We observe that about half of the R^2 values are smaller than 0.5, which indicates that their linear fits do not describe the $P-L$ correlations accurately. Some of the galaxies such as NGC 3198, NGC 3621, and NGC 4548 have extremely small correlation coefficients (smaller than 0.3). Even the greatest coefficients (NGC 2090) are smaller than 0.8. It is clear that the overall accuracy of our $P-L$ fits is not very high.

When we use the more accurate time inputs in Stage Three, we observe that there is some

Table 3.1. $P-L$ Slopes of the Recovered and Time-Corrected Data Using Less Accurate Time Inputs

Galaxy	RV km/s	Published	DCDFT Recovered	ANOVA Recovered	DCDFT Corrected	ANOVA Corrected
NGC 925	552	-2.839	-2.266	-1.609	-2.264	-1.629
NGC 1326A	1718	-2.476	-2.502	-1.938	-2.509	-1.445
NGC 1365	1665	-2.167	-1.339	-0.979	-1.365	-0.979
NGC 2090	923	-2.327	-2.059	-2.102	-1.894	-1.580
NGC 2541	557	-2.379	-2.238	-1.078	-2.253	-0.841
NGC 3031	-42	-2.170	-1.025	-0.904	-1.025	-0.907
NGC 3198	679	-0.250	-0.154	-0.344	-0.129	-0.244
NGC 3319	752	-2.070	-1.661	-1.659	-1.659	-1.654
NGC 3351	777	-2.284	-2.169	-1.003	-2.170	-1.065
NGC 3621	727	-1.809	-1.496	-0.973	-1.496	-1.006
NGC 4321	1570	-1.767	-1.680	-1.598	-1.680	-1.598
NGC 4414	717	-1.534	-1.683	-1.652	-1.637	-1.679
NGC 4535	1957	-2.796	-2.787	-1.784	-1.818	-1.63
NGC 4548	492	-1.575	-1.120	-0.193	-1.192	-0.201
NGC 4725	1207	-2.264	-1.353	-1.472	-1.335	-1.241
NGC 5457	267	-2.243	-1.953	-1.202	-1.956	-1.085
NGC 7331	818	-2.669	-2.484	-2.689	-2.536	-1.913

Table 3.2. The R^2 Values of the $P - L$ Slopes before and after Time Correction Using Less Accurate Time

Galaxy	Published	DCDFT Recovered	DCDFT Time-Corrected	ANOVA Recovered	ANOVA Time-Corrected
NGC 925	0.733	0.604	0.603	0.419	0.418
NGC 1326A	0.762	0.763	0.764	0.467	0.401
NGC 1365	0.517	0.586	0.586	0.210	0.213
NGC 2090	0.834	0.797	0.765	0.730	0.708
NGC 2541	0.663	0.649	0.655	0.170	0.098
NGC 3031	0.609	0.198	0.198	0.185	0.185
NGC 3198	0.013	0.006	0.005	0.049	0.031
NGC 3319	0.504	0.496	0.500	0.387	0.430
NGC 3351	0.427	0.405	0.406	0.145	0.153
NGC 3621	0.272	0.196	0.196	0.107	0.106
NGC 4321	0.493	0.459	0.459	0.422	0.422
NGC 4414	0.385	0.452	0.431	0.432	0.443
NGC 4535	0.642	0.662	0.567	0.515	0.487
NGC 4548	0.238	0.138	0.149	0.005	0.006
NGC 4725	0.648	0.386	0.382	0.494	0.489
NGC 5457	0.664	0.660	0.660	0.403	0.332
NGC 7331	0.723	0.685	0.698	0.790	0.800

Table 3.3. Comparison of the DCDFT and ANOVA Slopes in the Recovery Stage Using More Accurate Time

Galaxy	DCDFT Slope	ANOVA Slope
NGC 925	-2.131	-1.477
NGC 1365	-1.368	-0.980
NGC 3031	-1.025	-0.904
NGC 4535	-2.835	-1.832

disagreement in the recovery stage as compared to the outputs using less accurate time inputs. This disagreement suggests that the uncertainties in the time inputs are relatively large, which results in an even larger error in the $P-L$ fits. Table 2.22 shows that the errors in the $P-L$ slopes are mostly greater than 20%. Some galaxies such as NGC 4414 have errors as large as 50%.

The comparison of the DCDFT and ANOVA periods calculated using the more accurate time inputs before and after time correction are shown in tables 3.3 and 3.4. We do observe some significant changes in the periods for both high-velocity galaxies (such as NGC 4535) and low-velocity galaxies (such as NGC 3031). However, there is no clear evidence that these changes in periods are a direct result of time correction. Table 2.23 shows the errors in the $P-L$ slopes of these four galaxies using more accurate time inputs. We observe no improvement in accuracy if we compare the values with the ones in Table 2.22. Therefore, we conclude that the different values of $P-L$ slopes are more likely due to uncertainties in both the time inputs and the $P-L$ fits.

The answers the three questions we raised in Section 1.3 can be summarized as below:

1. Based on the our data, it is difficult to determine a critical recessional velocity at which a significant period change can be observed for a Cepheid. The low-velocity galaxies such as NGC 3031 show almost no change in Cepheid periods when time correction is applied. Even

Table 3.4. Comparison of the DCDFT and ANOVA Slopes in the Time-Correction Stage Using More Accurate Time

Galaxy	DCDFT Slope	ANOVA Slope
NGC 925	-2.133	-1.477
NGC 1365	-1.341	-0.953
NGC 3031	-0.616	-0.518
NGC 4535	-1.829	-1.598

Table 3.5. The R^2 Values of the $P-L$ Slopes before and after Time Correction Using More Accurate Time

Galaxy	Published	DCDFT Recovered	DCDFT Time-Corrected	ANOVA Recovered	ANOVA Time-Corrected
NGC 925	0.733	0.565	0.565	0.443	0.443
NGC 1365	0.517	0.588	0.587	0.213	0.221
NGC 3031	0.609	0.198	0.093	0.185	0.080
NGC 4535	0.642	0.714	0.600	0.564	0.484

the high-velocity galaxies such as NGC 1365 do not show a significant change in period.

2. We do observe some change in period after time correction. However, it is more reasonable to assume that these changes are due to the uncertainties in our data inputs instead of the time correction effect itself. Relatively high uncertainties are observed in the $P-L$ fits. Most of the $P-L$ slopes have errors greater than 20%. And the Pearson correlation coefficients of these fits suggest that the majority of the fits do not represnet strong correlations.

3. The overall effect of the time correction is hard to evaluate due to the large errors in the Key Project data. This deficiency is caused by the short observation baseline and insufficient data points. The short-period Cepheids tend to have lower uncertainties, while the long-period ones have larger uncertainties. More than half of the Cepheids in our sample are long-period ones. The short-baseline and insufficient data points have more influence on these long-period Cepheids, which leads to the large inaccuracies we have. Further studies need to be undertaken using data with better time coverage.

We conclude that the Cepheid data from the HST Key Project data do not cover a sufficient length in observational time for reliable period measurements. By observing the number of data points and the time duration as shown in Table 2.1, we conclude that the data set does not have sufficient time coverage for Cepheids with medium to long periods (roughly ranging from 10 to 70 days). The short-period Cepheids (less than 10 days) are better described. However, these are not the majority in our data set.

3.2 Impact of Length of Time String

An ongoing senior thesis project conducted by Rachel Hunter at Brigham Young University suggests that a reliable period calculation of a Cepheid-type star requires an observation that covers at least 4 of its complete variability cycles with the best results starting at 30 cycles. Simulations using an artificial observation time set for a theoretical 1-day period Cepheid yields periods as high as 1.2 days using slightly over 1 period. The analysis is repeated for data sets with a larger number of cycles included, up to approximately 100 cycles. Table 3.6 shows the number of cycles in the period calculation (first column) and the period calculated (second column). It can be seen that by 4 cycles we have reached a point of only a 1% error. We then reach a 0.1% error at about 15 cycles. To fully recover a pure 1 day period we needed to reach 30-35 cycles. The data from the HST Key Project covered in the range of 2.5 cycles for short period Cepheids to perhaps less than one cycle for some of the longest period Cepheids.

It is clear from the table that with a time coverage of approximately 4 cycles the calculated period will have an error smaller than 10%. Thus we conclude that for future studies that aim to calculate the periods of Cepheids with improved accuracy and to testify the results of the time correction, the observation needs to cover at least 4 variability cycles of the object. For a Cepheid sample with a mean period of about 30 days (which is the case of most of the galaxies used in this thesis), it implies that the duration of observation should be at least one year. This was not achieved by the Key Project Cepheid data, which makes our period calculation and the $P-L$ fits highly uncertain.

The study done by Riess and his colleagues (Riess et al. 2012) on M31 used data taken over a three-year survey. Its long observation baseline makes the study a great example for future studies on Cepheid periods. As we have mentioned in Section 1.1, the result from this study has good quality and agrees with a previous study using IR data. We would suggest future studies to either cover a long baseline for the long-period Cepheids or improve the sampling rate for the short-period ones. In reality, a long-baseline observation is difficult to achieve because most of the observation facilities have limited time for each study. A fast sampling rate might be an easier solution as now the Kepler space telescope is able to provide suitable data for the purpose of Cepheid studies,

Table 3.6. Varying Time Inputs (in the Number of Variability Cycles) and the Periods of a Theoretical 1-Day Period Cepheid

Number of Cycles	Period [Days]
1.0345	1.169317
2.0292	1.036198
3.0239	1.015985
4.0187	1.008878
5.0134	1.005901
6.0081	1.004016
7.0028	1.002942
8.0373	1.002138
9.0320	1.001603
10.026	1.001335
15.000	1.000534
20.014	1.000267
25.027	1.000267
30.001	1.000267
35.014	1
40.027	1
50.014	1
60.001	1
70.028	1
80.015	1
90.002	1
99.989	1

especially the short-period ones. We would also suggest future researchers to re-visit the objects that have been intensely observed through multiple epochs in time. Good examples of such would be the LMC and the SMC. By combining the data from multiple observations throughout time, it should be easier to see shifts in the Cepheid variability phase, which would be a clear indication of the time correction effect.

Bibliography

Berdnikov, L. N., Ignatova, V. V., Caldwell, J. A. R., & Koen, C. 2000, New Astronomy, 4, 625

Berdnikov, L. N., & Ignitova, V. V. 2000, The Impact of Large-Scale Surveys on Pulsating Star Research, ed. L. Szabados & D. Kurtz, Vol. 203 (San Francisco, CA: ASP Conference Series)

Berdnikov, L. N., & Turner, D. G. 2001, The Astrophysical Journal Supplement Series, 137, 209

Carroll, B. W., & Ostlie, D. A. 2007, An Introduction to Modern Astrophysics, 2nd edn., ed. A. R. S. Black (San Francisco, CA: Pearson), 1278

Ciatti, F., & Rosino, L. 1977, Astronomy and Astrophysics, 57, 73

Cox, J. P., & Whitney, C. 1958, The Astrophysical Journal, 127, 561

de Vaucouleurs, G. 1975, Galaxies and the Universe, ed. A. Sandage, M. Sandage, & J. Kristian, Vol. 9 (Chicago, IL USA: University of Chicago Press), 557

—. 1978, Astrophysics, 224, 710

de Vaucouleurs, G., de Vaucouleurs, A., Corwin, H. G., J., Buta, R. J., Paturel, G., & Fouquï£¡, P. 1991, Third Reference Catalogue of Bright Galaxies. Volume I: Explanations and references. Volume II: Data for galaxies between 0h and 12h. Volume III: Data for galaxies between 12h and 24h (New York, NY: Spinger) de Vaucouleurs, G., de Vaucouleurs, A., & Corwin, J. R. 1976, Second reference catalogue of bright galaxies (Austin, TX USA: University of Texas Press)

Eddington, A. S. 1919, Monthly Notices of the Royal Astronomical Society, 79, 177

Ferrarese, L., et al. 1998, The Astrophysical Journal, 507, 655

Ford, H. C., et al. 2009, SPIE, 4854, 81

Freedman, W. L., et al. 1994a, Astrophysical Journal, 435, L31

—. 1994b, Astrophysics, 427, 628

—. 2001, The Astrophysical Journal, 553, 47

Gibson, B. K., et al. 1999, Astrophysical Journal, 512, 48

Graham, J. A., et al. 1997, The Astrophysical Journal, 477, 535

—. 1999, Astrophysical Journal, 516, 626

Hughes, S. M. G., et al. 1998, Astrophysical Journal, 501, 32

Kelson, D. D., et al. 1996, Astrophysical Journal, 463, 26

—. 1999, The Astrophysical Journal, 514, 614

Kenney, J. D. P., Wilson, C. D., Scoville, N. Z., Devereux, N. A., & Young, J. S. 1992, Astrophysical Journal, 395, L79

Kolb, E. W., & Turner, M. S. 1990, The early universe, Vol. 69 (New York: Addison-Wesley)

Leavitt, H. S., & Pickering, E. C. 1912, Harvard College Observatory Circular, 173, 1

Macri, L. M., Stanek, K. Z., Bersier, D., Greenhill, L. J., & Reid, M. J. 2006, The Astrophysical Journal, 652, 1133

Macri, L. M., et al. 1999, Astrophysical Journal, 521, 155

Mallas, J. H., & Kreimer, E. 1978, The Messier album (Cambridge, Mass.: Sky Publication Co.)

Martin, C., & Plummer, H. C. 1914, Monthly Notices of the Royal Astronomical Society, 74, 225

Mould, J. R., et al. 2000, Astrophysical Journal, 528, 655

Ngeow, C., & Kanbur, S. M. 2006, The Astrophysical Journal, 650, 180

—. 2008, The Astrophysical Journal, 679, 76

Ngeow, C.-C., Kanbur, S. M., Neilson, H. R., Nanthakumar, A., & Buonaccorsi, J. 2009, The Astrophysical Journal, 693, 691

Patat, F., Barbon, R., Cappellaro, E., & Turatto, M. 1994, Astronomy and Astrophysics, 282, 731

Peacock, J. A. 1999a, Cosmological Physics (Cambridge, UK: Cambridge University Press), 704

—. 1999b, Cosmological Physics

Persson, S. E., Madore, B. F., Krzemiadski, W., Freedman, W. L., Roth, M., & Murphy, D. C. 2004, The Astronomical Journal, 128, 2239

Phelps, R. L., et al. 1998, Astrophysical Journal, 500, 763

Plummer, H. C. 1913, Monthly Notices of the Royal Astronomical Society, 73, 661

Prosser, C. F., et al. 1999, Astrophysical Journal, 525, 80

Pustilnik, S. A., & Tepliakova, A. L. 2011, Monthly Notices of the Royal Astronomical Society, 415, 1188

Rawson, D. M., et al. 1997, Astrophysical Journal, 490, 517

Riess, A. G., Fliri, J., & Valls-Gabaud, D. 2012, The Astrophysical Journal, 745, 156

Rubin, V. C., Peterson, C. J., & Ford, W. K., J. 1975, Astrophysical Journal, 199, 39

Sakai, S., et al. 1999, The Astrophysical Journal, 523, 540

Sandage, A. 1996, Astrophysical Journal, 111, 18

Sandage, A., & Bedke, J. 1985, Astronomical Journal, 90, 1992

Sandage, A., & Tammann, G. A. 1981, A revised Shapley-Ames Catalog of bright galaxies (Washington, DC: Washington: Carnegie Institution)

Sebo, K. M., et al. 2002, The Astrophysical Journal Supplement Series, 142, 71

Shapley, H. 1914, Astrophysical Journal, 40, 448

Silbermann, N. A., et al. 1996, Astrophysical Journal, 470, 1

—. 1999, Astrophysical Journal, 515, 1

Soszynski, I., et al. 2008, Acta Astronomica, 58, 163

Szabados, L. 1977, Mitt. Sternw. Ungarisch. Akad. Wiss., 1

—. 1980, Mitt. Sternw. Ungarisch. Akad. Wiss., 1

—. 1981, Mitt. Sternw. Ungarisch. Akad. Wiss., 1

—. 1989, Communications of the Konkoly Observatory, 11, 1

Tully, R. B. 1980, Astrophysical Journal, 237, 390

—. 1988, Nearby galaxies catalog (Cambridge and New York: Cambridge University Press), 221

Turner, A., et al. 1998, Astrophysical Journal, 505, 207

Turner, D. G. 1998, The Journal of the American Association of Variable Star Observers, 26, 101

Turner, D. G., Billings, G. W., & Berdnikov, L. N. 2001, The Publications of the Astronomical Society of the Pacific, 113, 715

Turner, D. G., Horsford, A. J., & MacMillan, J. D. 1999, The Journal of the American Association of Variable Star Observers, 27, 5

Udalski, A., Szymanski, M., Kubiak, M., Pietrzynski, G., Soszynski, I., Wozniak, P., & Zebrun, K. 1999, Acta Astronomica, 49, 201

van den Bergh, S. 1976, Astrophysical Journal, 206, 883

Veron, P., Lindblad, P. O., Zuiderwijk, E. J., Veron, M. P., & Adam, G. 1980, Astronomy and Astrophysics, 87, 245

Zaritsky, D., Smith, R., Frenk, C., & White, S. D. M. 1997, Astrophysical Journal, 478, 39